POLITECNICO DI MILANO

Scuola di Ingegneria Industriale e dell'Informazione

Corso di Laurea Magistrale in
Ingegneria Biomedica

Modulation and mathematical prediction of monoclonal Antibodies N-linked glycosylation in continuous CHO cell culture

Relatore: Prof. Massimo MORBIDELLI

Correlatore: Thomas VILLIGER

Autore:

Ernesto Scibona matr. 799459

Anno Accademico 2013/2014

Table of Contents

List of Tables

List of Figures

Abbreviations

2-AA	2- Anathralamide
ADP	Adenosine diphosphate
AMM	Ammonia
AMP	Adenosine monophosphate
ATF	Alternating tangential flow filtration
ATP	Adenosine triphospate
CDP	Cytinde diphosphate
CHO	Chinese Hamster Ovary
CMP	Cytidine monophosphate
CMP-Neu5Ac	Cytinde diphosphate N-acetylneuraminic acid
COPI	Coat Protein Complex I
CTP	Cytidine triphosphate
DoE	Design of Experiments
GDP	Guanosine diphosphate
GDP-Fuc	Guanosine diphosphate fucose
GDP-Hex	Guanosine diphosphate hexose
GDP-Man	Guanosine diphosphate mannose
Glu	Glucose
GMP	Guanosin monophosphate

GOD	Glucose oxidase
GTP	Guanosine triphosphate
ER	Endoplasmic reticulum
HILIC	Hydrophobic interaction chromatography
HPAEC	High pressure anion exchange chromatography
IgG	Immunoglobulin G
Lac	Lactic acid
LOD	Lactate oxidase
mAb	Monoclonal antibody
MALDI	Matrix-assisted laser desorption/ionization
MEIGO	MEtaheuristics for bIoinformatics Global Optimization
NADPH	Nicotinamide Adenine Dinucleotide Phosphate
NSD	Nucleotide sugar donor
ODE	Ordinary differential equation
RV	Reactor Volume
TFF	Tangential flow filtration
TGN	Trans-Golgi network
TOF-MS	Time-of-flight mass spectrometry
UDP	Uridine diphospate
UDP-Hex	Uridine diphospate hexose
UDP-HexNAc	Uridine diphospate N-acetylhexosamine

UDP-Gal	Uridine diphospate galactose
UDP-GalNAc	Uridine diphospate N-acetylgalactosamine
UDP-Glc	Uridine diphospate glucose
UDP-GlcNAc	Uridine diphospate N-acetylglucosamine
UDP-Xyl	Uridine diphospate xylose
UDP-GlcA	Uridine diphospate glucoronic acid
UMP	Uridine monophospate
UTP	Uridine triphosphate
Xv or VCD	Viable cell density

Amino Acids Nomenclature

ALA	Alanine
ARG	Arginine
ASN	Asparagine
ASP	Aspartic acid
CYS	Cysteine
GLN	Glutamine
GLU	Glutamic acid
GLY	Glycine
HIS	Histidine
ILE	Isoleucine
LEU	Leucine

LYS	Lysine
MET	Methionine
PHE	Phenylalanine
PRO	Proline
SER	Serine
THR	Threonine
TRP	Tryptophan
TYR	Tyrosine
VAL	Valine

Glycosylation Nomenclature

Man I	α-1,2 mannosidase I
Man II	α-1,3/ α-1,6 mannosidase II
GnT I	α-1,3 N-acetylglucosaminyl transferase I
GnT II	α-1,6 N-acetylglucosaminyl transferase II
FucT	α-1,6 fucosyltransferase (FUT8)
GalT	β-1,4 galactosyltransferase
SiaT	α-1,6 sialyltransferase
TP	Transport protein
M9	$Man_9GlcNAc_2$
M8	$Man_8GlcNAc_2$

M7	$Man_7GlcNAc_2$
M6	$Man_6GlcNAc_2$
M5	$Man_5GlcNAc_2$
HM	High mannose (M9, M8, M7, M6, M5)
A2	$GlcNAc_2Man_5GlcNAc_2$
FA1	$GlcNAcMan_5GlcNAc_2Fuc$
FA2G0	$GlcNAc_2Man_5GlcNAc_2Fuc$
FA2G1	$GalGlcNAc_2Man_5GlcNAc_2Fuc$
FA2G2	$Gal_2GlcNAc_2Man_5GlcNAc_2Fuc$
FA2G2S1	$SiaGal_2GlcNAc_2Man_5GlcNAc_2Fuc$
FA2G2S2	$Sia_2Gal_2GlcNAc_2Man_5GlcNAc_2Fuc$

Abstract

Over 30% of the biotechnological products marketed are therapeutic monoclonal antibodies (mAbs) employed for the treatment of cancer, autoimmune diseases and many other pathologies. These drugs are commonly humanized immunoglobulins Gs (IgGs) produced by genetic recombination using mammalian cells as hosts. All IgG-based mAbs are N-glycosylated in the Fc region and, like other glycoproteins, are produced as a pool of different isoforms that differ only for the type of N-glycan attached to the Asn-X-Tyr consensus sequence.

It has been largely demonstrated that these sugar moieties are of paramount importance for the clinical efficacy of these drugs in terms of immunogenicity, stability, pharmacokinetic properties (PK) and biological activity. For instance, IgGs bearing N-glycans which lack core fucose show a significant increase in antibody-dependent cell-mediated cytotoxicity (ADCC) (up to 100 fold), while terminal galactosylation has been linked with enhanced complement-dependent cytotoxicity (CDC) and prolonged serum half-life. N-glycosylation is therefore regarded as one of the main product quality attributes by regulatory agencies.

Even though the ability to control this post-translational modification is limited by the high degree of complexity and heterogeneity of the glycan structures and the non-template driven nature of glycosylation, it has been reported that presence of trace elements, waste metabolites accumulation and intracellular nucleotide sugar donors concentrations have a strong influence on this biological process.

With the aim of creating mAbs possessing a desired glycosylation profile, an experimental and mathematical framework for the prediction of the N-glycosylation pattern under different process conditions was developed.

In order to investigate the effect of ammonia production, manganese and galactose supplementation, a series of continuous cell cultivations was carried out under the design of experiments (DoE) methodology using Chinese hamster ovary (CHO) cells.

Compared to typical industrial fed-batches, perfused bioreactors allow a better control of process conditions due to the continuous exchange of culture medium. The use of this type of systems prevented waste product accumulation and changes in cellular metabolism by

culturing the cells in a steady environment. Moreover, thanks to this strategy, the levels of the three glycosylation effectors investigated were maintained to desired set points, resulting in constant glycosylation profiles.

During each run, different steady states in terms of viable cell density and medium components were performed in order to systematically assess the impact of the three considered process parameters. Antibody glycosylation profiles, intracellular metabolites levels, amino acids and ammonia accumulated were analyzed by means of HPLC, MALDI-TOF-MS and enzymatic assays. Measured quantities were used to tune a mathematical model whose performance, in terms of predictive capacity, was subsequently tested for a different point within the experimental space. The developed mathematical model consisted of a kinetic network consisting of 33 oligosaccharides connected by 43 enzyme-catalyzed reactions for a total of 40 coupled ODEs and was based on the work of del Val et. al [1]. To solve the system, the Golgi apparatus was considered as a single plug flow reactor (PFR), where recycling and compartmentalization of resident proteins was implemented by assuming their concentration across the apparatus following 3-parameters normal functions.

New enzyme kinetic equations were developed to provide a bridge between N-glycosylation and process conditions. The effect of ammonia was included by considering a reduction in enzyme activity in response to basification of the Golgi environment caused by this metabolite. Enzyme kinetics were modified to take into account the presence of Mn as essential cofactor for the reaction mechanism and galactose supplementation was reproduced by including equations for the nucleotide sugars transport into the Golgi compartment.

On the experimental side, N-glycosylation was successfully modulated by the implemented process strategy. Galactose and manganese were provided together with the culture medium, while different steady states for ammonia were obtained by regulating the cell density inside the bioreactor. Cell viability was always very high (above 90%) and no starvation in amino acids was detected. Galactose and Mn were not found to affect the process performance in terms of VCD or mAb specific productivity.

Intracellular metabolites analysis showed consistent nucleotides and nucleotide sugars profiles throughout all runs. The concentration of these species was found to be in line with other measurements for the same cell line and could be easily tuned by means of different

medium compositions: for instance, a 3-fold increase in UDP-Galactose was detected in response of 10 mM galactose supplementation.

The analytical protocol employed for the N-glycans analysis allowed the detection of more than 20 different oligosaccharide structures. A substantial increase in terminal galactosylation (up to 1.5-fold) was observed when cells were fed with either galactose or manganese, showing a synergistic effect when both components were added simultaneously. Elevated ammonia levels resulted in a decrease in terminal galactosylation and sialylation with a corresponding increase in high mannose structures.

The mathematical model successfully reproduced these changes and further predicted the glycosylation pattern under a set of conditions that was not included in the first optimization. Estimated parameters were found to be in the same range of experimental data for other mammalian cell lines and the number of parameters optimized per structures predicted was much lower compared to all other models published so far.

To provide a reference with statistical tools, the same set of data was used in parallel to develop a response surface methodology (RSM). Although correctly tuned to the experimental points, this approach lacked interpolating capacity, indicating the superiority of the mechanistic model with respect to the statistical one.

The model developed was capable not only to predict changes in glycosylation as a response to variations in medium components and process conditions, but provided insights about non-measurable quantities such as intra-Golgi concentration profiles of single N-glycans and nucleotide sugars. Computer simulations were used to determine the main chemical fluxes and how these fluxes were affected by the investigated process conditions.

For this reason, the mechanistic approach of this work could represent a base for metabolic engineering of the production of recombinant proteins with a desired glycosylation pattern.

***Keywords*:** N-linked Glycosylation, monoclonal antibodies, perfused bioreactor, mathematical model.

Sommario

Piú del 30% dei prodotti del settore biotecnologico attualmente sul mercato sono anticorpi monoclonali (mAbs) utilizzati per la cura di tumori, malattie autoimmuni ed altre patologie. Queste proteine, utilizzate come farmaci, sono nella maggior parte dei casi immunoglobuline G (IgGs) prodotte con la tecnologia del DNA ricombinante in cellule di mammifero. Le immunoglobuline G umane sono delle glicoporoteine ed in quanto tali sono prodotte come una serie di isoforme che differiscono per il tipo di oligosaccharide attaccato alla sequenza consenso Asn-X-Thr/Tyr.

Numerosi studi hanno dimostrato che il tipo e la struttura di questi zuccheri hanno un'importanza fondamentale per l'efficacia clinica dei farmaci prodotti in termini di immunogenicitá, stabilitá, proprieta farmacocinetiche (PK) ed attivitá biologica. Ad esempio, immunoglobuline G legate ad oligosaccaridi non fucosilati mostrano un aumento fino a 100 volte della citotossicitá mediata da cellule (ADCC), mentre la presenza di galattosio come unitá terminale é stata correlata ad un aumento della citotossicitá dipendente dal sistema del complemento (CDC) e dell'emivita in circolo. La N-glicosilazione é perció considerata dalle agenize regolatrici una delle proprietá piú importanti di questi prodotti biologici.

Anche se le possibilitá di controllare questa modifica post traslazionale sono limitate dall'alto grado di complessitá ed eterogeneitá di questi oligosaccaridi, cosí come dall'impossibilitá di ricondurre queste strutture ad un template in DNA, é stato dimostrato come la presenza di elementi traccia, l'accumulo di metaboliti di scarto e la concentrazione di glicosil-nucleotidi abbiano una forte influenza nel processo biologico durante la produzione industriale di glicoproteine.

Al fine di creare anticorpi monoclonali con il profilo di glicosilazione desiderato, nel presente lavoro é stato sviluppato un quadro sperimentale e modellistico al fine di predire l'effetto di diverse condizioni di processo sulla biosintesi di questi oligosaccaridi.

Una serie di colture cellulari in sistemi a perfusione secondo la metodologia del Design degli Esperimenti (DoE) é stata effettuata per investigare gli effetti causati da ammoniaca, galattosio e manganese sulla N-glicosilazione di anticorpi monoclonali prodotti in cellule

di linea CHO. Rispetto ai processi semi-batch, tipicamente utilizzati nell'industria biofarmaceutica, l'utilizzo di bioreattori perfusi garantisce un miglior controllo delle condizioni di processo. La continua aggiunta di nutrienti e rimozione di sottoprodotti permettono l'ottenimento di un ambiente costante nel reattore. Inoltre, il ricambio continuo del medium consente di regolare finemente i livelli di ammoniaca, galattosio e manganese durante l'esperimento, mentre la rimozione di sottoprodotti evita l'accumulo di sostanze di scarto che possono determinare modifiche nel metabolismo cellulare.

In ogni coltura cellulare sono stati studiati diversi stati stazionari in termini di densitá cellulare e composizione del mezzo di coltura in modo da analizzare sistematicamente l'impatto dei parametri considerati. I profili di glicosilazione e le concentrazioni di metaboliti intracellulari, amminoacidi ed ammoniaica sono stati analizzati mediante HPLC, MALDI-TOF e saggi enzimatici. I valori ottenuti sono stati utilizzati per calibrare un modello matematico, la cui capacitá predittiva é stata poi testata per un diverso punto all'interno dello spazio sperimentale. Il modello matematico sviluppato, basato sul lavoro di del Val et. al [1], consiste in un *network* cinetico di 33 oligosaccaridi connessi da 43 reazioni, per un totale di 40 equazioni differenziali ordinarie. Per risolvere il sistema l'apparato di Golgi é stato modellizzato come un singolo reattore chimico PFR, in cui gli effetti di riciclo e compartimentalizzazione degli enzimi sono stati implementati assumendo profili di concentrazione di questi ultimi descritti da funzioni normali a tre parametri.

Nuove equazioni cinetiche sono state sviluppate per consentire di legare le condizioni di processo alla N-glicosilazione. L'effetto dell'ammoniaca é stato incluso considerando una riduzione dell'attivitá enzimatica in seguito alla basificazione dell'apparato di Golgi causata da questo metabolita, il manganese é stato inserito nel meccanismo di reazione come cofattore mentre la presenza di galattosio é stata riprodotta includendo nel modello le equazioni del trasporto di glicosil-nucleotidi all'interno dell'apparato.

Dal punto di vista sperimentale, la strategia utilizzata ha permesso una corretta modulazione della N-glicosilazione: galattosio e manganese sono stati forniti alle cellule all'interno del mezzo di coltura, mentre diversi livelli di ammoniaca sono stati ottenuti semplicemente regolando la densitá cellulare all'interno del reattore. La vitalitá cellulare é risultata molto alta, superiore al 90%, senza aver riscontrato alcuna limitazione in amminoacidi e fonti di carbonio. Le due sostanze aggiunte nel mezzo non hanno inficiato

la performance del processo in termini di vitalitá cellulare o produttivitá specifica di anticorpi.

L'analisi dei metabolti intracellulari ha mostrato, negli stati stazionari investigate, profili costanti nel tempo sia dei nucleotidi che dei glicosil-nucleotidi. La concentrazione di questi ultimi si é rivelata in accordo con altre misurazioni per la stessa linea cellulare ed é stata correttamente controllata variando la composizione del mezzo di coltura. Ad esempio, la concentrazione di UDP-Gal é stata incrementata di 3 volte in seguito all'aggiunta di galattosio 10 mM.

Il protocollo analitico utilizzato per l'analisi degli oligosaccaridi ha permesso la determinazione di oltre 20 strutture differenti. Un sostanziale aumento in galattosio terminale (fino a 1.5 volte) é stato riscontrato quando le cellule sono state coltivate in presenza di manganese o dello zucchero stesso. I due componenti hanno inoltre mostrato un effetto sinergico quando sono stati introdotti contemporaneamente all'interno del reattore. Elevati livelli di ammoniaca hanno invece prodotto una diminuzione della frazione relativa di strutture recanti galattosio o acido sialico terminale, con un correspondente aumento nella quantitá di strutture ricche in mannosio.

Il modello matematico é riuscito con successo a riprodurre questi effetti e a predire il profilo di glicosilazione per un diverso set di condizioni. I parametri stimati sono risultati essere dello stesso ordine di grandezza registrato per altre linee cellulari, mentre il numero di parametri ottimizati per numero di strutture riprodotte é risultato molto inferiore rispetto a quello utilizzato dai modelli ad oggi pubblicati.

Per offrire un confronto con metodi statistici, lo stesso set di dati é stato applicato per sviluppare una superficie di risposta (RSM). Sebbene correttamente calibrata dai punti sperimentali, questa tecnica non é riuscita ad interpolare un diverso punto sperimentale, indcando la superioritá del modello meccanicistico a paritá di condizioni.

Il modello sviluppato si é inoltre rivelato capace non solo di predire cambiamenti nella glicosilazione in risposta a variazioni nelle condizioni di processo, ma ha anche consentito di ottenere delle informazioni sui profili di concentrazione delle diverse strutture olgiosaccaridiche e dei glicosil-nucleotidi all'interno dell'apparato di Golgi, non misurabili mediante tecniche sperimentali. Simulazioni a computer hanno permesso di determinare i principali flussi chimici e come questi venissero modificati dalle condizioni di processo investigate. Per questi motivi, l'approccio meccanicistico proposto in questo lavoro puó

rappresentare la base per la produzione di proteine ricombinanti con il profilo di glicosilazione desiderato.

***Parole chiave*:** N-glicosilazione, anticorpi monoclonali, bioreattore perfuso, modello matematico.

Chapter 1: Introduction

1.1 N-linked Protein Glycosylation

Glycosylation is the most abundant post translational modification for mammalians and refers to the attachment of oligosaccharides to specific amino acid sequences on newly synthesized proteins. This protein modification is known to be involved in many fundamental biological functions such as cell-cell and cell-matrix interactions, as well as protein folding, stability and circulatory half-life. In contrast to nucleic acids and peptides, the synthesis of oligosaccharides is a non-template driven process which relies on the segregation of several enzymatic steps in different compartments. Moreover, the types of structures assembled in this way are typically branched molecules that differ in chain length, type of linkage, anomery (α or β) and branching points [2]. Due to this intrinsic high complexity and the failure in predicting these structures from a DNA template, studies on glycobiology only began in the 80s with the advent of more sophisticated analytical techniques.

Different types of glycosylation observed in nature can be classified according to the nature of the sugar-amino acid linkage, namely N- and O-glycosylation, C-mannosylation, phosphoglycation and glypiation [3]. While N-glycosylation and glypiation are characterised by the *en bloc* transfer of an oligosaccharide precursor to particular residues of the protein, all other types of linkage are formed by the enzymatic transfer of activated monosaccharides directly to the polypeptide [3].

N-glycosylation, the main focus of this work, has been widely recognized to be the most important and frequent sugar-amino acid bond in eukaryotes. For reference, it has been estimated that 64.9 % of the cell proteins contain potential glycosylation sites and that 9 out of 10 of them are N-glycosylation specific [4]. In this case, the glycosidic linkage occurs between the N-acetylglucosamine of the oligosaccharide precursor and the amide group of specific asparagine residues located within the Asn-X-Thr/Ser consensus sequence, where X can be any amino acid except proline. The mechanisms through which

this precursor sugar attached to the protein and subsequently modified will be descripted in the next chapter.

1.2 N-Glycan Synthesis

N-linked glycosylation starts at the cytoplasmic face of the ER of eukaryiotic cells with the synthesis of a membrane-bound dolichol-linked precursor oligosaccharide composed of 3 glucose residues, 9 mannose residues and 2 N-acetylglucosamines ($Glc_3Man_9GlcNAc_2$), linked together as depicted in Fig. 1A. The synthesis of this precursor is carried out by the sequential action of particular enzymes, referred to as glycotransferases, catalysing the transfer of sugar moieties from nucleotide-activated sugars (nucleotide sugar donors, NSDs) to specific acceptor molecules [5]. Once formed, the glycan is translocated across the ER membrane and exposed towards the luminal side, where under the activity of a multimeric enzymatic complex called oligosaccharyl transferase (OST) is *en bloc* transferred to proteins exposing the Asn-X-Thr/Ser consensus sequence [6]. Once the sugar-amino acid bond is formed, newly synthetized proteins are encapsulated inside lipid vesicles and transported throughout the ER and Golgi compartments to have their sugar

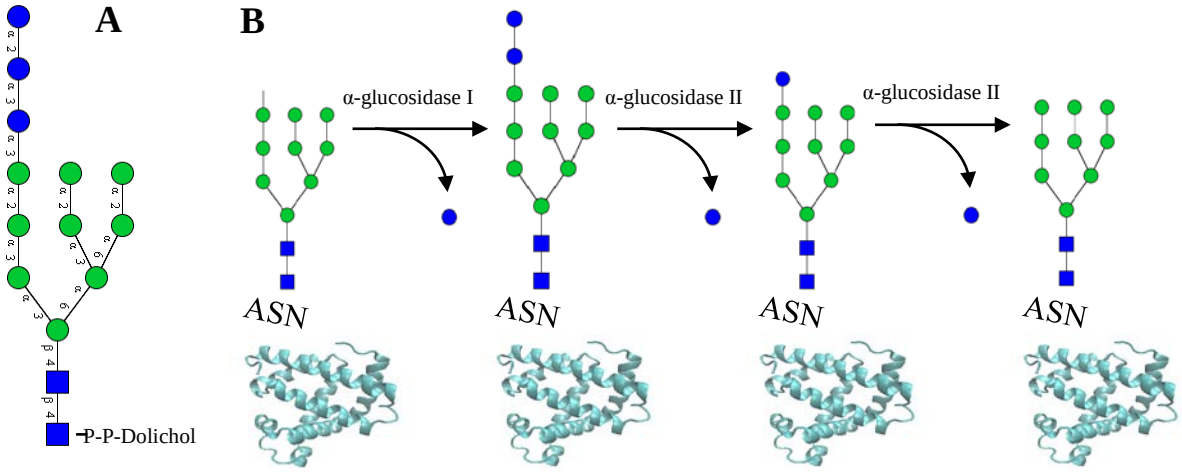

Figure 1 The dolichol-linked oligosaccharide precursor (A). Modifications of the precursors during protein folding (B)

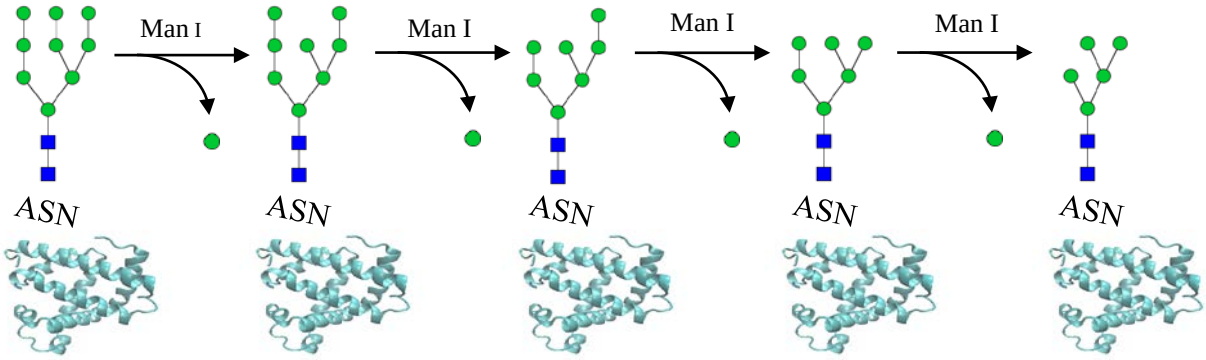

Figure 2 N-Glycan processing in the *cis*-Golgi

moieties modified. Since every compartment (ER, *cis*-, *medial*- and *trans*- Golgi) has its own set of enzymes, the glycan processing can be nominally divided into a sequence of successive reactions. The first step of this process consist of the sequential removal of glucose residues from the acceptor sugar (i.e. the glycan attached) catalysed by α-glucosidases I and II (Fig. 1B), in a process which is known to be involved in the quality control of protein folding in the ER. Once 2 of the 3 glucose residues are removed, the polypeptide encounters molecular chaperones, a class of proteins apt to prevent aggregation and misfolding and provide a reducing environment to aid the formation of disulphide bonds [7]. Removal of the last glucose unit provides a mean to signal that the protein is properly folded and ready to be transferred to the *cis*-Golgi. Most of the proteins are now characterised by a so called "high mannose" (HM) glycan, composed of 2 N-acetylglucosamines (GlcNAc) and 8-9 Mannose residues linked together in a branched structure as depicted in Fig. 2. While in the *cis*-Golgi, up to 4 mannose residues are removed under the action of successive α-mannosidases to produce the $Man_5GlcNAc_2$ oligosaccharide, a key intermediate for the production of more complex N-glycans (Fig. 2). Starting from the *medial-Golgi*, glycan modifications mainly involve the addition of different sugar monomers to the growing structure catalysed by glycotransferases. This pathway is initiated by the action of N-acetylglucosaminyl transferase I (GnTI) with the addition of a GlcNAc molecule to the α1-6 arm of the core $Man_5GlcNAc_2$. This step is required for the Golgi α-mannosidase II to cleave the remaining mannose residues in the α1-3 arm of the glycan (Fig. 2). The enzyme N-acetylgucosaminyl transferase II (GnTII) later adds a second GlcNAc to the glycan to form a bi-antennary structure (Fig. 3). While the addition of a second GlcNAc is common for most of the mammalians, some organisms,

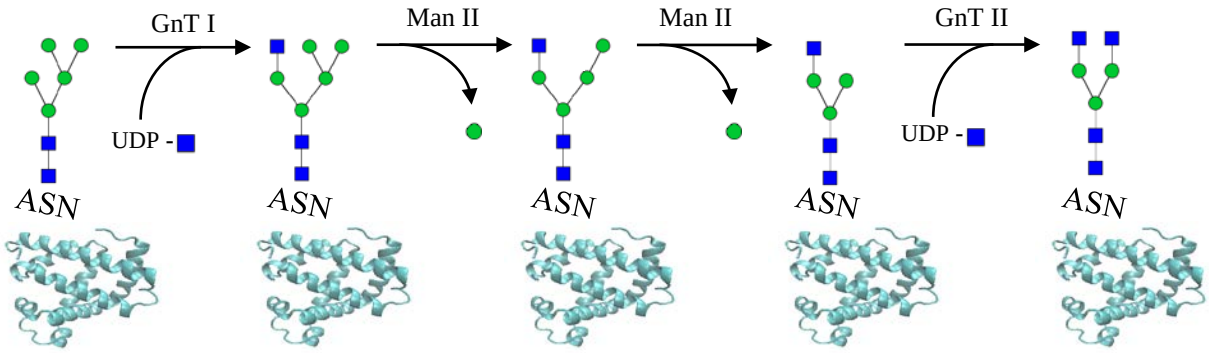

Figure 3 N-Glycan processing in the *medial*-Golgi

such as humans, also express other N-acetylgucosaminyl transferases which allow the formation of tri- and tetra-antennary glycans [7].

The final processing is carried out in the *trans*-Golgi to form more complex structures in a series of steps that is different for each species (among a single cell of a single organism) and it is dependent on which protein is being glycosylated. In general, the first modification applies to the core and consists in the addition of a fucose molecule to the GlcNAc bound to the asparagine (mainly via α1–6 linkages) catalysed by enzymes of the fucosyl transferases subclass. Subsequently, the branched structures are elongated with the attachment of galactose in β position by the action of galactosyltransferases. Other decorations involve the addition of sialic acid, fucose, galactose, N-acetylgalactosamine, and sulfate to the branches, mainly in α position [7]. An overview of the most common reactions occurring is presented in Fig. 4.

1.3 N-Glycosylation Heterogeneity

Despite every consensus sequence is in principle available for linkages with oligosaccharides, the transfer of the N-glycan may be impaired due to conformational constraints or other limitations occurring during the glycoprotein folding. Given that only a subset of all possible Asn-X-Thr/Ser motifs is involved in such linkages, proteins with multiple binding sites may present different combinations of site occupancies, giving rise to a type of structural diversity referred to as macroheterogeneity. Moreover, it's commonly observed that even a single consensus sequence may be bound to different types

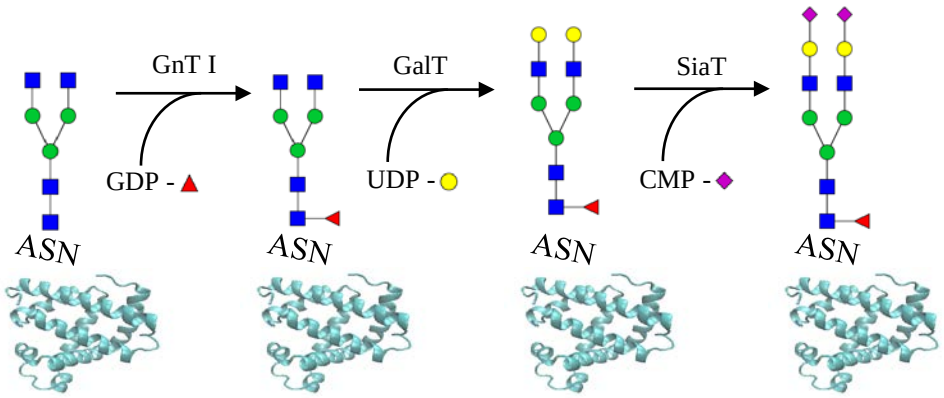

Figure 4 N-Glycan processing in the *trans*-Golgi and *TGN*.

of N-glycans, leading to a second type of heterogeneity, called microheterogeneity. Glycoproteins are thus produced as pools of heterogeneous N-glycans bound to an invariant polypeptide backbone. This phenomenon greatly enhances the diversity of glycoproteins that a single cell might produce, causing the glycome to become much bigger in size with respect to both genome and proteome. For example, human immunoglobulins G (IgGs) present complex bi-antennary glycan structures with six main different forms (Tab. 1), although more than 1000 different forms can be present [8].

Table 1 Key N-glycans in human IgG1.

N-linked glycosylation site	Terminal GlcNAc	Terminal galactose	Terminal sialic acid	Core fucosilation
Asn-297	35 %	50 %	10-15 %	69%

1.4 Human Immunoglobulins as Glycoproteins

Immunoglobulins (IgGs), also referred to as Antibodies (Abs), are the most important secretory products of the adaptive immune system [9]. A single IgG unit is a Y-shaped macromolecule consisting on two identical light and heavy chains, both comprising defined structural domains of about 100 amino acid residues each. Once the folding is completed, single chains are linked together by disulphide bridges giving rise to three

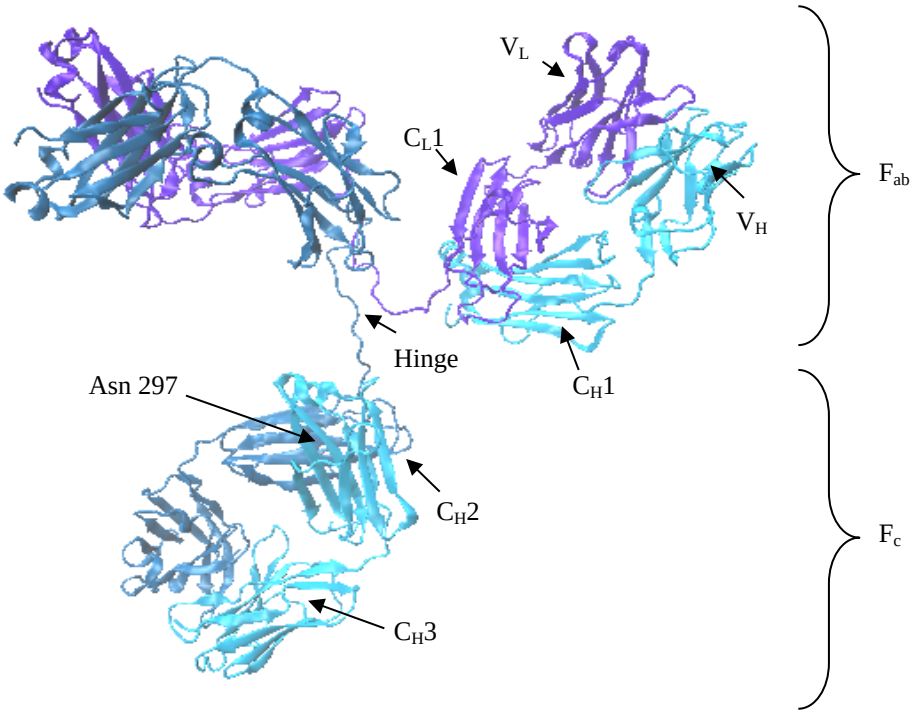

Figure 5 Representation of an IgG1 molecule and location of the most important domains.

defined regions separated by a flexible hinge (Fig. 5). The constant domains, located at the C-term, constitute the crystallisable fragment (Fc) and define the isotype of the Ig (α, β, ε, γ and δ), while the variable regions on both heavy and light chains pair to establish two antigen-binding fragments (Fab).

The general mechanism of action of antibodies involves first the binding of the antibody's respective antigen (Ag) mediated by the Fab, followed by the recognition of the Ab–Ag complex by the immune system of the host organism. Antibodies belonging to the IgG1 subclass represent the vast majority of antibodies approved for clinical practice and can activate the immune response by means of antibody-dependent cellular cytotoxicity (ADCC) and complement-dependent cellular cytotoxicity (CDC). Both mechanisms are based on the recognition of specific interaction sites on the Fc region by surface receptors of natural killer cells (FcγRI, FcγRII and FcγRIII) or by the C1q component of the complement systems. The recognition site in the IgG-Fc is determined by the pairing of the CH2 and CH3 domains of the heavy chains, where the CH2 domain is N-glycosylated at asparagine-297. Most recombinant antibodies are thus glycoproteins bearing two N-oligosaccharides in the constant region. The presence of these sugars directly influences

the structure of the crystallisable fragment and is responsible for the biological activity of such molecules as briefly reviewed in the next paragraph.

1.5 Effect of N-Glycosylation on Antibodies

Glycosylation is a post-translational modification and therefore does not directly affect the biological function of a protein, which is mainly due to its amino acid sequence, but instead plays a key role in modulating its physiochemical properties such as solubility, stability and conformation. Hence, glycosylation deeply affects the *in vivo* biological activity of proteins and is of paramount importance for the quality of therapeutic recombinant immunoglobulins.

As previously mentioned, the presence of the N-glycan on mAbs is required for the obtainment of a correct spatial conformation: this is due to the extensive non-covalent interactions occurring between the oligosaccharide (which is integrated in the Fc region as revealed by X-ray crystallography [10]) and the peptide backbone. These mutual interactions are known to influence and stabilize the structure of the entire macromolecule. Two studies based on differential scanning micro-calorimetry [11] and differential scanning fluorimetry [12] established that non-glycosylated antibodies show a lower free energy of stabilisation (ΔG), mainly due to a less stable structure, and a lower temperature of exposure of the hydrophobic regions (T_H). Both quantities directly correlate with the unfolding temperature and the overall stability of the molecule, suggesting non-glycosylated antibodies to be more prone to misfolding and therefore less stable.

Besides affecting the overall stability, the Fc region conformation can also enhance (or suppress) the effector function of mAbs by modulating the affinity between the CH2 domain and the Fcγ receptors: although the interaction is dependent on the protein moiety only, the presence of the oligosaccharide at Asn-297 partially modulates the structure of the Fc region, therefore affecting the binding with the effector ligands. This is critical for non-glycosylated antibodies which, despite retaining their binding affinity towards the antigen, no longer elicit their therapeutic mechanism. The missing binding activity of leukocytes or complement components was confirmed *in vitro* by measuring the affinity between non-glycosylated crystalline Fc regions and soluble Fcγ receptors [13].

Considering glycosylated antibodies, numerous other studies demonstrated the possibility to modulate the affinity of Fc receptors and effector ligands by changing only the type of sugar attached. For instance, IgGs bearing N-glycans without core fucose showed an increased ADCC (up to 50-fold) with respect to fucosylated ones [14], while terminal galactosylation enhanced CDC [15].

When dealing with drugs pharmacokinetic properties have also to be assessed to develop an efficient product. In case of antibodies, these properties are strongly influenced by the type and structure of their sugar moieties. In this view, antennary structures bearing terminal galactose and sialic acid present longer serum half-life compared to high mannose or N-acetylglucosamine oligosaccharides [16]. This is due to the presence on the surface of dendritic cells of the mannose receptor, a C-type lectin (i.e. a carbohydrate-binding protein) with the task of inducing the selective clearance of circulatory proteins bearing terminal mannose and N-acetylglucosamine. Moreover, since the region near the Asn-297 site is partially hydrophobic, glycosylated monoclonal antibodies present improved solubility, reduced tendency to aggregate [17] and higher resistance towards proteases [18], again resulting an increase in serum half-life.

In some cases glycosylation is proven to have detrimental effects: although carbohydrates are generally not immunogenic, specific glycosylation pattern can be recognized as foreign by the human immune system, especially when xenogenic host cells are used for their production. Commonly found non-human epitopes are for instance the galactose-alpha-1,3-galactose (α-gal) linkage and the N-glycolylneuraminic acid (NGNA) sugar, introduced in N-glycans produced by CHO or mouse NS0 cells. Controlling the glycosylation is therefore absolutely necessary to produce safe and efficient drugs.

1.6 Mammalian Cell Cultures for the Production of Therapeutic Proteins

Therapeutic monoclonal antibodies currently represent the highest selling product in the biopharmaceutical industry, with their sales occupying over 30% of the biotechnological products market in the United States (US) and continuously growing [19]. As of march 2012, 28 different mAbs have been currently marketed either in Europe or in the US. The

vast majority of mAbs (26/28) is produced by mammalian cell hosts like Chinese hamster ovary (CHO) (43%, 12/28), SP2/0 (25%), NS0 (18%) or hybridoma cells (7%), with the remaining two products in the market being antigen-binding fragments manufactured in bacterial cultures of *E. coli* [20]. As seen from the data published by the Food and Drug Administration (FDA), mammalian cells nowadays represent the main system for the production of recombinant proteins. The choice for mammalian hosts resides both in their superior capability compared to bacteria, plants and yeast to assure proper folding and post-translational modifications [21] and the possibility to be cultured in large-scale suspension bioreactors. Among mammalian cells, CHO cells dominate the industrial production due to their robustness, high productivity and fidelity in reproducing human-like post-translational modifications [21]. Recent advances in cell culture technology in terms of clone screening, media development and process optimization have led to a drastic improvement in productivity of mammalian cells, which can be now grown in large-scale suspension cultures (up to 20000L) in chemically defined medium. Despite the fact that stirred-tank reactors now represent the industry's technology of choice, the operation mode remains diversified, with fed-batch and perfusion cultures being the dominant systems for industrial manufacturing.

Operation Modes for the Production of Biopharmaceuticals

Fed-batch currently represents the most established operation mode for the production of recombinant proteins at industrial scale due to its scalability properties, process reliability and operational simplicity. Compared to simple batch operation, fed-batch cultures involve a controlled feeding strategy to prevent nutrient depletion, thus allowing for a prolonged culture time (up to 17 days) at higher viable cell densities (VCD), and providing higher product concentrations due to accumulation of the product inside the reactor [22]. State-of-the-art fed-batch processes can reach more than $25 \cdot 10^6$ cells/ml and final product titers beyond 10 g/L.

In continuous (or perfused) cultures the product is continuously harvested from the bioreactor by means of cell retention devices such as hollow fibers [22], while fresh medium is fed at the same rate to keep the culture volume constant. The continuous exchange of medium compensates for nutrient utilization and reduced the accumulation of

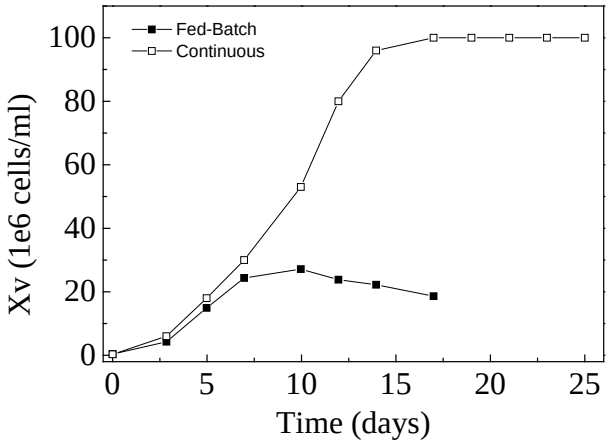

Figure 6 Viable cell density profiles for a typical fed-batch and continuous run.

toxic metabolites in the bioreactor, thus allowing much higher cell densities (up to $100 \cdot 10^6$ cells/ml) and prolonged culture time (~ months) to be reached. In addition, a ‘’cell bleed’’ (i.e. direct removal of content from the bioreactor) might be applied to keep the viable cell density constant. When compared to fed-batches, continuous cultures provide superior productivity due to higher cell densities, steady-state quality of the product and require a smaller scale for the operation (500-1000 L versus 15000-20000L). On the other hand, these systems are limited in terms of horizontal scalability (i.e. scale-out) due to the absence of cell retention devices for small scale operations. A quick comparison of the VCD profiles in the 2 operation modes is presented in Fig. 6.

1.7 Protein Glycosylation Control

N-glycosylation is considered by regulatory agencies as one of the main product’s critical quality attributes because of its role in affecting the therapeutic performance of recombinant proteins. Knowing how different manufacturing conditions influence this post-translational modification is therefore of paramount importance for the biopharmaceutical industry. The main strategies for modulating glycosylation of recombinant proteins reported in literature include (I) host cell engineering and clone selection, (II) media components and (IV) operating parameters.

Host Cell Engineering and Clone Selection

Cell lines used for the production of recombinant IgGs are normally genetically engineered to express products with reduced immunogenicity and enhanced *in vivo* performances. For instance, NS0 and SP2/0 cells express the α1,3-galactosylatransferase which is responsible for the α 1,3 linkage between two galactose units, an epitope not present in humans and therefore highly immunogenic [23]. On the other hand, CHO and NS0 cells produce glycoproteins bearing small quantities of N-glycolyl-neuraminic acid (a form of sialic acid) recognized as foreign by the human immune system. In other cases, clone screening using lectins can be employed to select subpopulations of cells with interesting characteristics like absence of fucosylation or galactosylation.

The therapeutic efficacy of IgGs can be measured in terms of ADCC, which is determined by the affinity between the Fc region and the FcγRIII receptors on the surface on natural killer cells (FcγRIII-A for neutrophilis). ADCC has been showed to increase up to 50-100 times for non-fucosylated antibodies, leading many industries and research groups to find strategies to knock out the fucosyltransferase FUT8 gene [24] to prevent the attachement of this type of sugar. Another mean to prevent fucosylation involves the increase of GlcNAc-bisected glycans [25], since it was demonstrated that the presence of the bisecting GlcNAc inhibits the action of FUT8.

Culture Conditions

The main process parameters that are known to significantly affect glycosylation are temperature, pH and dissolved oxygen (DO). Briefly, temperature has been found to affect the ratios between bi- tri- and tetra-antennary structures for erythropoietin (EPO) produced in CHO cells [26], pH variations between 6.8 and 7.8 have been linked to differences in galactosylation and sialylation up to 50% for mAbs produced by a murine hybridoma cell line [27], and decreasing DO causes a shift towards less galactosylated structures [28]. Other authors also cited osmolarity as a factor influencing N-glycosylation, but its effect is not fully understood [29]. Despite implementing different set points for these parameters they could be used to modulate the N-oligosaccharide synthesis, the results are most of the times contradictory and a general trend cannot be derived. Moreover, deviations from the

optimal values negatively affect the culture performance in terms of lower cell viability and productivity. It is therefore much more convenient to control glycosylation through the supplementation of specific molecules whose effect is limited to the N-glycan biosynthetic pathway.

Many authors indicated that type and availability of carbon sources has a great impact on protein glycosylation, most likely due to the influence of monosaccharides on synthesis of the nucleotide sugar donors. Rearick et. al [30] showed that the absence of glucose in culture medium reduces the biosynthesis of the lipid-linked oligosaccharide precursor, resulting in lower site occupancy and glycosylation profiles for monoclonal antibodies [31]. When cells are supplemented with sugars that are involved in the NSDs biosynthesis, intracellular concentrations of the corresponding nucleotide sugar precursors are increased [32], and can be directly correlated in changes of the resulting glycosylation pattern. For instance, cells cultured in presence of galactose (up to 18 mM) show an increase in UDP-Galactose, resulting in the production of more galactosylated antibodies, while other works reported that the addition of N-acetylmannoamine and fucose could be linked with larger extents of terminal sialylation and core fucosylation [32]. Sugars not directly involved in the NSDs synthesis can have a significant impact on glycosylation as shown recently by Hossler *et al.* [33], who described how CHO cells supplemented with sucrose and tagatose produced a higher percentage of high mannose non-fucosylated species.

A strong way to direct glycosylation towards more processed N-glycans (i.e. glycans presenting terminal galactose/sialic acid) is represented by the addition of uridine and manganese. The first molecule raises intracellular levels of uridine-based nucleotide sugars (UDP-Galactose, UDP-Glucose, UDP-GlcNAc, UDP-GalNAc), while Mn is a primary cofactor for GnTI [34], GnTII [29] and GalT[35] and its presence increases the turnover number of these glycotransferases.

Another possibility to modulate glycosylation involves the presence of the N-glycan biosynthetic pathway inhibitors in the culture medium with the aim of slowing down or stopping specific reactions by I) blocking the catalytic site of specific enzymes or II) lowering their activity (turnover number). The main example with reference to the first point is kifunesine, an inhibitor of the mannosidase I enzyme which has been employed to produce antibodies with enhanced ADCC [36], since the glycosylation pathway for cells treated with this substance is blocked in the first stages (i.e. before fucosylation can take

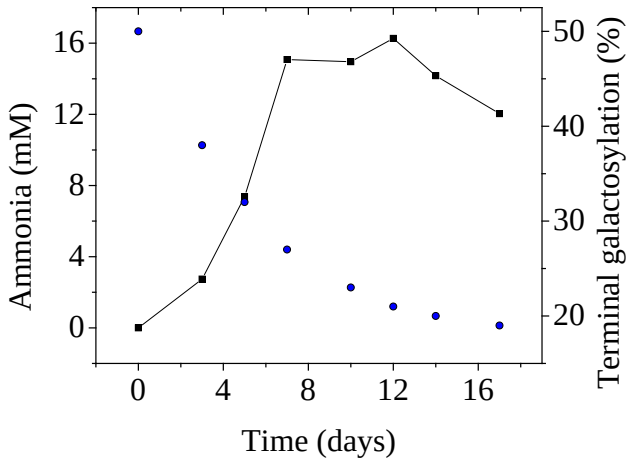

Figure 7 Time-dependent concentration profiles of ammonia and intracellular metabolites of CHO cells when when cultured in fed-batches and the resulting N-linked glycosylation pattern in terms of terminal galactosylation of monoclonal antibodies produced (blue dots).

part). Regarding the second type of inhibitors, the main example in this case is represented by ammonia, a basic metabolite arising from the metabolism of amines which is thought to increase the pH in the Golgi apparatus thus preventing enzymes to work in optimal conditions. Cell cultured in presence of high ammonia levels typically show an increase in high-mannose and non-galactosylated structures. Other inhibitors are sodium butyrate [37] and polyamines like spermine and spermidine [38], both negatively affecting sialylation of glycoproteins.

Process Operation Mode

The most common manufacturing modes for the production of therapeutic proteins are fed-batch and continuous cultures. Other systems, like batch cultures, hollow fiber bioreactors and biphasic bioreactors have been employed but will not be discussed due to their scarce industrial relevance. In fed-batch systems the content inside the reactor is harvested (i.e. removed) only at the end of the operation in order to purify the product. This leads both to accumulation of waste metabolites in the medium and depletion of nutrients over time, which leads to changes in the glycosylation pattern throughout the culture (Fig. 7). The change in glycosylation is manifold and includes different intracellular levels of nucleotide sugars [39], increasing ammonia concentrations and possible changes in gene expression of

important glycosylation enzymes [40]. These issues can be easily solved by the use of perfusion systems, where the nutrient consumption is compensated by the continuous addition of fresh medium while the waste byproducts are continuously washed out by means of cell retention devices. This allows for lower ammonia levels resulting in an overall increase of terminal galactosylation and sialylation compared to fed-batch conditions. Moreover, continuous systems allow a better control of process conditions since the level of every substance can be kept to a specific set point, and resulting in a constant product quality. This topic will be further discussed in the experimental section.

1.8 Modelling N-linked Glycosylation

In order to promote a continuous improvement in the production of biopharmaceuticals regulatory agencies like FDA are encouraging companies to implement the quality by design (QbD) paradigm for the design and development of new products. One of the main points of the Q10 directive states that ‘’Quality by design means designing and developing manufacturing processes during the product development stage to consistently ensure a predefined quality at the end of the manufacturing process’’, meaning that a thorough understanding of the product and its manufacturing process, including the identification of product’s critical quality attributes (CQAs) and how different process conditions affect CQAs, is required. N-linked glycosylation has been proved to greatly affect the therapeutic performance of recombinant glycoproteins and is therefore considered one of the main CQA for mAbs [19]. In line with the QbD scope, the development of detailed mathematical frameworks to model the N-linked glycosylation biosynthetic pathway aims to provide a fast and cheap alternative to experimental screening to achieve specific glycoform distributions via metabolic or genetic engineering. Furthermore, computational models represent useful resources for understanding the biological mechanisms underneath the glycosylation process.

Four main mechanistic models of N-linked glycosylation describing microheterogeneity have been proposed so far (Umaña and Bailey [41], Krambeck and Betenbaugh [42], Hossler et. al [43] and del Val et. al [1]). The main aim of these models was the

characterization of the glycoprotein crossing through the Golgi compartments and the maturation of its N-oligosaccharide catalysed by the work of the glycosylation enzymes.

The first model was developed by Pablo Umaña and James Bailey in 1997 [41] with the goal of predicting qualitative changes in the N-linked glycoform distribution resulting from different levels of the enzymes involved in the oligosaccharide biosynthesis. In this model the Golgi apparatus is divided into four different compartments (*cis*-, *medial*-, *trans*- Golgi and the trans-Golgi network), represented by single reactors with characteristic enzyme concentrations connected to create a system of four reactors in series, thus allowing for the spatial distribution of enzymes along the apparatus to be resembled. The model considered a restricted reaction network involving only a small subset of commonly found oligosaccharides and reaction rates were assumed to follow simplified Michaelis-Menten kinetics under saturation of co-substrates. By solving the corresponding mass balance, the authors were able to estimate the N-linked oligosaccharide distribution of a protein given a set of conditions (mainly different enzymes levels). The main limitations of this model are related to the very small reaction network and the assumption of enzyme saturation by nucleotide-sugar cofactors, which have been showed to be one of the limiting factors in the entire process [44].

The second model, developed by Krambeck and Betenbaugh [42], retained the same basic structure comprised of four reactors in series described by Umaña and Bailey. The biggest contribution was extending the model by I) considering an increased number of oligosaccharide structures such as fucosylated, galactosylated and sialylated N-glycans, and II) implementing the effect of donor substrate concentrations in the Michaelis-Menten equation. This allowed for a wider range of glycosylation patterns to be predicted.

Hossler et. al [43] used the computational approach to compare the main mechanisms hypothesized for glycoprotein transport through the Golgi, i.e. cisternal maturation and vesicular transport. The vesicular transport model postulates that Golgi cisternae are stationary compartments (i.e. fixed in space) holding different enzymes, and that proteins travel across them inside vesicles that bud off one chamber and fuse to the next one. In the cisternal maturation model cargo proteins are stationary with respect to the cisterna, which in turn undergoes a maturation process by traversing the Golgi stack and at the same time modifies its enzyme composition. From an engineering point of view, the first case is equivalent to a series of stirred tank reactors (CSTR's) where the product is continuously

transported downstream after spending a certain holding time inside one compartment, while the second one corresponds to a plug-flow reactor (PFR). By analysing the N-glycan distribution predicted by the two mathematical models (4 CSTR and 4 PFR in series respectively) the authors suggested that the mechanism of cisternal maturation was more likely to occur. This hypothesis was further confirmed by direct experiments on living yeast [45].

The most recent model, proposed by del Val et. al in 2011 [1] was based on the cisternal maturation assumption and introduced many other features such as the recycling of Golgi-resident proteins mediated by COPI vesicles [46] and different kinetic mechanisms for each enzyme catalysed reaction. The transport of NSDs into the Golgi was included to link glycosylation and cellular metabolism. The model was successfully used to reproduce the glycosylation profile of marketed antibodies, with a superior performance with respect to the previous ones.

Although these models are capable of reproducing certain glycosylation patterns, they cannot provide a link to the manufacturing condition, and most of the parameter values used are either taken from the literature or computationally estimated. Therefore, these models are not able to predict the effect of pH variations or supplementation of specific precursors.

The main idea of this work is therefore to combine the continuous cultivation system and mathematical modelling to I) generate data in controlled conditions, II) modulate the glycosylation under the Design of Experiments (DoE) methodology, and III) predict the behaviour of the system with the aid of computational tools.

Design of Experiments is a systematic approach used to maximize the amount of information obtained from experimental data with the goal of determining the relationships between the inputs and the output of a specific process. The methodology was implemented in this work to generate different glycosylation patterns as follows:

1) CHO cells were cultured in continuous bioreactors to generate different steady-states. On average, three different steady states were performed on a single bioreactor run by maintaining the cells for 7-10 days under the same process conditions.
2) Each steady state corresponds to a point of the DoE.

3) Steady states differ between them only for the concentration of manganese, galactose and ammonia inside the bioreactor.
4) While manganese and galactose were provided by the culture medium, ammonia was regulated by changing the VCD inside the bioreactor.
5) A two-level full factorial DoE was developed where each parameter was changed between a high and a low level for all the possible permutations, thus generating a cube as depicted in Fig. 8. Additionally, a central point experiment was carried out with all process parameters assuming an intermediate value.
6) The edge points of the cube were used to calibrate the model (parametric optimization), while the middle point was exploited to test its predictive capability.

In order to compare the mechanistic approach with statistics a simple response surface methodology (RSM) was performed on parallel with the mathematical model. A schematic representation of the DoE and the experimental strategy implemented is presented in Fig. 8.

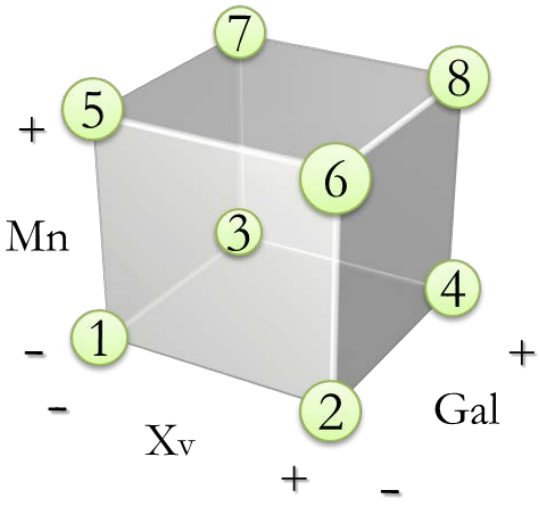

DoE Point	Mn µM	Xv 1e6cells/mL	Gal mM
1	0.01	20	0
2	0.01	60	0
3	0.01	20	10
4	0.01	60	10
5	1	20	0
6	1	60	0
7	1	20	10
8	1	60	10
Middle	0.1	40	5

Figure 8 Representation of the DoE and values used for the experiments (table on the left).

Chapter 2: Materials and Methods

2.1 Cell Culture

Cell Line

A single transfected Chinese hamster ovary cell line secreting a recombinant humanized monoclonal antibody (IgG1 isotype) was used for the experiments described in this work. The cell line is adapted for suspension cultures and was kindly provided by an industrial partner.

Culture Medium

A proprietary serum-free medium was used for all the cultures. A total of three different medium compositions were used to optimize different culture stages, namely expansion, production and production at high cell densities. Under $30 \cdot 10^6$ cells/ml cells were cultured in a so-called ‘’base’’ production medium, mixed with a concentrated ‘’feed’’ at different fractions for higher viable cell densities (VCDs). The feed was enriched in D-Glucose (Acros organics, Geel, Belgium), L-Cysteine (Merck, Germany), L-Tyrosine (Sigma Aldrich, Switzerland) and L-Asparagine (PanReac AppliChem, Germany) to account for the increased consumption of nutrients and avoid limitations in these components. N-glycosylation was modulated through the addition of D-Galactose (Acros organics, Geel, Belgium) and Manganese (II) Chloride (Sigma Aldrich, Switzerland).

Expansion and Inoculation

Cells stored in liquid nitrogen were initially thawed in a water bath at 37 °C and centrifuged (300 rpm, 3 min) to remove the DMSO-containing supernatant. Fresh expansion medium was added to achieve a VCD of $0.3 \cdot 10^6$ cells/ml and the suspension transferred to a 50 mL spin tube (TPP, Switzerland). Cells were then incubated for three days at 36.5 °C, 90% humidity and 5% pCO_2. After this period, cells were diluted with new expansion medium every two days to lower the final cell density to $0.3 \cdot 10^6$ cells/ml. Once the culture volume reached 100 mL, cells were transferred to roller bottles. Cells were first inoculated in a perfusion seed bioreactor and, upon reaching high cell densities (up to $40 \cdot 10^6$ cells/ml), transferred to the bioreactors used for the described experiments. This strategy, already reported in literature for fed-batch systems [47], allows the elimination of the growth phase and reduces the time needed to reach steady state. By sterile transferring an aliquot from the seed bioreactor directly to other systems, VCD at time zero in production bioreactor was set as $20 \cdot 10^6$ cells/ml.

2.2 Reactor Design

Continuous cultures were carried out in two perfused bioreactor setups differing only for the type of external loop and retention device (Alternating Tangential Flow, ATF, and Tangential Flow Filtration, TFF). In both systems, the cell suspension flows through a hollow fiber that allows the permeation (or filtration) of molecules whose dimension is smaller compared to the pore size of the material itself, while retaining cells in the bioreactor. The hollow fibers used (MiniKros® Filter Modules, SpectrumLabs.com, USA) are made in Polyethersulfone (276) and were designed to have 1570 cm^2 surface area, 1mm fiber diameter and 0.5 µm pore size. In the TFF setup the flow inside the hollow fiber is regulated by the action of a centrifugal pump and is therefore unidirectional, while in the ATF the liquid is pumped through the action of a diaphragm, creating an alternating flow which has been reported to reduce the fouling inside the fiber [48]. The two systems will be proved to be equivalent in terms of N-glycosylation in the results and discussions section. Bioreactor design is based on a DASGIP parallel bioreactor system (DASGIP

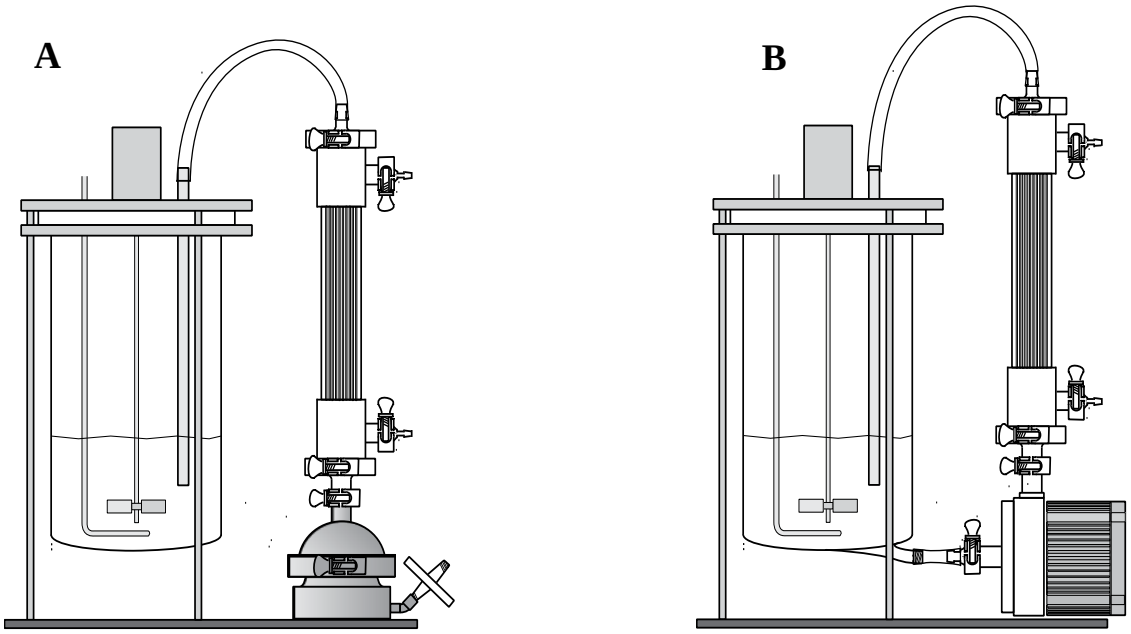

Figure 9 Bioreactor setups used for the cultivations. ATF (A) and TFF (B) systems differ only for the external loop configuration.

Technology, Eppendorf, Switzerland) and is shown in Fig. 9 with a comparison of the two external loops.

2.3 Reactor Operation

The VCD in production bioreactors during the inoculation was set to $20 \cdot 10^6$ cells/ml. In order to achieve the steady state condition required for the mathematical model, accumulation of cells inside of the reactor due to cell divisions was prevented by removal of liquid (‘’bleeding’’). For reactors equipped with the biomass sensor this operation was performed automatically by the control unit by switching on an external pump each time the measured VCD exceeded the desired set point. In all the other cases the bleeding was performed manually by I) offline measuring of VCD, II) calculating the bleeding volume according to Eq. 1, III) removal of liquid with the use of a pump connected to the bleed line.

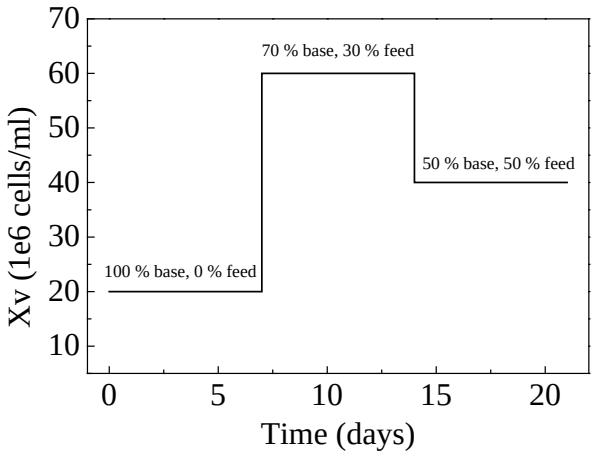

Figure 10 VCD profile and medium composition used for the bioreactor runs.

$$V_{bleed} = \frac{VCD - VCD_{setpoint}}{VCD} RV \quad (1)$$

Cultures were carried out to reproduce the ideal VCD profile presented in Fig. 10. Cells were kept at $20 \cdot 10^6$ cells/ml for at least one week to ensure steady state and cultured under base production medium. VCD was then set to $60 \cdot 10^6$ cells/ml while the medium composition was switched to 70% concentrated feed and 30% base medium. Finally, cells were bled to $40 \cdot 10^6$ cells/ml and cultured under 50% concentrated feed and 50% base medium. During the transition between the steady state, the feed fraction was gradually changed to the optimal composition over 1-2 days. Manganese chloride and galactose were added to the base or feed fraction to reach the desired concentrations in the culture medium.

2.4 Reactor and Process Control

Process parameters such as viable cell density, glucose and lactate concentrations, bioreactor pH, dissolved oxygen (DO) and CO_2 pressure (pCO_2) were monitored daily by means of both online and offline measurements.

Online Process Control

Both bioreactor setups were equipped with online pH-sensors (05-DPAS-SC-K8S pH Probe, Mettler Toledo, Switzerland), DO-sensors (InPro® 6820, Mettler Toledo, Switzerland), CO_2-sensors (Autoclavable CO2 sensor, PreSens Sensing GmbH, Germany) and temperature sensors. Harvest rate from all the bioreactors was fixed to 1 Reactor Volume (RV) per day while the bleed rate was defined to maintain VCD to the desired set point. To keep the culture volume constant to 1.5 L, perfusion rate was automatically adjusted by the process control unit to compensate the reduction of the volume inside the reactor. Temperature was set to 36.5 °C throughout the culture and DO was maintained to 50% of air saturation by applying a gas flow rate of 20 L/h controlling the inlet fractional composition of O_2, air and N_2. The pH was fixed to 7.10 and deviations were controlled through pulsed sparging of CO_2. Stirring speed was set to 250 rpm and sparging was performed with an open pipe sparger (1mm hole size). During the last runs, bioreactors were equipped with an online biomass sensor (Aber, UK) which allowed the automation of the bleeding process.

Viable Cell Density (Offline)

Cell number and viability were estimated every 24h according to the trypan blue exclusion method using a CedeX cell counter (Innovatis, Germany). To ensure a more accurate cell counting cells were suspended in a Trypsin – EDTA solution (10x) from Sigma Aldrich (Switzerland) and incubated at 37 ˚C for 3 min. This allowed a re-dispersion of formed aggregates to simplify the visual recognition performed by the program.

Glucose/Lactate (Offline)

Glucose and lactate levels in cell cultures were measured enzymatically using a Hitado Super GL compact instrument (Hitado, Germany). The instrument is fully automated and exploits an electrochemical sensor to measure the metabolites oxidation catalyzed by glucose oxidase (GOD) and lactate oxidase (LOD).

pH Measurements (Offline)

Throughout the cultures the pH inside the reactor was monitored by the online probe described in the online process control section and automatically adjusted to 7.1. The online probe was calibrated on a daily basis by offline measurements performed by an independent FiveEasy Plus Mettler Toledo pH probe (Mettler Toledo, Switzerland).

2.5 Sampling Protocols

For future analysis of ammonia, titer, amino acids, metabolites and glycosylation profiles, the reactor was sampled on a daily basis. Except for the metabolite extraction, samples were prepared by withdrawing 20 mL of reactor liquid with the use a sterile syringe, centrifuging at 300g for 5 min and filtering the supernatant into Eppendorf tubes (approximately 1 mL each). Samples were put in a -20 ˚C fridge for long term storage.

Metabolites Extraction

A suspension containing $5 \cdot 10^6$ cells was sampled from the reactor and centrifuged at 1000 g for 1 min (4 ˚C) in a 1.5 ml Eppendorf tube. The supernatant was collected in a separate vial and stored at -80 ˚C. The cell pellet was resuspended in 1 ml 10 mM ammonium acetate buffer (pH 7.2) and centrifuged at 1000 g for 1 minute. After the supernatant was discarded the cell pellet was destroyed by vortexing the Eppendorf tube at maximum speed for 1 min. 12 µl of internal standard solution (0.5 mM $^{13}C^{15}N$ ATP, 0.5 mM D4-Alanine), 400 µl of MTBE (100 µM DSPC), 150 µl of methanol and 150 µl of water were added in this order. After vortexing for 30 seconds, the suspension was centrifuged at 10000 g for 2.5 min (4 ˚C). Different phases were collected into separate vials by pipetting and the samples stored at -80 ˚C before analysis.

2.6 Analytics

Amino Acids

Amino acids were determined by reversed-phase chromatography using a C18 analytical column (Agilent Zorbax Eclipse Plus). Pre-column OPA/FMOC derivatization was used while the separation was carried out by applying a gradient of mobile phase A (10 mM Na_2HPO_4 : 10 mM $Na_2B_4O_7$) and mobile phase B (acetonitrile : methanol : water 45 : 45 : 10, v : v : v) from 2 to 57 % of buffer B over 20 minutes. Concentrations of amino acids were obtained by interpolating from a standard curve. Prior to analysis each sample was filtered using Vivaspin 500 (5000 Da) centrifugation filters (Sartorius Stedim Biotech, Germany) at 4000 g for 20 min (4 ˚C).

Nucleotides Nucleotide Sugar Donors / MALDI-TOF

The concentration of intracellular metabolites was determined both by mass-spectroscopic (MALDI-TOF) and chromatographic analysis. MALDI-TOF was performed on a commercial instrument (AB Sciex 5800) according to Steinhoff et al. [49] with the ND:YAG laser operating in reflectron negative mode. Briefly, small aliquots of analytes (4 µL droplets) were deposited upon an indium-tin-oxide microarray (Sigma Aldrich, Switzerland) and crystallized using 10 mg/mL 9-Aminoacridine (Fluka-Chemie AG, Germany) in 90 % ethanol. Measured masses were normalized with respect to the internal standard ($^{13}C^{15}N$ ATP).

Nucleotide Sugar Donors / HPAEC

Intracellular metabolites were also determined by high-pressure anion exchange chromatography (HPAEC) using an Agilent 1200 HPLC system (Agilent Technologies, USA) equipped with a CarboPac PA-1 column and a PA-1 guard column (Dionex, Sunnyvale, CA). The method has been adapted from *Tomiya et al.* [50] using 1mM sodium hydroxide (E1) and 1M sodium acetate trihydrate in 1mM sodium hydroxide (E2) as

eluents. The flow rates of all eluents were set to 1mL/min and the column thermostat was set to 25°C. Elution was performed by the following gradients: T0 = 20% (v/v) E2; T10 = 55% (v/v) E2; T25 = 55% (v/v) E2; T35 = 80% (v/v) E2; T40 = 90% (v/v) E2; T50 = 100% (v/v) E2. Nucleotides and sugar nucleotides were detected by UV absorbance at 260 nm. The target components were calibrated by serially diluting stock mixtures in deionized water including ATP, AMP, ADP, CTP, CDP, CMP, GTP, GDP, GMP, UTP, UDP, UMP, CMP-Neu5Ac, UDP-GalNAc, UDP-GlcNAc, UDP-Gal, UDP-Glc, GDP-Fuc and GDP-Man. All of the above chemicals were purchased from Sigma-Aldrich.

Titer

Titer (i.e. total antibody concentration) analysis was performed on an Agilent 1200 HPLC system (Agilent Technologies, USA) using a Protein A affinity column model 2-1001-00 (Applied Biosystems, USA). 10 mM NaH_2PO_4, 150 mM NaCl (pH 7.5), 10 mM HCl, 150 mM NaCl (pH 2.0) and 20% Acetic Acid were used as loading (A), elution (B) and cleaning (C) buffer respectively according to the following method: T_0 = 100% A; $T_{1.50}$ = 100% B; T_4 = 100% C; $T_{4.70}$ = 100% A. Antibodies were detected by reading the absorbance at 280 nm and the corresponding concentration was calculated according to the following equation:

$$c_{Titer} = \frac{A_{Peak} \cdot F}{Inj.Vol \cdot K} \tag{2}$$

Where K is a specific calibration factor, A_{Peak} the measured peak area, F the flow rate through the column (set to 1 ml/min) and the injection volume is 5 µL.

Ammonia

Ammonia concentrations were evaluated using the Ammonia (Rapid) Assay kit (Megazyme, Ireland) on a 96 well plate (TPP, Switzerland). Briefly, 10 µL of sample solution was pipetted into wells, followed by the addition of 200 µL of Millipore water, 30

µL of supplied Buffer 1 (pH 8.0), 20 µL of supplied concentrated NADPH solution and 2 µL of glutamate dehydrogenase (GIDH) solution. Absorbances were read using an EnSpire 2300 Multilabel Reader (Perkin Elmer, USA) before and after enzyme addition and ammonia concentrations were obtained by interpolating from a standard curve. Samples corresponding to steady state with high viable cell densities were diluted with Millipore water (1:3 for $60 \cdot 10^6$ cells/mL and 1:2 for $40 \cdot 10^6$ cells/mL) to get an estimated level of ammonia below 0.4 g/L as suggested by the manufacturer.

2.7 N-linked Glycosylation Analysis

The analysis of the glycosylation profiles was performed on three different stages. First, the oligosaccharides were enzymatically detached from the antibodies, purified from the rest of the mixture and fluorescently labeled. Secondly, chromatographic separation was carried out to determine the relative quantity of each N-glycan. Single peaks were finally resolved by means of Time-Of-Flight Mass-Spectroscopy (MALDI-TOF). A more detailed version of the single procedures is provided below.

N-linked Glycans Purification

For the analysis of the glycosylation pattern mAbs were first purified from the supernatant using Vivapure miniprepA purification kit (Sartorius Stedim Biotech, Germany) according to the manufacturer's protocol. N-linked glycans were enzymatically detached from the peptide backbones by incubating for 14 h at 37 ˚C in presence of 2 µl concentrated PNGase F (New England Biolabs, USA). Before treating with the enzyme, purified mAbs were incubated in the supplied denaturation buffer (SDS) at 37 ˚C for 10 min.

Released N-glycans were isolated using Superclean ENVI-Carb column tubes (Sigma Aldrich, Switzerland) by loading the samples in 2% acetonitrile / 0.1 M ammonium acetate solution and eluting with 50% v/v acetonitrile in H_2O. Eluted fractions were collected and dried overnight under vacuum in a Vacufuge® plus (Eppendorf, Germany).

In order to be fluorescently labeled, solvent-free N-linked oligosaccharides were dissolved in 20 µl of 70% DMSO 30% acetic acid, 1 M sodium cyanoborohydride solution

containing 0.35 M 2-Anathralamide (2-AA) (Sigma Aldrich, Switzerland) according to Bigge *et al.* [51] and incubated in the same solution at 65 ˚C for 2 h. Hereafter, the mixture was cooled to room temperature and diluted with 380 µL acetonitrile.

To remove the excess of unreacted dye, all samples were loaded to 3 Whatman 3MM filter paper disks placed on Ultrafree® MC (0.5 mL) centrifugal filter units (PTFE membrane, 0.45 µm pore size) (Millipore, USA) as described by Merry *et al.* [52]. The system was washed 3 times with 95% acetonitrile and oligosaccharides were eluted 3 times using 50 µl of Millipore water (Millipore, USA). After drying, samples were dissolved in 30 µl Millipore water and 70 µl acetonitrile.

HILIC Analysis

Different N-glycan structures were separated by hydrophilic interaction chromatography (HILIC) using a GlycoSep N-Plus column (4.6 mm x 150 mm, Prozyme, USA) equipped on an Agilent 1200 HPLC system (Agilent Technologies, USA). The analysis was carried out at 30 ˚C using 10 mM formic acid, 80% w/w acetonitrile (pH 4.4) and 30 mM formic acid, 40% acetonitrile (pH 4.4) as mobile phase A and B respectively. The gradient started from 70% and was reduced to 35% mobile phase A over 90 min at 0.6 ml/min. After the gradient, the column was washed for 10 min with 0.5 % formic acid and re-equilibrated at 30% mobile phase B before next analysis. For each sample the injection volume was set to 90 µl. Fluorescence-labeled N-glycans were detected with an excitation wavelength of 250 nm and an emission wavelength of 410 nm. Fractions containing separated oligosaccharides were collected every minute using a FC 203B (Gilson, Switzerland) fraction collector. Each sample was completely dried in a Vacufuge® plus (Eppendorf, Germany), resuspended in 10 µL of Millipore water and stored at -20 °C prior to mass spectroscopy analysis.

MALDI-TOF

MS analysis was performed at the Functional Genomic Center Zurich using a 4800 Plus MALDI TOF/TOF system (AB SCIEX, USA) equipped with a 200 Hz Nd:YAG laser as

described previously [27]. Briefly, samples containing 2-AA labeled oligosaccharides were first desalted using ZipTip µ-C18 pipette tips (Millipore, USA) equilibrated with Milli-Q water (Millipore, USA), and spotted onto a 384 Opti-TOF MALDI target plate together with 0.9 µL of 2,5-dihydroxybenzoic acid (DHB) (10 g/L) in 70% Acetonitrile. The instrument was operated in both reflectron positive and negative ion mode and masses were analyzed in a range from 750 to 400 m/z. Mass peaks were detected by comparison with the GlycoWorkBench2 database [53].

Chapter 3: Mathematical Model

3.1 Model Overview

The mathematical model has been developed with the aim to predict changes in the N-glycosylation pattern of humanized monoclonal antibodies in response to different media composition and process conditions. The model can be formally divided in two different parts, a first one used to describe briefly the cell culture kinetics in terms VCD and metabolism, and the second one focused on the glycosylation reactions taking place inside the Golgi apparatus. Under the hypothesis that the glycan processing within the ER is fully completed, every Fc region entering the *cis*-Golgi is represented by a high mannose structure (M9) that under the action of different glycosidases and glycotransferases will be converted to a series of different mature forms. The N-glycans pattern that the model aims to characterize is the one typical of humanized mAbs, i.e. core-fucosylated biantennary structures terminating with galactose, N-acetylglucosamine and sialic acid. The reaction scheme used to described these structures is composed by 33 N-glycans connected through a network of 43 reactions and is shown in Fig. 11.

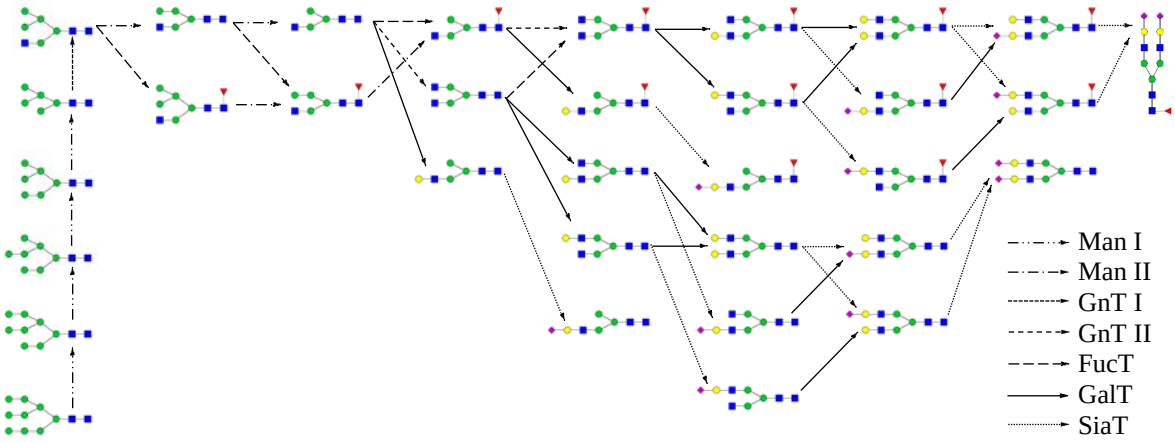

Figure 11 Fc region N-linked glycosylation network implemented in the model.

3.2 Cell Culture Dynamics

A description of the cell culture dynamics was included to provide a first link between process conditions (average viable cell density, perfusion rate, medium composition) and cellular metabolism. Under conventional assumptions of perfect mixing, the mass balance for viable cells (X_v) is:

$$\frac{\mathrm{d}(VX_{\mathrm{v}})}{\mathrm{d}t} = \mu VX_{\mathrm{v}} - \mu_{\mathrm{d}} VX_{\mathrm{v}} - Q_{\mathrm{bleed}} X_{\mathrm{v}} \tag{3}$$

Where V is the bioreactor volume, Q_{bleed} the volumetric cell bleed, and μ the specific growth rate, defined as a function of extracellular ammonia (AMM) through the following equation:

$$\mu = \mu_{max}\left(\frac{K_{AMM}^{\mu}}{K_{AMM}^{\mu} + [AMM]}\right) \tag{4}$$

K_{AMM}^{μ} is a saturation constant for the ammonia dependency of the growth rate. The specific antibody production was defined as:

$$\frac{dV[mAb]}{dt} = q_{\mathrm{mAb}} VX_{\mathrm{v}} - (Q_{\mathrm{bleed}} + Q_{\mathrm{harvest}})[mAb] \tag{5}$$

At steady state the specific productivity q_{mAb} (mol·cell^{-1}·day^{-1}) can be obtained as a function of X_v and the flow rates out of the reactor:

$$q_{\mathrm{mAb}} = \frac{(Q_{\mathrm{bleed}} + Q_{\mathrm{harvest}})[mAb]}{VX_{\mathrm{v}}} \tag{6}$$

Ammonia production was calculated as a function of X_v and asparagine in the feed medium as follows:

$$\frac{dV\left[AMM\right]}{dt} = q_{AMM} V X_v + K_{d,ASN}\left[ASN_{feed}\right] - \left(Q_{harvest} + Q_{bleed}\right)\left[AMM\right] \tag{7}$$

With q_{AMM} and $K_{d,ASN}$ representing the specific productivity of ammonia due to cellular metabolism and dissociation constant of asparagine, respectively.

3.3 Mechanistic Model of N-linked Glycosylation

Many of the equations and assumptions present in the second part of the model are based on the cisternal maturation assumption with recycling of Golgi resident proteins proposed by Del Val et al. [1]. In this context, the Golgi apparatus was modelled as a single plug flow reactor (PFR) with constant flow linear velocity and diameter. Neglecting axial dispersion, the mass balances for the species involved in the glycosylation process can be computed as follows.

N-glycan (oligosaccharides) balance:

$$\frac{\partial OS_i}{\partial t} = -\frac{4q}{\pi D^2}\frac{\partial OS_i}{\partial z} + \sum_{j=1}^{N.R.} \nu_{i,j} r_j \tag{8}$$

Nucleotide sugars balance inside the Golgi apparatus:

$$\frac{\partial NS_k^{\text{golgi}}}{\partial t} = F_{T,k} - \frac{4q}{\pi D^2}\frac{\partial NS_k^{\text{golgi}}}{\partial z} + \sum_{j=1}^{N.R.} \nu_{k,j} r_j \tag{9}$$

Nucleotides balance:

$$\frac{\partial N_k^{\text{golgi}}}{\partial t} = -F_{T,k} - \frac{4q}{\pi D^2}\frac{\partial N_k^{\text{golgi}}}{\partial z} + \sum_{j=1}^{N.R.} \nu_{k,j} r_j \tag{10}$$

Where *OS* indicates the glycan attached to the Fc region of a mAb and $\sum v_{k,j} r_j$ the reaction term of a given species, (*N*). $F_{T,k}$ is the rate of transport of nucleotides and nucleotide sugars described in the transport kinetics section.

Golgi structural parameters are derived from the work of del Val et al. [1], and are reported in Table 1.

Table 2 Golgi structural parameters value and description

Parameter	Value	Description
A_g	99 μm^2	Surface area of the Golgi compartments
V_g	25 μm^3	Volume of the Golgi apparatus
D	7.82 μm	Golgi internal diameter
q	1.12 μm^{3}min^{-1}	Volumetric flow rate through the Golgi

For the N-glycan balance, the initial conditions for the system of differential equations (i.e. the total glycoprotein concentration entering the Golgi at z = 0), were calculated as:

$$OS_{z=0} = \frac{q_{mAb}}{Q_{Golgi}} \tag{11}$$

The initial concentration of NSDs and nucleotides was assumed to be equal to the intracellular concentration (i.e. once being formed, the vesicle containing the glycoprotein encapsulates intracellular components as well at the same concentration as in the surrounding fluid). Due to the high activity of nucleoside diphosphatases in the Golgi, UDP, GDP and CDP were assumed to be instantaneously converted to the corresponding nucleotide monophosphates.

Golgi resident proteins distribution

Every reaction considered in the model is catalysed by Golgi-resident enzymes which are known to be compartmentalized [54] and recycled to preceding stacks by means of COPI vesicles [55]. To resemble this mechanism the concentration of Golgi enzymes (*E*) and transport proteins (*TP*) are assumed to follow three–parameter normal distributions:

$$E_j(z) = E_j^{\max} \exp\left[-\frac{1}{2}\left(\frac{z - z_j^{\max}}{\omega_j}\right)^2\right] \tag{12}$$

$$TP_k(z) = TP_k^{\max} \exp\left[-\frac{1}{2}\left(\frac{z - z_k^{\max}}{\omega_k}\right)^2\right] \tag{13}$$

Where $E_{j,max}$ and $TP_{k,max}$ represent peak concentration, $z_j^{\max}$ $z_{j,max}$ and $z_k^{\max}$ peak position, $\omega_{z,j}$ and $\omega_{z,k}$ distribution width respectively. Values implemented in the model are taken from the previous optimization performed by del Val et. al [1], with the peak concentration of all the enzymes divided by a factor 2 to take into account the lower specific productivity of the CHO cells used in this work. The list of parameters used is reported in Table 2, while Fig 12 includes a graphic representation of the enzyme and transport protein localization across the Golgi compartments.

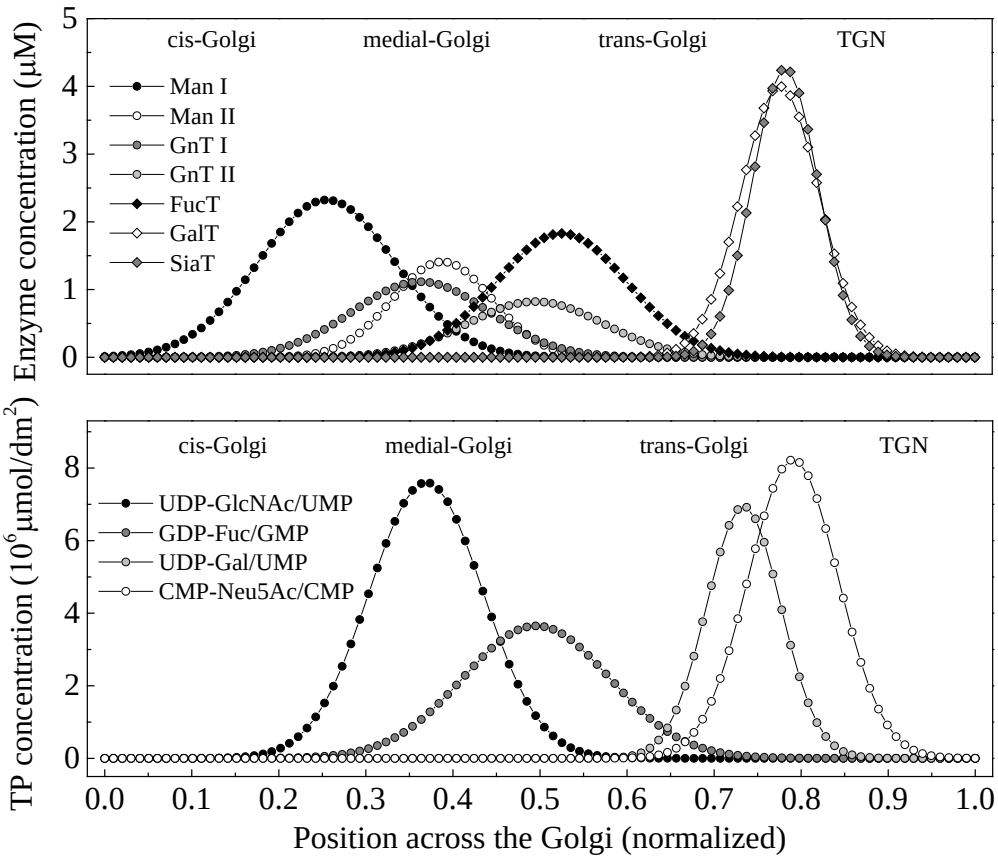

Figure 12 Graphical representations of the calculated enzymes and transport protein distribution in the Golgi apparatus.

Table 3 Enzyme and transport proteins distribution paramters.

Enzyme	E_{max} (μM)	z_{max} (norm.)	ω_z (norm.)
ManI	1.161	0.255	0.0785
ManII	0.705	0.388	0.0575
GnTI	0.557	0.363	0.0783
GnTII	0.411	0.495	0.0781
FucT	0.914	0.525	0.0753
GalT	2.000	0.776	0.0450
SiaT	2.132	0.782	0.0379
Transport protein	TP_{max} (μmol/dm^2)	z_{max} (norm.)	ω_z (norm.)
UDP-GLCNAc/UMP	$7.60 \cdot 10^{-6}$	0.369	0.0651
GDP-Fuc/GMP	$3.65 \cdot 10^{-6}$	0.496	0.0843
UDP-Gal/UMP	$6.94 \cdot 10^{-6}$	0.734	0.0426
CMP-Neu5Ac/CMP	$8.23 \cdot 10^{-6}$	0.791	0.0516

Enzyme Kinetics

Three different kinetic mechanisms have been used according to literature reports: Michaelis Menten kinetics (Eq. 14), Sequential-order Bi-Bi kinetics (Eq. 15), and Random order Bi-Bi kinetics (Eq. 16). Every reaction mechanism includes competitive and product inhibiting reactions as derived by [1].

Michaelis-Menten kinetics (*Man I* [56], *Man II* [57])

$$r_j = \frac{k_{f,j} \cdot \left[E_j\right] \cdot \left[OS_i\right]}{K_{d,i} \cdot \left(1 + \frac{\left[OS_i\right]}{K_{d,i}} + \sum_{z=1}^{NC} \frac{\left[OS_z\right]}{K_{d,z}} + \frac{\left[OS_{i-1}\right]}{K_{d,i-1}}\right)} \tag{14}$$

Sequential-order Bi-Bi kinetics (*GnTI* [58], *GnTII* [59], *GalT* [35])

$$r_j = \frac{k_{f,j} \cdot \left[NS_k^{\text{golgi}}\right] \cdot \left[OS_i\right] \cdot \left[E_j\right]}{K_{d,k} \cdot K_{d,i} \cdot \left(\frac{\left[NS_k^{\text{golgi}}\right]}{K_{d,k}} + \frac{\left[NS_k^{\text{golgi}}\right]}{K_{d,k}} \cdot \frac{\left[OS_i\right]}{K_{d,i}} + \frac{\left[NS_k^{\text{golgi}}\right]}{K_{d,k}} \cdot \sum_{z=1}^{NC} \frac{\left[OS_z\right]}{K_{d,z}} + \frac{\left[N_k^{\text{golgi}}\right]}{K_{d,Nk}} \cdot \frac{\left[OS_{i+1}\right]}{K_{d,i+1}} + \frac{\left[N_k^{\text{golgi}}\right]}{K_{d,Nk}}\right)} \tag{15}$$

Random-order Bi-Bi kinetics (*FucT* [60], *SiaT* [61])

$$r_j = \frac{k_{f,j} \cdot \left[NS_k^{\text{golgi}}\right] \cdot \left[OS_i\right] \cdot \left[E_j\right]}{K_{d,k} \cdot K_{d,i} \cdot \left(1 + \frac{\left[NS_k^{\text{golgi}}\right]}{K_{d,k}} + \frac{\left[OS_i\right]}{K_{d,i}} + \sum_{z=1}^{NC} \frac{\left[OS_z\right]}{K_{d,z}} + \frac{\left[NS_k^{\text{golgi}}\right]}{K_{d,k}} \cdot \frac{\left[OS_i\right]}{K_{d,i}} + \frac{\left[NS_k^{\text{golgi}}\right]}{K_{d,k}} \cdot \sum_{z=1}^{NC} \frac{\left[OS_z\right]}{K_{d,z}} + \frac{\left[N_k^{\text{golgi}}\right]}{K_{d,Nk}} \cdot \frac{\left[OS_{i+1}\right]}{K_{d,i+1}} + \frac{\left[N_k^{\text{golgi}}\right]}{K_{d,Nk}} + \frac{\left[OS_{i+1}\right]}{K_{d,i+1}}\right)} \tag{16}$$

In the notation used, $K_{d,I}$, $K_{d,\ i+1,\ z}$ and $K_{d,k}$ symbolize the dissociation constant for the enzyme-oligosaccharide and the enzyme-nucleotide sugar complexes, respectively. Subscripts *i* was used for the N-glycan being modified and *z* to indicate competitive inhibitors. N_k symbolizes the nucleotide byproduct while OS_{i+1} (or OS_{i-i}) represents the glycan product. In the case of byproducts the dissociation constant of the nucleotide-enzyme complex $K_{d,Nk}$ was assumed to be 10 times the corresponding $K_{d,k.}$ The catalytic step was assumed to be irreversible and was represented by the turnover rate $k_{f,j}$, estimated from the maximum velocity rate and the molecular weights of the enzymes reported in

literature. The complete list of values implemented for the enzyme turnover rates and dissociation constants is provided in table 4 and 5. Parameters indicated with * where computationally estimated.

Table 4 Enzyme kinetic parameters

Enzyme	k_f (min^{-1})	Source
ManI	888	Human, purified[62]
ManII	1924	Rat liver, purified[63]
GnTI	1022	Rabbit liver, purified[34]
GnTII	1406	Rat liver, purified[59]
FucT	291	Porcine brain, purified[64]
GalT	872	Rat liver, purified[65]
SiaT	491	Rat, purified[66]

Table 5 Dissociation constants for Golgi resident enzymes

Enzyme	Substrate	K_d (µM)	K_k (µM)	Source
Man I	M9	60.5	-	Estimated[56]
	M8	110.0	-	Human, purified[62]
	M7	30.8	-	Estimated[56]
	M6	74.1	-	Estimated[56]
Man II	M5	200	-	Human adenocarcinoma, purified[67]
	M4	100	-	Estimated[68]
GnTI	M5	260	170	CHO, purified[69]
GnTII	CoreGlcNAc1	*	960	Rat liver, purified[59]
FucT	Non-fucosylated glycoprotein	*	46	Porcine brain, purified[64]
GalT	FA2G0	*	65	Rat liver, purified[70]
	FA2G1	*		
SiaT	Asialo glycoprotein	*	50	Rat, cloned[71]

Together with the transport of NSDs, enzyme kinetics provides a link between the process conditions and the resulting glycosylation pattern. Modifications of the previous equations to take into account the effect of ammonia production and manganese supplementation is hereby described.

Effect of Ammonia in the Kinetic Mechanism

Ammonia is a toxic waste product resulting mainly from the metabolism of glutamine and asparagine whose accumulation during cell cultures is known to affect cell growth as well as increasing intracellular pH [72]. In terms of N-linked glycosylation, high levels of ammonia have been correlated to a decrease in terminal galactosylation and sialylation as stated in the introductory chapter. Various mechanisms have been proposed in attempt to explain this effect, including changes in gene expressions, redistribution of enzymes, disturbances in the balance of NSDs and basification of the Golgi apparatus. The latter has been assumed to be the prevailing effect, since ammonia molecules can readily diffuse through lipid membranes due to their hydrophobicity and small hydration radius, thus neutralizing the pH in the Golgi environment, which is normally slightly acidic. To mathematically reproduce this effect the turnover rate ($k_{f,j}$) for all the glycostransferases has been assumed to vary with the Golgi pH (pH^{golgi}) according to:

$$k_{f,j} = k_{fmax,j} \cdot e^{-\frac{1}{2}\left(\frac{pH_{opt}^{\text{golgi}} - pH^{\text{golgi}}}{\omega_{f,j}}\right)^2} \tag{17}$$

In order to resemble the turnover rate's pH-dependency the $k_{f,j}$ for Golgi resident enzymes was modeled as a Gaussian function centered at the optimum pH (pH_{opt}), with amplitude $k_{fmax,j}$ (Tab. 3) and width $\omega_{pH,j}$. Experimental points were first obtained from literature data using Plot Digitizer [73] and interpolated with Gaussian using pH_{opt} and $\omega_{pH,j}$ as fitting parameters. All the enzymes were assumed to have different $\omega_{pH,j}$ and a single optimal pH. Interestingly, the best pH value fitting the entire set of data was found to be 6.59, which is very close to other literature measurements of 6.58 [74]. Nevertheless, other authors reported the existence of a pH gradient in the Golgi, with the terminal regions of the secretory pathways being more acidic [75]. This type of behaviour was not implemented since all the enzymes considered were found to have approximately the same optimal pH. The estimated values are reported in Tab. 6 while Fig. 13 gives a graphical representation of the curves obtained. It's worth noting that the α-mannosidases (I & II) and the α-fucosyltransferase were found to be poorly affected by pH variations (large ω, Fig. 13 A, B and E), while β-galactosyltransferase and α-sialyltransferase showed narrow pH/activity

profiles, thus suffered an important loss of activity when the environment was basified by ammonia (Fig.13 F and G).

Golgi pH was assumed to be a function of the ammonia level in the culture medium through the following relation:

$$pH^{\text{golgi}} = pH_{opt}^{\text{golgi}} + log\left(\frac{\gamma_{Amm}^{\text{golgi}} + [AMM]}{\gamma_{Amm}^{\text{golgi}}}\right) \quad (18)$$

The parameter pH_{opt} indicates the pH in the Golgi in physiological conditions (estimated to be 6.59) and γ_{AMM} is a saturation constant used as sole fitting parameter to describe the effect of ammonia. Ammonia was included inside a logarithmic operator (base 10) to avoid the summation of a linear scale to a log scale (pH).

Table 6 Enzyme pH-dependent activities parameters

Enzyme activity profiles parameters		Source
pH_{opt}	6.59	Estimated
ω *Man I*	1.71	Rat liver Golgi, purified [56]
ω *Man II*	1.40	BHK, purified [76]
ω *GnT I*	1.08	Human, cloned [77]
ω *GnT II*	0.96	Rat kidney, purified [78]
ω *FucT*	2.01	Porcine brain, purified [79]
ω *GalT*	0.77	CHO cells, purified [80]
ω *SiaT*	0.60	CHO cells, purified [80]

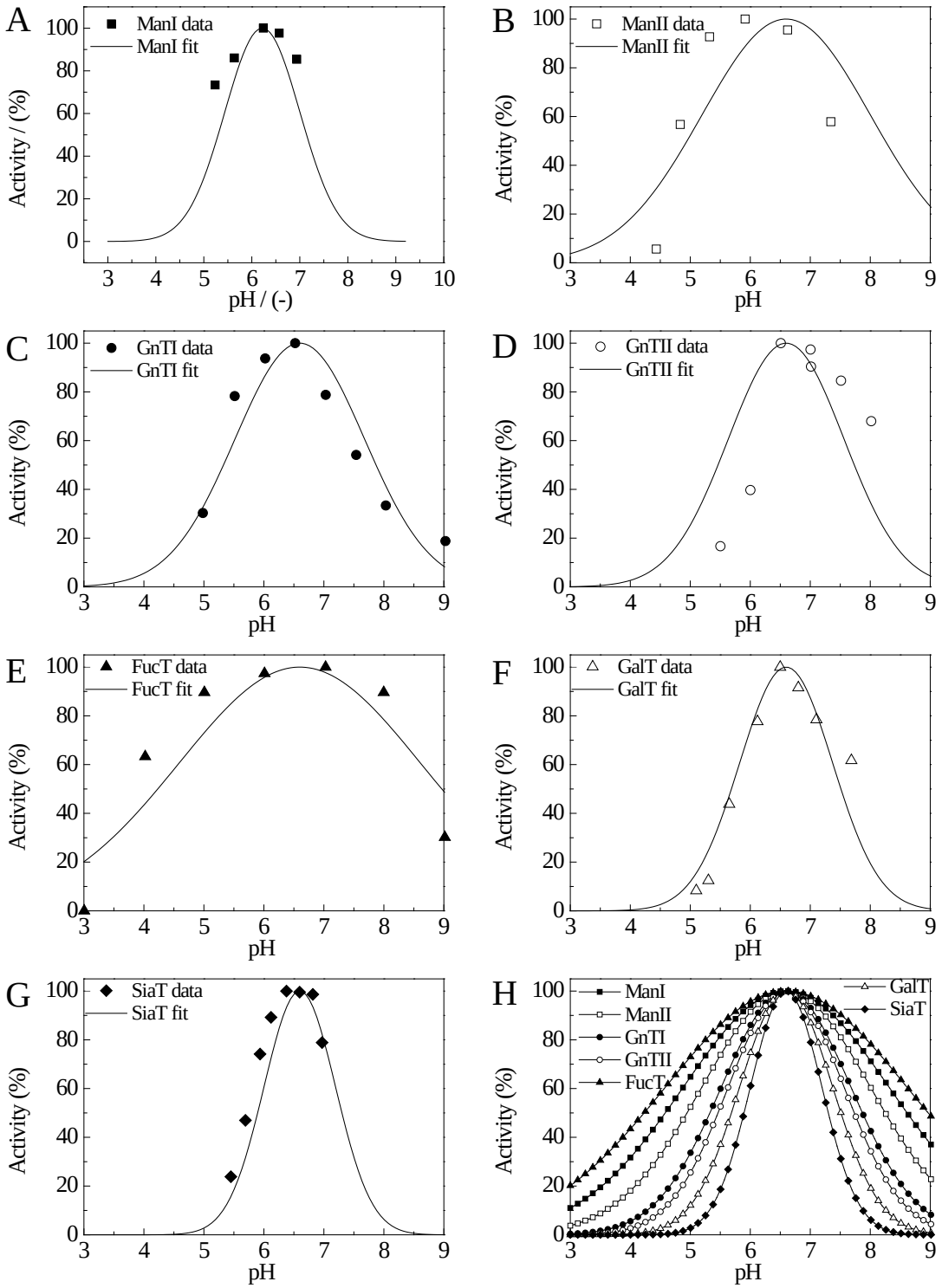

Figure 13 Graphical representation of Golgi resident enzymes activity as a function of Golgi pH.

Effect of Manganese in the Kinetic Mechanism

Supplementation of manganese salts such as $MnCl_2$ in the culture medium has been linked to increased levels of galactosylation and sialylation for recombinant glycoproteins [81]. The mechanism underneath this effect lies in the enhanced activity of many glycotransferases, including GnTI [34], GnTII [29] and GalT [35], requiring Mn in the oxidation state 2+ as cofactor. In order to represent this effect, the kinetic mechanism for the enzyme GalT (Sequential-order Bi-Bi) was modified by including the binding Mn to the enzyme as first step of the catalytic cycle. GnTI and GnTII were assumed to be independent to Mn concentration because this effect could not be detected by the data collected during this work. The result is shown in Eq. 19, whose complete derivation is reported in the S1 supplementary information. The dissociation constant introduced for the enzyme-cofactor complexes $K_{d,Mn}$ was used as fitting parameter to optimize the model.

Modified Sequential-order Bi-Bi kinetics

$$r_j = \frac{k_{f,j} \cdot \left[NS_k^{\text{golgi}}\right] \cdot [OS_i] \cdot [E_j]}{K_{d,k} \cdot K_{d,i} \cdot \left[1 + \frac{K_{d,\text{Mn}}}{[Mn]} + \frac{\left[NS_k^{\text{golgi}}\right]}{K_{d,k}} + \frac{\left[NS_k^{\text{golgi}}\right]}{K_{d,k}} \cdot \frac{[OS_i]}{K_{d,i}} + \frac{\left[NS_k^{\text{golgi}}\right]}{K_{d,k}} \cdot \sum_{z=1}^{NC} \frac{[OS_z]}{K_{d,z}} + \frac{K_{d,\text{Mn}}}{[Mn]} \cdot \frac{\left[N_k^{\text{golgi}}\right]}{K_{d,Nk}} \cdot \frac{[OS_{i+1}]}{K_{d,i+1}} + \frac{K_{d,\text{Mn}}}{[Mn]} \cdot \frac{\left[N_k^{\text{golgi}}\right]}{K_{d,Nk}}\right]} \quad (19)$$

Nucleotide Sugar Donors Transport

The NSDs are activated form of sugar synthetized by eukaryotic cells in the cytosol (UDP-GlcNAc, GDP-Fuc and UDP-Gal) or in the nucleus (CMP-Sia), which act as donors in the glycosylation reactions. Being co-substrates for many glycosyltransferases, these molecules must be first transferred to the ER/Golgi by means of highly specific transport proteins (TP) localized across the membranes of these compartments. The mechanism of action reported for all the transport proteins considered in this model is counter transport between the nucleotide sugars from the cytosolic side and the corresponding nucleotide mono-phosphate on the Golgi side. For instance, a molecule of UDP-Gal is transported inside the Golgi while a molecule of UMP is removed. The transport rate for all TPs

considered was found to follow saturation kinetics [82], mathematically represented by the expression reported by [1] (Eq. 20).

$$F_{k,in} = k_{T,k}[TP_k]\frac{A^{\text{golgi}}}{V^{\text{golgi}}}\left(\frac{[NS_k^{\text{cyt}}]}{K_{NSD}^{\text{cyt}} + [NS_k^{\text{cyt}}]}\right)\left(\frac{[N_k^{\text{golgi}}]}{K_N^{\text{golgi}} + [N_k^{\text{golgi}}]}\right) \quad (20)$$

Where k_T is the transport turnover number while K_{NSD}^{cyt} and K_N^{golgi} indicate the affinity of the membrane receptors towards the substrates and were assumed to be the same due to lack of data. Moreover, they were assumed to be half of the intracellular concentration of their nucleotide sugar substrate (Tab. 7). The constant relative to the UDP-Gal/UMP antiport has been used as fitting parameter to represent the effect of increasing UDP-Gal concentrations in response of galactose supplementations.

Table 7 Transport kinetic parameters

Transport protein	k_T (min^{-1})	K_{NSD}^{cyt} (µM)	Source
UDP-GLCNAc/UMP	1084	811	Rat liver [83]
GDP-Fuc/GMP	130	21.5	Rat liver [84]
UDP-Gal/UMP	689	*	Rat liver [85]
CMP-Neu5Ac/CMP	397	19.9	Rat liver [86]

3.4 Model Simulation and Parameter Estimation

During continuous cultures the perfusion of fresh medium, together with the removal of liquid from the reactor at the same rate, prevents waste product accumulation and allows the cells to remain in a steady environment. In terms of mathematical modelling, this is equivalent to consider all time derivatives equal to zero, since the system is operating at steady-state. In addition to this, all process parameters considered (X_v, NH_3, Mn, nucleotides and nucleotides sugar concentrations) are assumed to be constant for each point of the DoE considered (the average measurement over the entire steady state was

used if not stated otherwise) and listed in Tab. 8 and Fig. 8 (introductory chapter). Other parameters related to the enzyme kinetics were taken from literature or estimated from previously developed model.

The ODE system corresponding to the kinetic scheme presented was solved numerically using the ODE15s solver in MATLAB (Mathworks, Inc. Version R2014a). In order to describe quantitively the N-linked microheterogeneity for 7 structures, the K_ds for GnT I, GnT II, GalT (addition of first and second galactose), FucT and SialT, were used as fitting parameters. One more fitting parameter was added to capture the effect of different conditions: $K_{d,Mn,Gal}$ for manganese, $K^{\mathrm{cyt}}_{UDP-Gal}$ fir galactose and γ_{NH3}ammonia.

The objective function used to estimate these parameters is shown in eq. 21 and was minimized using the MATLAB MEtaheuristics for bIoinformatics Global Optimization (MEIGO) toolbox [87]. This global optimization toolbox implements metaheuristics and includes a scatter search method for parameter estimation.

$$X = \sum_{n=1}^{N} f_n^{predicted} - f_n^{measured} \tag{21}$$

Where X is the vector of parameters to be optimized, $f_n^{predicted}$ is the fraction of glycans of type n predicted by the model and $f_n^{measured}$ are the corresponding measured values. The glycoforms used for optimization are FA1, A2, FA2G0, FA2G1, FA2G2, FA2G2S1 and FA2G2S2.

Table 8 Nucleotide and Nucleotide sugars values implemented in the model

DoE Point	UDP-GlcNAc	GDP-Fuc	UDP-Gal	CMP-Neu5Ac	UMP	CMP	GMP
	mM	mM	mM	mM	mM	mM	mM
1	1.7502	0.0461	0.1207	0.0513	1.9415	0.2473	0.4962
2	1.7502	0.0461	0.1207	0.0513	1.9415	0.2473	0.4962
3	1.4898	0.0402	0.2956	0.0295	1.9415	0.2473	0.4962
4	1.4898	0.0402	0.2956	0.0295	1.9415	0.2473	0.4962
5	1.7502	0.0461	0.1207	0.0513	1.9415	0.2473	0.4962
6	1.7502	0.0461	0.1207	0.0513	1.9415	0.2473	0.4962
7	1.4898	0.0402	0.2956	0.0295	1.9415	0.2473	0.4962
8	1.4898	0.0402	0.2956	0.0295	1.9415	0.2473	0.4962
Middle	1.6485	0.0418	0.1610	0.0352	1.9415	0.2473	0.4962

Chapter 4: Results and Discussion

4.1 Experimental Results

Cell Culture Performance

The approach chosen to modulate glycosylation involved changing the medium components (manganese and galactose) and viable cell density with the system operating at steady-state. This strategy was developed according to the design of experiments methodology and implemented in two different bioreactor setups that differ only with respect to the external loop (ATF and TFF). Cells were inoculated into the two systems at a viable cell density of $20 \cdot 10^6$ cells/ml and cultured under 100% base medium for 7 days while keeping VCD constant thanks to the adaptive bleeding strategy described in the materials and methods section. At day 8 the feed fraction was gradually changed to 70% concentrated feed and 30% base medium to allow a cell density to reach $60 \cdot 10^6$ cells/ml. This steady state was maintained for 7 days before bleeding the VCD down to $40 \cdot 10^6$ cells/ml. Medium composition switch was performed on day 1 of each steady state and glycosylation profiles were measured only after 4 days to ensure at least 98% removal of the previous medium (residence time in the bioreactor ~ 1 day). At least two different samples were taken for each point of the DoE.

The performance of two illustrative runs is hereby presented. The first one was performed on an ATF setup with adaptive bleeding performed manually twice per day, to generate the points of the DoE corresponding to $20 \cdot 10^6$ cells/ml, 0 mM Gal, 0.01 µM Mn, $60 \cdot 10^6$ cells/ml, 0 mM Gal, 0.01 µM Mn and $40 \cdot 10^6$ cells/ml, 5 mM Gal, 0.1 µM Mn (middle point). As shown in Fig. 14 A the desired viable cell density profile has been reached without VCD variations exceeding 10% of the set point, while viability was maintained above 90% throughout the entire culture (Fig. 14 B). Additionally, measured ammonia profiles well correlate with the three different VCD steady states demonstrating the

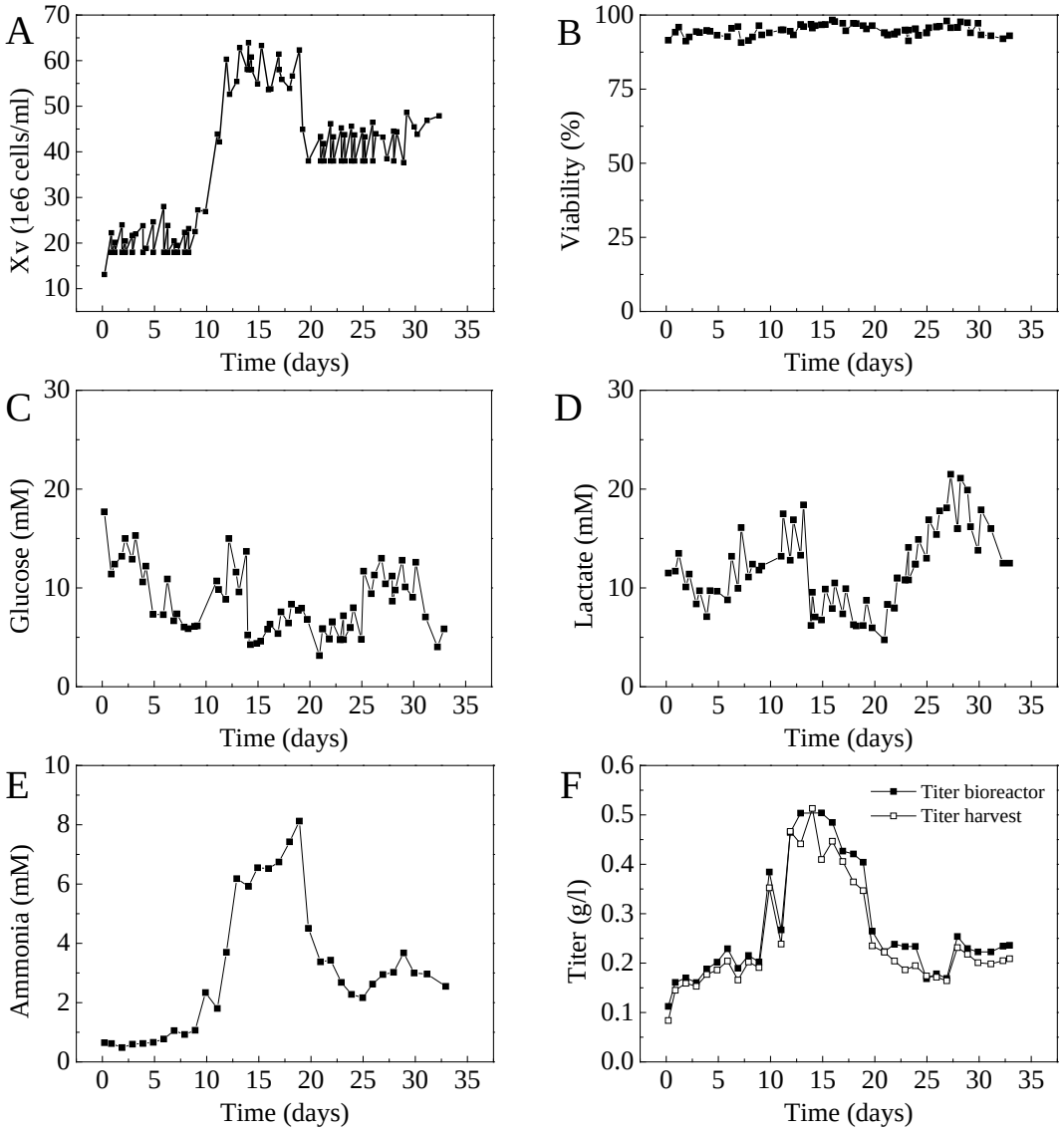

Figure 14 Viable cell densiy (A), viability (B), glucose and lactate levels (C, D) ammonia (E) and antibody concentration (F) for the first bioreactor run (ATF).

effectiveness of the strategy in modulating different process parameters (Fig. 14 E). The possibility of modulating ammonia was enhanced by the presence of additional (7.5 mM) asparagine in the feed medium: the amide group in the side chain of this amino acid is known to be subjected to hydrolysis by living cells, therefore supplementation of asparagine resulted in an increase of ammonia in the culture medium up to 7-fold, while VCD only increased 3-fold. For completeness glucose, lactate and titer profiles are also reported in Fig 14C-D. These graphs prove that I) both carbon sources never dropped to zero even in presence of high VCD and II) the absence of protein retention in the external

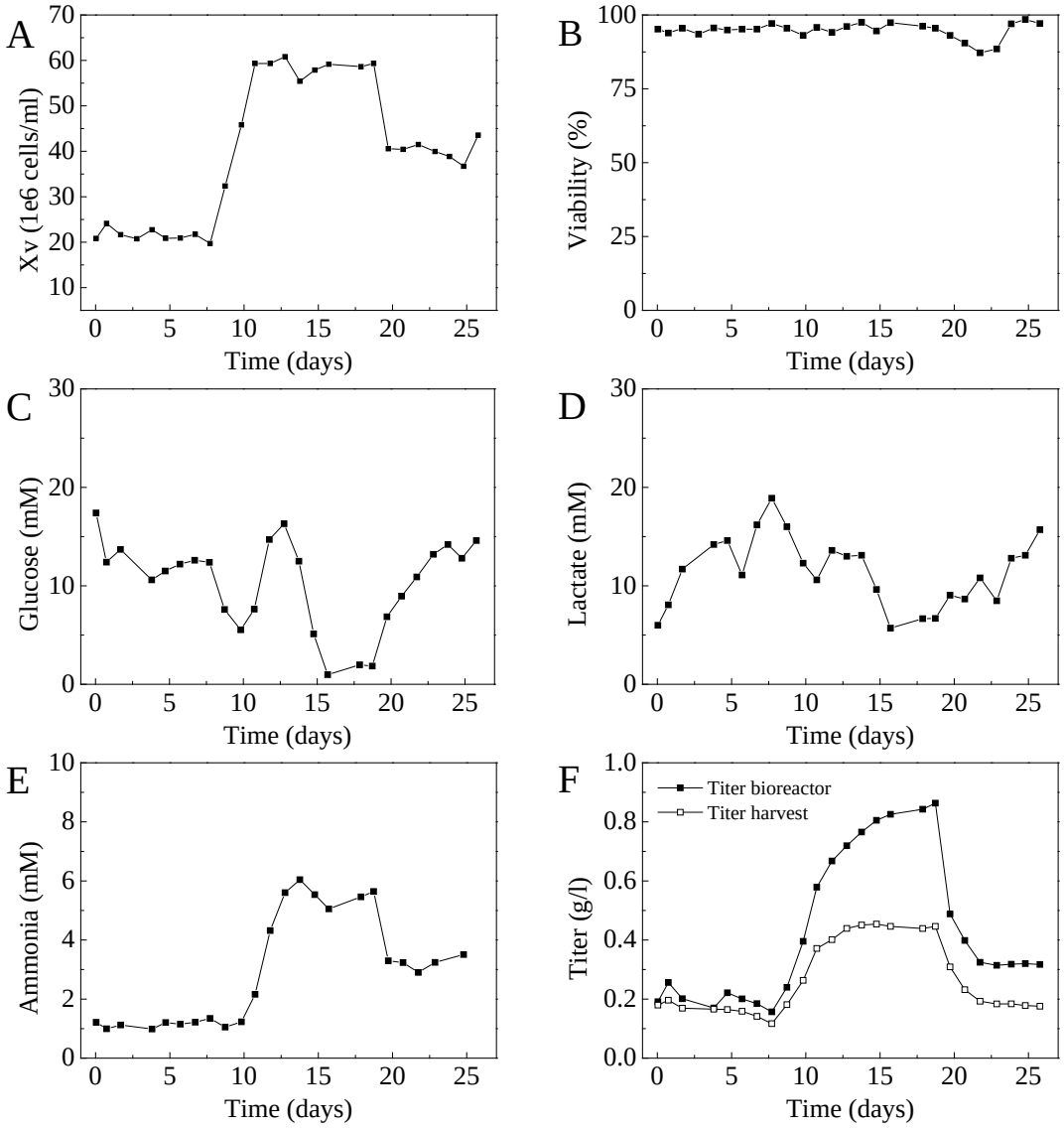

Figure 15 Viable cell densiy (A), viability (B), glucose and lactate levels (C, D) ammonia (E) and antibody concentration (F) for the second bioreactor run (TFF).

loop given by the ATF pump (i.e. antibody concentration inside the reactor and in the harvest flow are exactly the same).

Fig. 15 shows the performance of the second run, performed in a TFF-equipped perfused system in the presence of an automated biomass sensor. The bleeding procedure was no longer performed by the operator but was automatically performed thanks to the continuous VCD monitoring performed by the sensor, resulting in a much smoother VCD profile (Fig. 15 A). Even in this case, ammonia and titer profiles clearly correlate to the VCD, although the fouling of the external loop caused retention of the protein product

inside the fiber as shown in Fig. 15 F, resulting in a lower mAb concentration in the harvest. The only effect on glycosylation is a small increase in the amount of time required to reach steady state quality of the proteins. The first steady state is relative to the $20 \cdot 10^6$ cells/ml with low Mn and high galactose (10 mM), the second one has high VCD and Mn (1 µM), while the third point is again the middle point of the DoE. By comparing the two runs it was demonstrated that presence in the culture medium of Mn and galactose did not affect viability or glucose and lactate consumption, therefore proving the consistency of the process performance in presence of different medium compositions.

Amino Acids

Limitations in amino acids are detrimental for cell cultures in terms of limitation in protein productivity or even misincorporation of amino acids in the peptide sequence. CHO-S cells are particularly sensitive towards this condition, especially when it comes to asparagine starvation [88]. While analyzing the amino acid profiles of previous cultures, depletion of particular amino acids such as asparagine, cysteine and tyrosine was detected (Fig. 16, panel F).

Based on these findings, and with the goal of avoiding such limitations, the feed composition used in the successive runs was enriched with the addition 0.0375% v/v of concentrated Cys/Tyr solution and Asn powder for a final concentration of 7.5 mM. The modified medium composition was tested on another run and resulted in higher amino acid levels with respect to the starting condition, especially asparagine as seen from panel F of Fig. 17. The new feed composition was implemented for all following cultures.

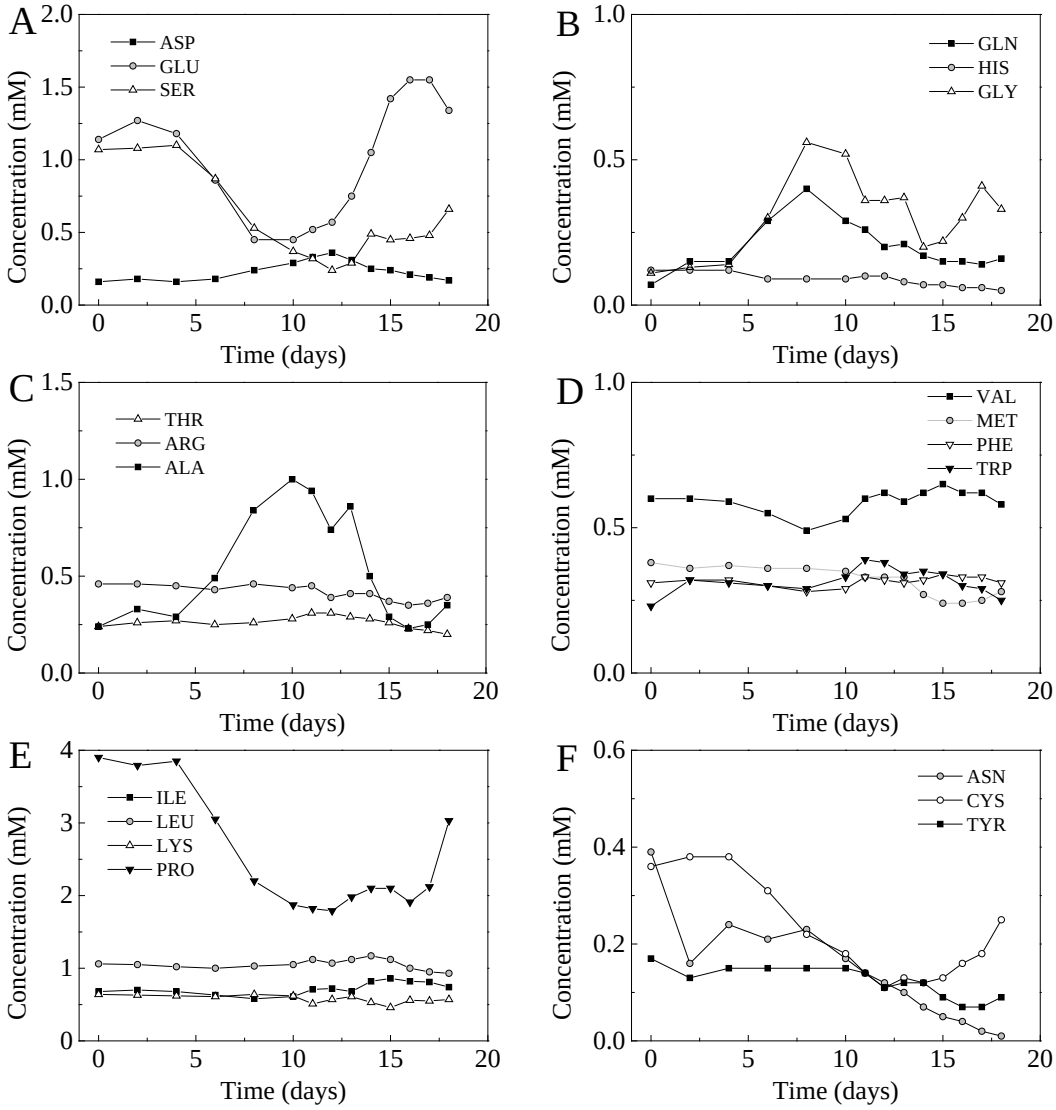

Figure 16 Amino acid concentrations throughout a bioreactor run with non-modified feed composition. As seen from panel F, asparagine, cysteine and tyrosine concentration drop to very low levels after one week of cultivation**.**

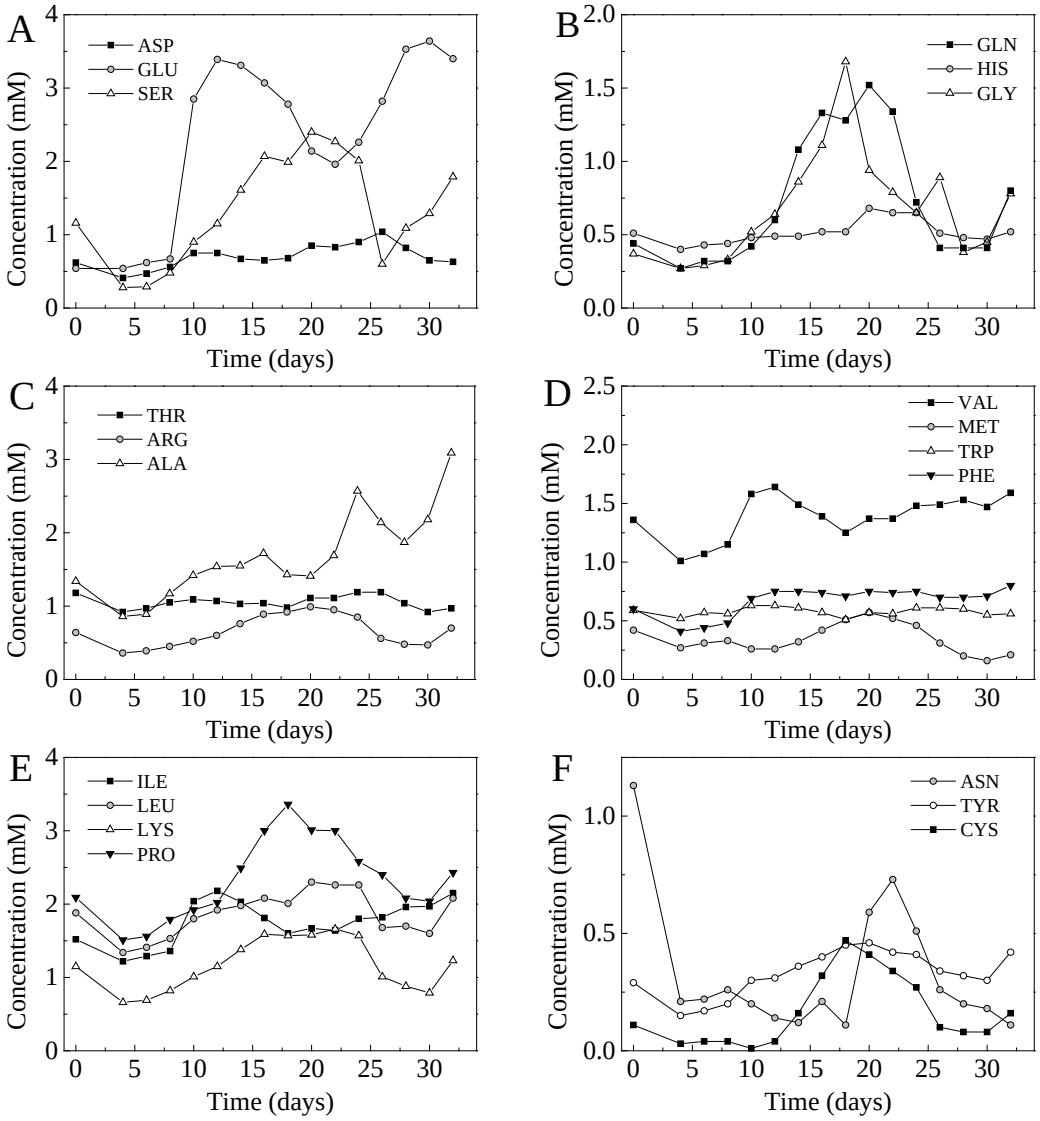

Figure 17 Amino acid concentrations throughout a bioreactor run with increased concentrations of asparagine, cysteine and tyrosine in the feed composition. As seen from panel F, amino acids levels, especially asparagine, are sensibly higher.

Nucleotides and Nucleotide Sugars

Intracellular nucleotides and nucleotides sugars concentrations were determined by means of mass spectroscopic and anion exchange chromatography analysis respectively. The use of both methods relies on the fact that, despite being more quick and precise, MS alone is not able to distinguish between sugar monomers with the same masses, such as hexoses (hex) and hexoses-N-Acetylglucosamines (hexNAc). In turn, chromatography is capable of

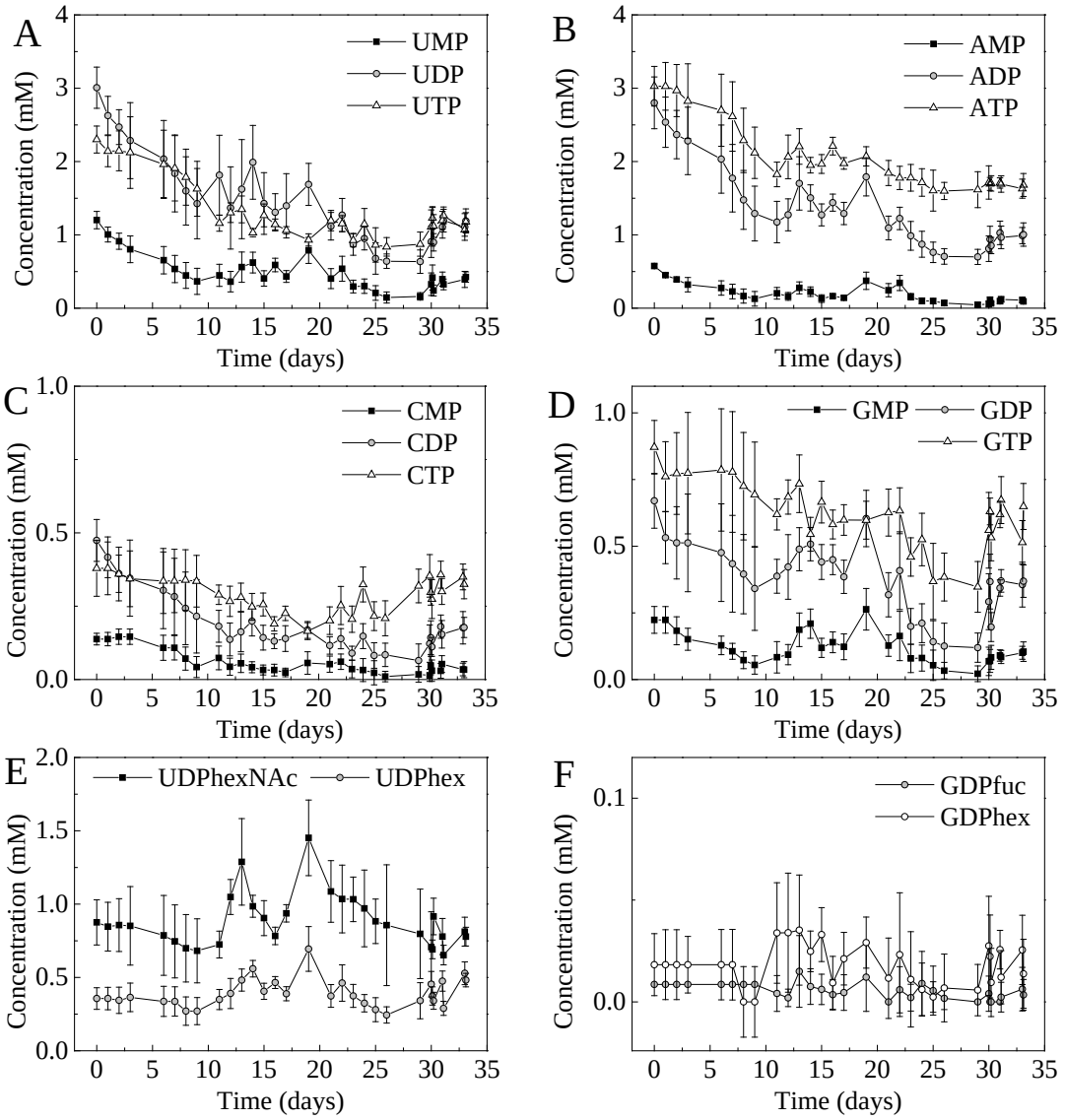

Figure 18 Nucleotides (A, B, C, D) and nucleotide sugars (E, F) concentrations measured with MALDI-TOF analysis for the first bioreactor run (ATF). St. devs were obtained over n = 10 measurements.

distinguishing sugars with the same masses (i.e. glucose/galactose) due to the diverse retention times on the stationary phase as a consequence of the different conformations assumed. For consistency, nucleotide concentrations used for the development of the mathematical model were extrapolated from MS, while chromatography was employed for the determination of the nucleotide sugars concentrations. Nucleotides levels were found to be in the mM range (Fig. 19 A-D), in line with other measurements found in literature for CHO cells [32], and relatively constant throughout the various cultures (experimental deviations encountered have to be accounted to the difficulty of sampling exactly 5 million

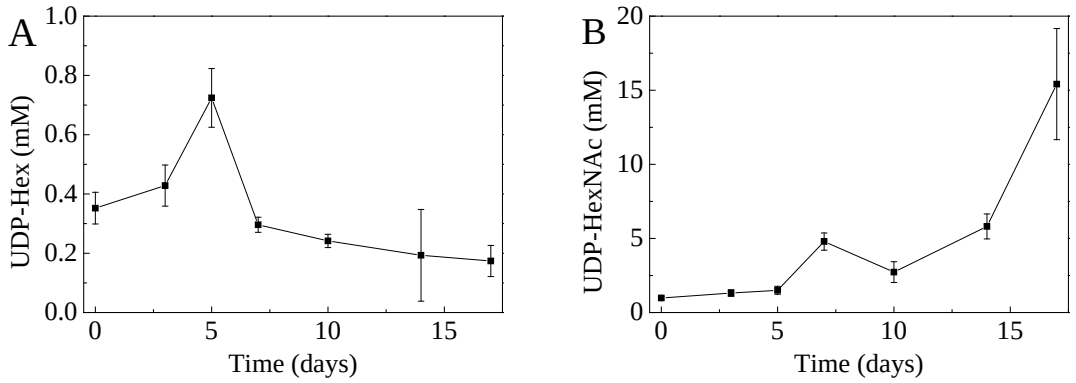

Figure 19 Typical UDP-Hex (A) depletion and UDP-HexNAc (B) accumulation observed in 17 days fed-batch cultivations (taken from Villiger et al. in press).

cells during the extraction procedure). Nucleotide-3-phosphates (NTPs) were found to be always in higher levels with respect to both diphosphate and monophosphate nucleotides, with the latter being the least concentrated species. ATP and UTP resulted in the highest concentrations (2 and 1.5 mM respectively), followed by GTP (0.75 mM) and CTP (0.4 mM). GDP-hex was detected only with MS due to its very low concentrations (below 0.02 mM). Illustrative results for the MS analysis of the first ATF run are shown in Fig. 18 while Fig 19 offers a comparison with a typical fed-batch run. It is worth noting that the use of a perfused system prevented the depletion of UDP-Hexoses (UDP-Galactose and UDP-Glucose) and the accumulation of UDP-HexNAc (UDP-N-Acetylglucosamine and UDP-N-Acetylgalactosamine): both events are regarded to as detrimental for glycosylation since they inhibit the latest step of the N-glycan processing.

Anionic exchange chromatography allowed the identification of 17 different metabolites, including molecular species with the same masses (illustrative chromatogram with all the species detected included in Fig. 20). Nucleotide-sugars concentrations where found to be in the µM range, apart from the two UDP-HexNAc species (around 1.5 mM for UDP-GlcNAc and 0.8 mM for UDP-GalNAc).

Chromatographic analysis confirmed the increase in UDP-Gal in response to galactose supplementation from 0.12 mM to 0.18 (5 mM gal fed) and 0.30 mM (10 mM gal fed) with no significant difference in UDP-Glc. The elution peak related to GDP-Fucose was very low but still measurable (GDP-Fuc was found to be around 40 µM, in line with the MS measurement for GDP-Hex) while GDP-Man was detected only with MS.

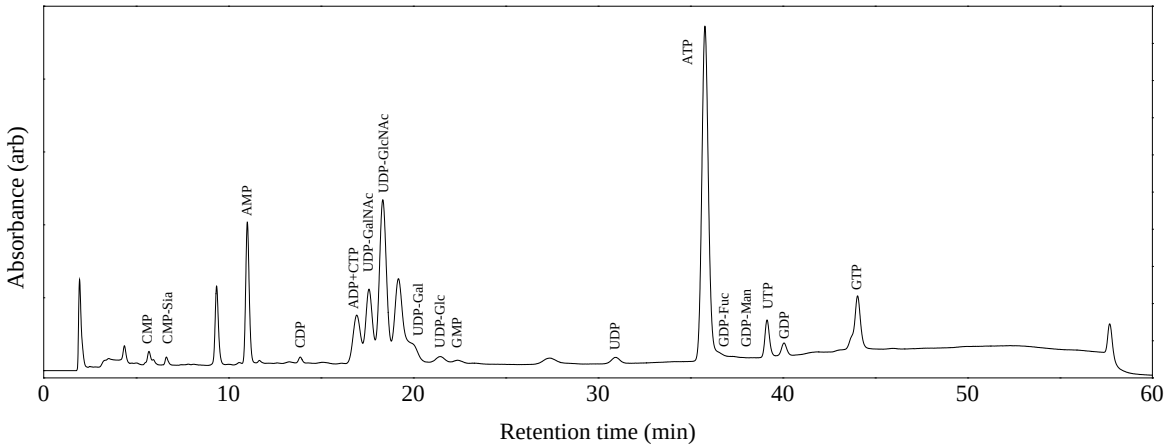

Figure 20 Anion exhange chromatogram for nucleotide and nucleotide sugars analysis with corresponding elution times.

Different levels of manganese were not found to affect intracellular metabolites concentrations, while supplementation of galactose resulted in an increase in the UDP-Gal/UDP-Glc ratio from around 0.5 to 1 as shown in Fig. 21. Surprisingly, the same effect was not detected for UDP-GalNAc and UDP-GlcNAc (Fig 21). Higher levels of ammonia could be correlated with an accumulation of UDP-GlcNAc and UDP-GalNAc, although the trend is not totally clear. No significant variations in intracellular metabolites profiles were detected in the 2 different set ups (Fig. 22). Complete results of the chromatographic analysis are reported in Tab. 9.

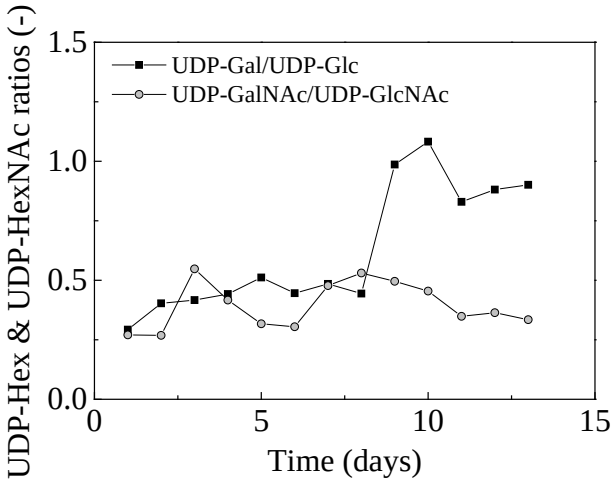

Figure 21 Variation in uridine-based nucleotides sugars in response to galactose supplementation after day 7.

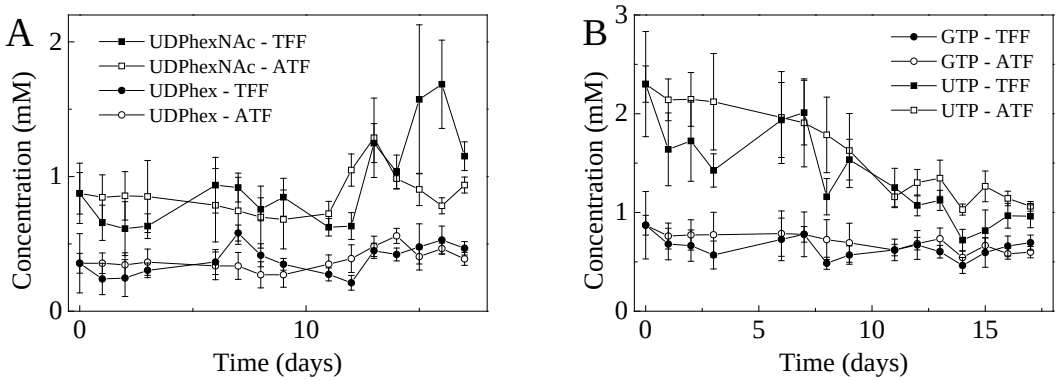

Figure 22 Equivalence of the two set-ups in terms of intracellular metabolites . Data shown only for UDP-HexNAc (A), UDP-Hex (A), GTP (B) and UTP (B).

Table 9 NSD concentrations measured with HPAEC.

Gal	Mn	NH_3	UDP-GalNAc	UDP-GlcNAc	UDP-Gal	UDP-Glc	GDP-Fuc	CMP-Neu5Ac
			mM	mM	mM	mM	mM	mM
High	Low	Low	0.531 ± 0.133	1.490 ± 0.190	0.296 ± 0.049	0.315 ± 0.040	0.0401 ± 0.006	0.0295 ± 0.004
Low	High	High	0.803 ± 0.201	1.750 ± 0.236	0.124 ±0.015	0.335 ± 0.055	0.0581 ± 0.009	0.0370 ± 0.007
Low	Low	Low	0.472 ± 0.060	1.511 ± 0.325	0.110 ± 0.016	0.268 ± 0.008	0.0365 ± 0.003	0.0440 ± 0.005
Low	Low	High	0.814 ± 0.060	2.425 ± 0.378	0.122 ± 0.020	0.267 ±0.043	0.0503 ± 0.011	0.0544 ± 0.008
Mid	Mid	Mid	0.548 ± 0.064	1.649 ± 0.261	0.181 ± 0.023	0.298 ± 0.048	0.0418 ± 0.009	0.0351 ± 0.008

4.2 Glycosylation Results

N-Glycan Structures Detected

The combination of HILIC and MALDI-TOF allowed the detection of more than 20 different oligosaccharide structures. Similarly to metabolites analysis, the complete characterization of the glycan structures required the use of two orthogonal analytical methods: MS was employed to uniquely identify the mass to charge ratio of the structures, while information on anomery of the bonding and type of hexose (glucose, galactose or mannose) was recovered thanks to a previous chromatographic separation: structural isomers were resolved in HILIC since the retention time is based on the hydrophilic potential of the molecule, which is a function of composition, structure and branching of the oligosaccharides. The complete series of structures detected is reported in Fig 23 in terms of retention times and in Tab. 10 with the complete list of the mass to charge ratios. Structures indicated with the symbol * have not been included into the model's kinetic scheme due to their extremely low relative concentrations (< 0.1 % of the total glycoprofile). The double peak registered at elution time 51 min correspond to the 2 FA2G1 structures (galactose attached to the α2-3 or α2-6 arm), with the galactosylated α2-6 arm eluting first. The same behavior was found for the FA1G1S1 (min 55), FA2G1S1 (min 58), A2G2S1 (min 63) and FA2G2S1 (min 74) structures. As seen from the chromatogram, the higher the elongation of the antennary arm, the longer was the retention time in the column. Therefore sialylated glycans eluted last (min 75+), while heavily trimmed oligosaccharides eluted in the first 30 minutes. Another factor determining the elution time was the presence of core fucose, whose absence reduced the elution time by approximately 10 minutes, as seen for instance in case of the A2-FA2 and A2G2-FA2G2 forms.

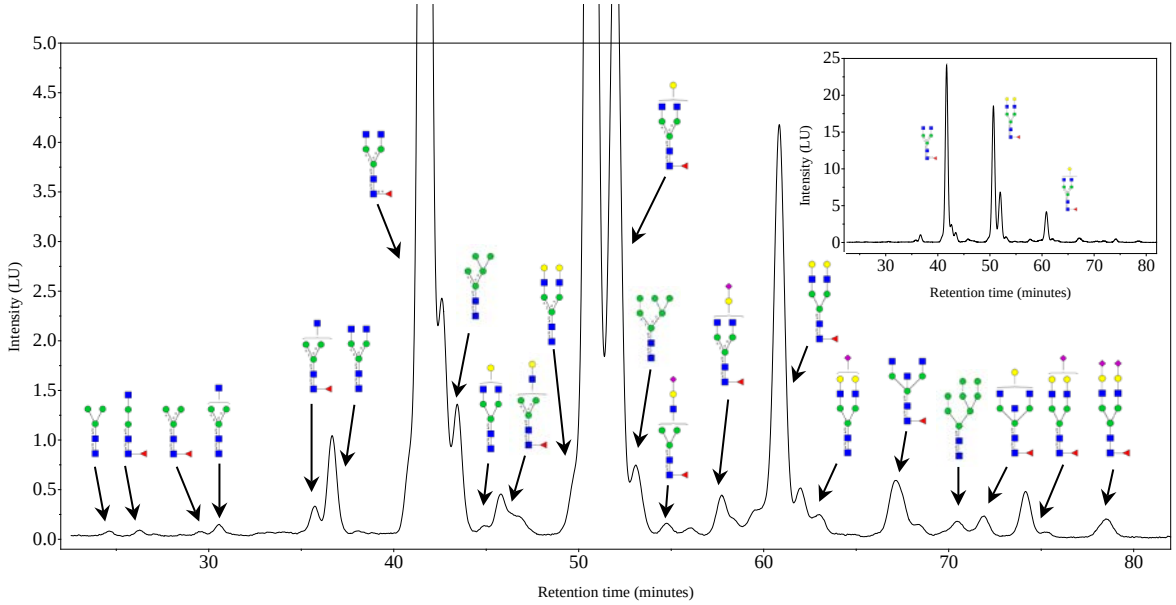

Figure 23 Fc region N-glycans illutrative chromatogram and elution times for all detected oligosaccharides.

Table 10 List of N-glycan structures detected with MALDI-TOF.

Glyco structure	Symbol	Theoretical mass (Da)	Measured m/z	
			$[OS+Na]^+$	$[OS+H]^-$
2AA-($HexNAc_2Hex_3$) *		1030.96	1053.43	-
2AA-($HexNAc_2Hex_3$)dHex *	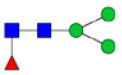	1177.11	1199.45	-
2AA-($HexNAc_2Hex_3$)HexNAc		1234.15	1256.51	-
2AA-($HexNAc_2Hex_3$)--HexNAcdHex		1380.30	1402.59	-
2AA-($HexNAc_2Hex_3$)$HexNAc_2$	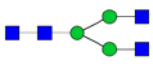	1437.35	1459.62	-
2-AA-($HexNAc_2Hex_3$)Hex_3	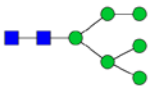	1517.54	1539.49	-
2AA-($HexNAc_2Hex_3$)--HexNAcHexdHex		1542.45	1564.50	1743.75

2AA-($HexNAc_2Hex_3$)$HexNAc_2$dHex	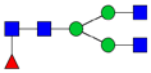	1583.49	1605.65	1581.72
2AA-($HexNAc_2Hex_3$) $HexNAc_2$HexdHex	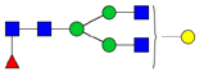	1746.62	1767.58	-
2AA-($HexNAc_2Hex_3$)$HexNAc_2$Hex	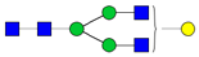	1599.49	1621.62	-
2AA-($HexNAc_2Hex_3$)Hex_2	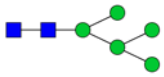	1646.58	1377.54	-
2AA-($HexNAc_2Hex_3$)$HexNAc_2Hex_2$	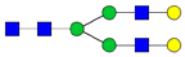	1761.65	1783.54	-
2AA-($HexNAc_2Hex_3$)- -HexNAcHexNeuAcdHex	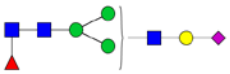	1833.67	-	1831.81
2AA-($HexNAc_2Hex_3$) $HexNAc_2Hex_2$dHex	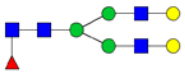	1907.79	1929.65	-
2-AA-($HexNAc_2Hex_3$)- -$HexNAc_3$dHex *	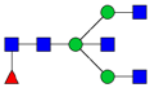	1787.68	1785.85	-
2AA-($HexNAc_2Hex_3$)Hex_5	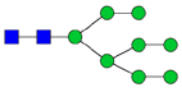	1970.69	1863.60	-
2AA-($HexNAc_2Hex_3$)- -$HexNAc_2$HexNeuAcdHex	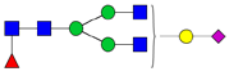	2036.90	2058.70	2034.88
2AA-($HexNAc_2Hex_3$)	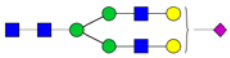	2052.74	-	2050.89
2-AA-($HexNAc_2Hex_3$)- -$HexNAc_3$HexdHex *	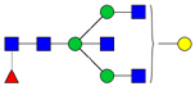	949.82	1947.9	-
2AA-($HexNAc_2Hex_3$)- -$HexNAc_2Hex_2$NeuAcdHex	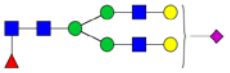	2199.05	-	2196.90
2AA-($HexNAc_2Hex_3$)- -$HexNAc_2Hex_2NeuAc_2$dHex	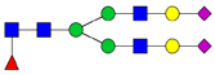	2489.89	-	2488.15

Equivalence of the two Systems in terms of N-Glycosylation and Achievement of Steady State

The ATF and TFF setups were found to behave equivalent in terms of viable cell density, metabolites levels, ammonia production and antibody specific productivity. To further prove the equivalence of the 2 systems in terms of N-glycosylation, two different steady states were carried out in both reactors simultaneously. As seen from the results reported in Fig. 24 A, deviations were found to be well below the experimental error and all the measured glycoforms showed similar values for both set ups. The external loop was therefore proven to not affect glycosylation, thus justifying the use of the two systems for the development of the DoE. Moreover, by measuring the glycoprofile at two different time steps at least 3 days away from each other only differences below 2.5 % in the major peaks were detected (Fig. 24 B), ensuring the correctness of the steady state assumption for glycosylation.

Modulation of Glycosylation in the DoE

A body-centered Design of Experiments model was developed to investigate the effect of manganese, galactose and ammonia on N-linked glycosylation of recombinant mAbs produced in continuous cultures and subsequently produce a model capable of predicting how these variables modulate mAbs glycosylation.

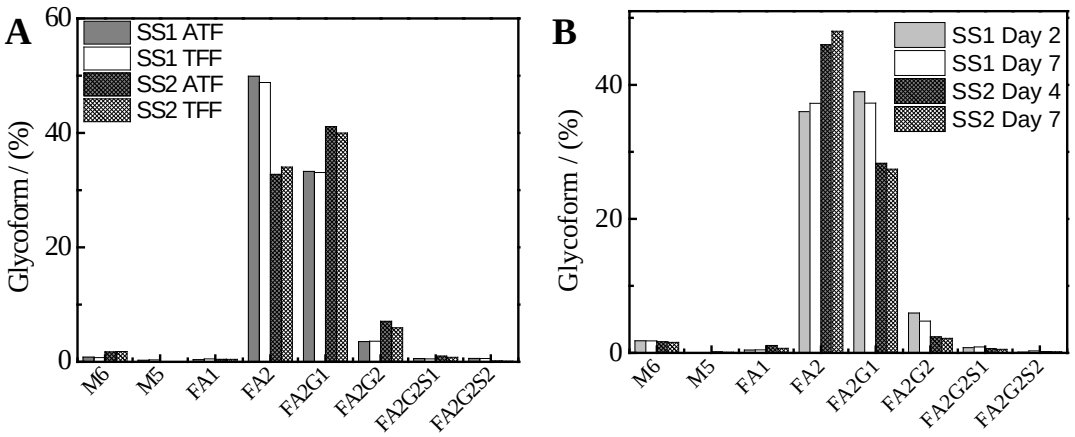

Figure 24 Comparison of glycosilation profiles between the two different reactor set-ups and at two different time points within a single steady state.

For the following report, only the species with highest relative concentrations of Tab. 10 will be reported (M5, FA1, A2, FA2, FA2G1, FA2G2, FA2G2S1 and FA2G2S2), with no distinction between antennary arms that differ only for the addition of one sugar monomer (i.e. FA2G1 = FA2G1α2-3 + FA2G1α2-3). The reason underlying this choice lies in the extremely low concentration of some structures and the fact that some of them were not found in every point of the DoE. Moreover, the eight structures considered represent on average 95% of the total glycoprofile, thus well resembling the effect of medium composition and process conditions.

Concerning the three major peaks (FA2G0, FA2G1 and FA2G2, together accounting for almost 90% of the total glycoprofile), a clear trend was detected for all the different conditions evaluated. As expected, a significant increase in mAb galactosylation was observed when cells were supplemented with either galactose or Mn. For instance, a Mn switch from 0.01 (Low) to 1 µM (High) in presence of low ammonia concentrations resulted in a 10% and 3.5% increase in FA2G1 and FA2G2 forms respectively, while the corresponding increase for $60 \cdot 10^6$ cells/mL was 16% and 3%. Similar values were found with the addition 10 mM galactose: 11.6% and 4.3% increase in FA2G1 and FA2G2 for low ammonia (+11.23% and +1.6% for high ammonia). Moreover, a synergistic effect was detected when the two substances were added simultaneously (+17% and +16.4% for FA2G1 and +9.5% +5.5% for FA2G2). The increase in galactosylated structures is in great part attributable to a decrease in the FA2G0 form, which from being the predominant peak in the control runs (56% and 59.8% depending on ammonia if no gal or Mn was added) was reduced to 39.4% and 36.9 % with a concomitant increase in FA2G1 and FA2G2 in case of 1 µM Mn and 10 mM gal addition, as seen in Tab. 11. This phenomenon is clearly seen in case of conditions that differ only for the amount of ammonia in the culture medium.

High mannose structures (M5, M6 and M8) were always found to increase at high viable cell densities due to higher ammonia concentrations, though never exceeding 3.5%. For reference, antibodies produced in fed batch runs normally show up to 15% HM with respect to the total amount of oligosaccharides [29]. For these structures, the effect of manganese and galactose was minor and did not show a predictable trend, mostly due to their very low relative concentrations and the partial co-elution of M5 and M6 with FA2G0 and FA2G1 during HILIC analysis.

Sialylated structures (FA2G2S1 and FA2G2S2) only represented a small portion (up to 2%) of the entire glycopattern. Such low values are common for human antibodies, since the sugar moieties attached at ASN-297 are deeply embedded in the peptide structure and therefore less accessible to glycosyltransferases. For this reason, Mn and gal supplementation could not be completely correlated to an increase in both FA2G2S1 and FA2G2S2. For example, monosilalylated structures were found to increase with Mn in case of high ammonia and galactose, but decreased if Mn was added to cell cultured with no galactose and in presence of low ammonia (Tab. 10). Other single sialylated structures (FA1G1S1, FA2G1S1) did not exceed 1% and no significant trend was detected.

A2 and FA1 structures represent 2 glycans whose processing stopped in the medial Golgi. Although their relative concentration was relatively low (2% and 1% respectively), both forms were found to increase with ammonia: this is due to the fact that successive processing is partially inhibited, resulting in higher fraction of less modified glycans. Manganese and galactose were not found to affect A2 and FA1 levels.

Table 11 Glycosylation results for the 9 points of the DoE

Gal	Mn	NH_3	M5 %	FA1 %	A2 %	FA2 %	FA2G1 %	FA2G2 %	FA2G2S1	FA2G2S1
Low	Low	Low	0.15	0.72	1.10	56.00	28.69	3.05	1.27	0.18
Low	Low	High	3.18	2.82	2.12	59.75	22.88	2.05	1.63	0.20
High	Low	Low	0.20	0.45	1.32	42.95	40.33	7.39	1.47	0.19
High	Low	High	0.60	1.89	3.01	52.64	34.11	3.60	0.91	0.18
Low	High	Low	1.00	0.64	2.04	41.97	41.26	6.73	0.76	0.80
Low	High	High	1.85	0.87	2.06	42.69	39.26	5.11	1.20	0.29
High	High	Low	0.60	0.58	1.11	34.04	45.34	12.51	0.62	0.20
High	High	High	1.82	0.94	2.44	39.38	39.27	7.56	1.36	0.70
Mid	Mid	Mid	2.00	0.57	1.67	36.85	42.94	8.73	1.22	0.45

4.3 Modeling Results

Cell Culture Dynamics

Growth rate was found to be 0.45 ± 0.16 day^{-1} for $20 \cdot 10^6$ cells/mL, 0.12 ± 0.05 day^{-1} for $60 \cdot 10^6$ cells/mL and 0.24 ± 0.04 day^{-1} for $40 \cdot 10^6$ cells/mL (data reported as averages ± st. devs over single steady states, st.devs calculated over 7 measurements), meaning that ammonia acted as inhibitor for cell division and proliferation. Maximum growth rate μ and K_{AMM}^{μ} were estimated as 1.10 day^{-1} and 0.79 mM respectively (R^2=0.9849) according to Eq. 4.

Antibody specific productivity was calculated according to Eq. 6 and was found to vary over different steady states: the q_{mAb} was 11.95 pg/cell/day at $20 \cdot 10^6$ cells/mL and 9.06 pg/cell/day at $60 \cdot 10^6$ cells/mL. Knowing the MW of human IgG1s (approx. 150000 g/mol), this resulted in 79.66 and 60.3 pmol/$\cdot 10^6$ cells/day for the two steady states. Manganese and galactose were not found to have an impact on the q_{mAb}.

The glycoprotein concentration at $z = 0$ was calculated as 140 µM according del Val's calculation considering the average productivity of the two steady states. This value is significantly lower than the one defined by previous models, therefore enzyme concentrations were reduced by a factor 2 as described in the mathematical model section.

Ammonia specific productivity due to cellular metabolism q_{AMM} was estimated as 98.59 nmol/cell/day (R^2=0.976), while the specific productivity in response of asparagine feed $K_{d,ASN}$ was found to be very close to zero and therefore not considered (Eq. 7).

Mechanistic Model of N-linked Glycosylation

The validation of the mathematical model can be schematized as follows: the eight edge points of the DoE were using to optimize unknown parameters and dissociation constants listed in the mathematical model section, while the central point was used to test the predictive capacity of the model. With reference to the first step, the model correctly was capable of reproducing the three major peaks without producing significant deviations for

all the other structures considered (FA1, A2, FA2G2S1 and FA2G2S2). Fitting of experimental data was achieved for all the different conditions investigated, as reported in Fig. 25. The reason for the lack of precision in capturing the smallest peaks is most likely attributed to the absence of a predictable trend across different conditions. This is particularly true for the double sialylated form, which was never found to exceed 0.8% of the total glycoprofile and was always underestimated in the model simulations.

The overall deviation of the model with respect to the experimental data was on average 6% for a single DoE point. This means that, on average, the model was able to fit 94% of the considered glycoprofile.

For comparison, the best performing glycosylation model published so far [1] resulted in an average deviation of 4% from glycosylation data of commercial mAbs. However, it is important to mention that the previous model required 6 fitting parameters to reproduce 7 N-glycan structures, while in the present work only 9 parameters were sufficient for a total of 56 structures for 8 different process conditions.

The estimated parameters are reported in Tab. 12. Dissociation constants for the enzymes-glycan complexes were generally found to be in the same order of magnitude (µM or mM) of literature reports. GalT and SiaT were found to have very high dissociation constants (around 10-20 mM), which could be explained by the low accessibility of the N-glycan to these enzymes because of the incorporation of the elongated antennas inside the Fc domain. The dissociation for manganese was estimated around 40 nM, a reasonable value when considering the change of glycosylation even at very low Mn concentration. The kinetic parameter for the transport of UDP-Galactose was found to be above the intracellular concentration of its nucleotide sugar substrate. This could be due to some assumptions underlying the model such as the absence of other glycoproteins inside the Golgi apparatus from antibodies.

To subsequently validate the mechanistic approach, the mathematical model was given VCD, manganese and galactose fed as input and was required to predict the glycosylation pattern of the central point of the cube. As seen in Fig. 26, the model successfully estimated the glycosylation profile with a correct reproduction of the major peaks. Even in this case, some of the minor peaks were not correctly predicted for the previously explained reasons (FA1 and FA2G2S2, with variations of -0.6 and +0.4% respectively).

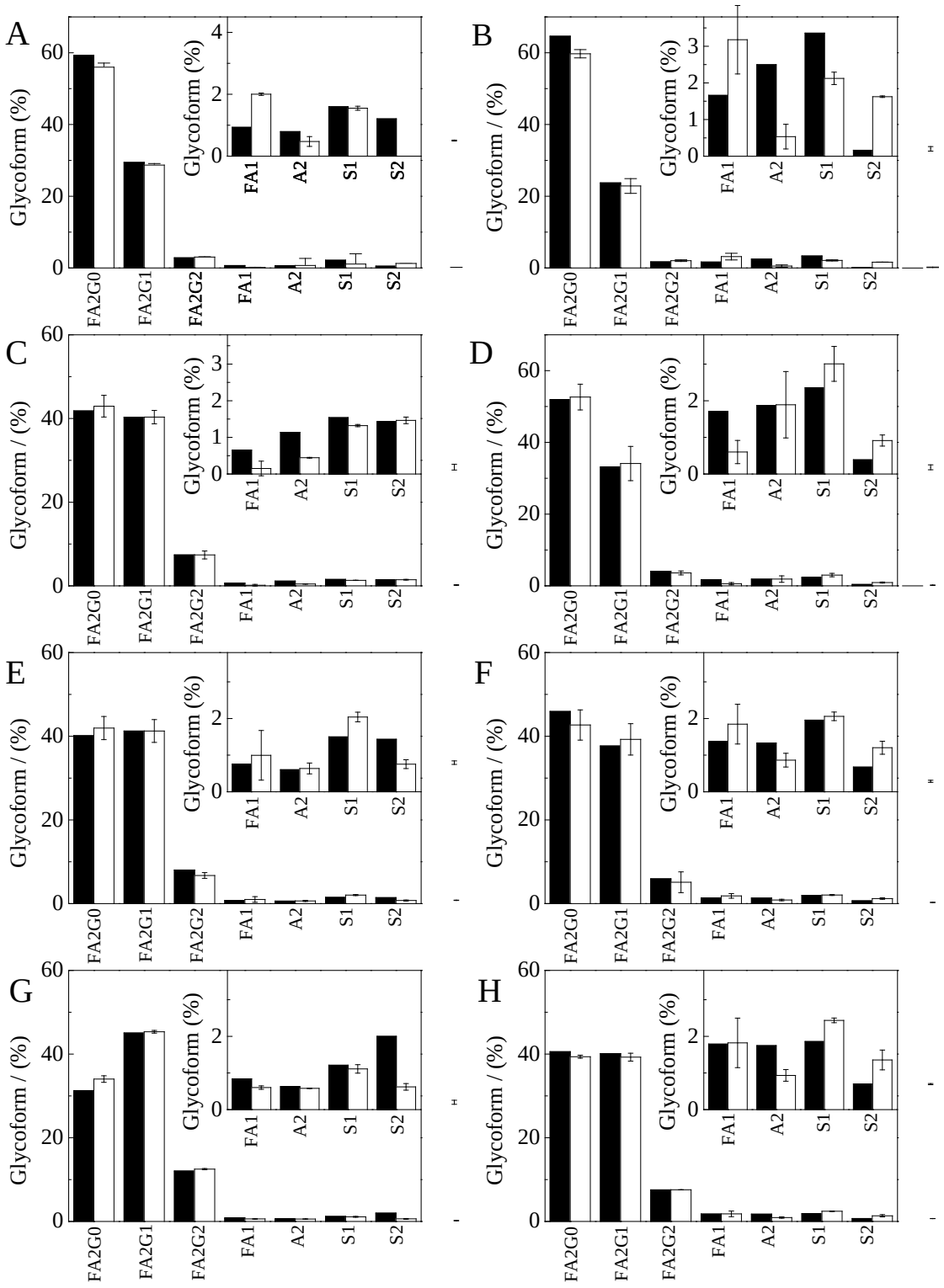

Figure 25 Calculated (black bars) vs Experimental (white bars) glycosylation profiles for the edge points of the DoE. A = low Xv, low Mn, low gal. B = high Xv, low Mn, low gal. C = low Xv, low Mn, high gal. D = high Xv, low Mn, high gal. E = low Xv, high Mn, low gal. F = high Xv, high Mn, low gal. G = low Xv, high Mn, high gal. H = high Xv, high Mn, high. Gal.

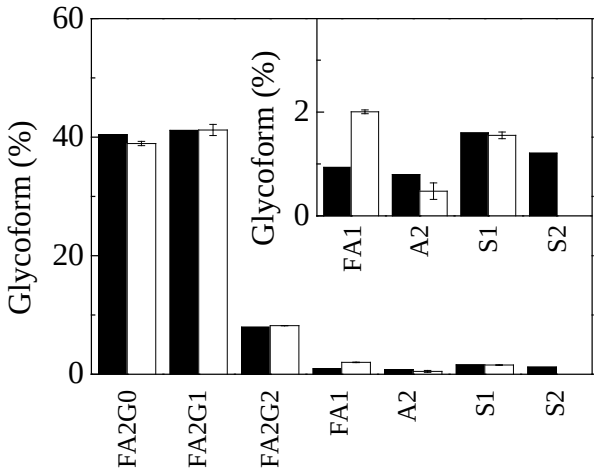

Figure 26 Middle point prediction by the model (black bars) and experimental data (white bars).

Table 12 Results of the parametric optimization.

Parameter	Value
K_d *GnT I*	785.6 µM
K_d *GnT II*	665.2 µM
K_d *FucT*	474.8 µM
K_d *GalT* (first addition)	9734 µM
K_d *GalT* (second addition)	12090 µM
K_d *SiaT*	18330 µM
K^{cyt} (UMP/UDP-Gal)	982.8 µM
K_d *Mn* (GalT)	0.038 µM
γ_{AMM}	1.714

Mechanistic vs Statistic Approach

To study differences in performance between the mechanistic model and statistical methods a very simple RSM was implemented as follows: a restricted third-order model with 8 unknown coefficients (Eq. 23) was used to develop a functional relation between the three input variables (NH_3, Mn, Gal) and glycosylation peaks. In order to compare the two different approaches, these coefficients were used in a second instance to estimate the glycoform distribution of the middle point of the DoE.

$$RSM = a_1 + a_2 \cdot Mn + a_3 \cdot NH_3 + a_4 \cdot Gal + a_5 \cdot Mn \cdot NH_3 + ...$$
$$+...a_6 \cdot Mn \cdot Gal + a_7 \cdot NH_3 \cdot Gal + a_8 \cdot Mn \cdot NH_3 \cdot Gal \quad (22)$$

To limit the amount of parameters used, RSM was applied only to the three major peaks (FA2G0, FA2G1 and FA2G2). The estimated coefficients are reported in Tab. 13.

Table 13 DoE coeeficients estimated for the RSM.

FA2G0				FA2G1				FA2G2			
a_1	55.2	a_2	-13.6	a_1	30.1	a_2	12.2	a_1	3.23	a_2	4.29
a_3	0.70	a_4	-1.40	a_3	-1.08	a_4	1.14	a_3	-0.18	a_4	0.48
a_5	-0.48	a_5	0.44	a_5	0.48	a_5	-0.61	a_5	-0.31	a_5	0.20
a_6	0.10	a_6	-0.22	a_6	0.00	a_6	-0.05	a_6	0.048	a_6	0.00

The statistical methodology successfully fitted the experimental points in the DoE, even with a very small deviation (below 10^{-6}), but did not predict the middle point correctly (Fig. 27). This can be attributed both to overfitting and lack of a sufficient number of experimental points to produce a correct response.

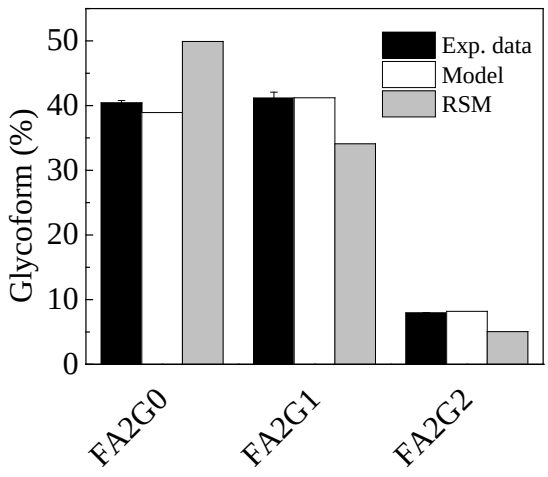

RSM prediction	Experimental Data
FA2G0: 49.92 %	FA2G0: 36.85 %
FA2G1: 34.09 %	FA2G1: 42.49 %
FA2G2: 5.06 %	FA2G2: 8.73 %

Figure 27 Graphical and numerical representation of the middle point prediction for the mechanistic model and the statistical response surface.

Nevertheless, eight experiments were sufficient for the mechanistic model to estimate the middle point glycosylation correctly, even employing less fitting parameters (9 compared to 24). Additionally, the statistical model diverges outside the space of experiments as shown in Fig. 28: at high Mn and Gal concentrations, unrealistically high levels of FA2G1/FA2G2 are predicted, while the mechanistic model shows both a more realistic dynamics and a saturation behavior after 2 µM Mn and 025 mM UDP-Gal.

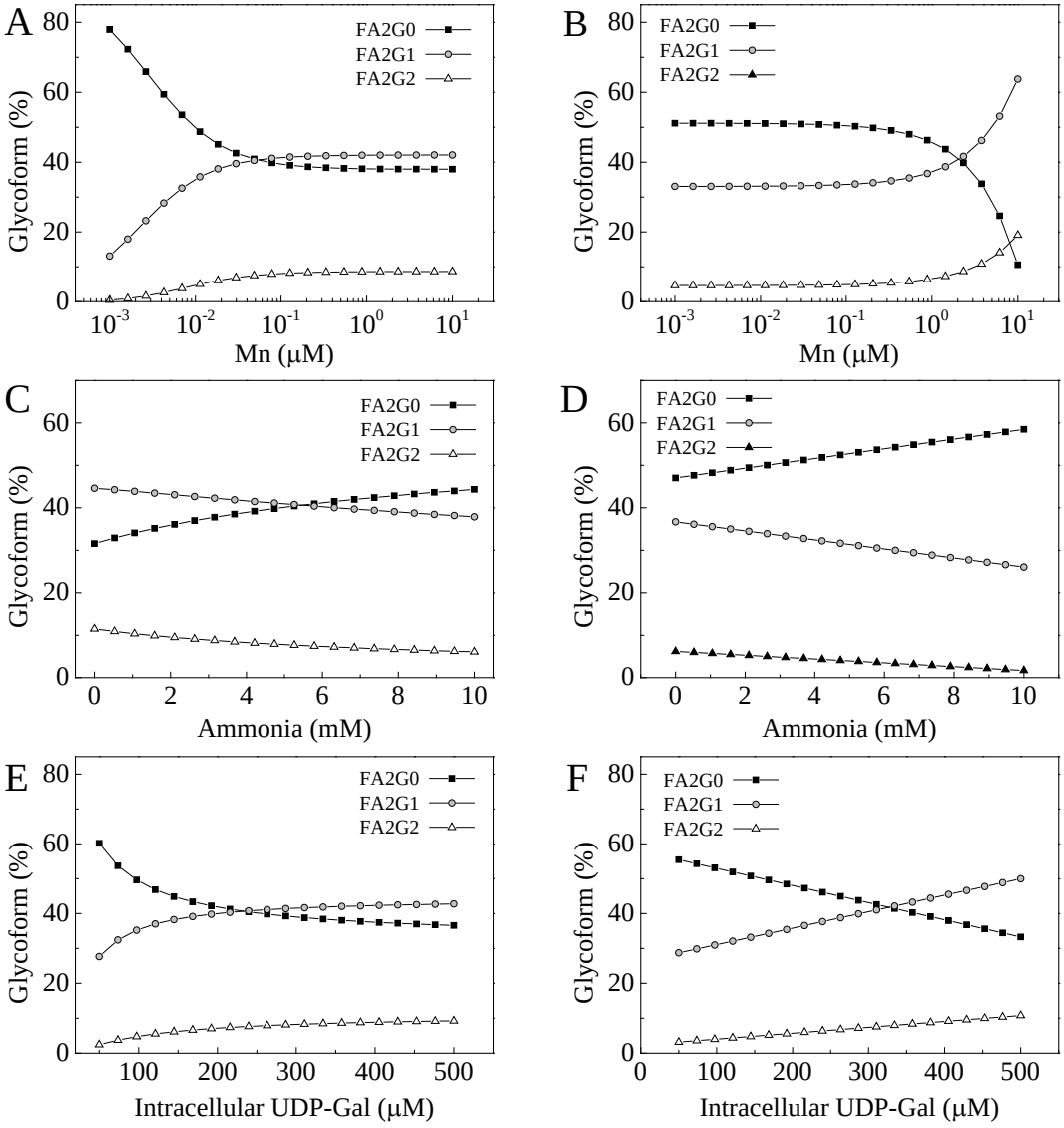

Figure 28 Behaviour of the mechanistic (A, C, E) and statistic (B,D,F) approaches inside and outside the DoE box.

4.4 Case studies

Intra-Golgi concentration profiles

One of the main advantages of this mathematical model is the possibility to not only calculate the glycosylation of secreted proteins but also to obtain insights about concentration profiles of glycans and nucleotide sugars across the Golgi.

For instance, by looking at the glycan profiles across the Golgi, one can identify the main chemical fluxes and how these fluxes are modified by different process conditions. With reference to the first point, by looking at Fig. 29 it is seen that the vast majority of the glycans is transformed from M9 to M5, A1 A2 and FA2 in this sequence. This means that, for example, the second GlcNAc is mostly attached before fucosylation takes part. By looking at FA2G0, one can also observe that its relative fraction can go over 90% in certain locations of the Golgi, while the amount secreted was usually lower than 60% during the experiments performed. This implies that the Golgi enzyme machinery in the *trans*-Golgi is not able to completely process the FA2G0 produced in the previous compartments. Once these glycans bearing terminal N-acetylglycosamines reach the TGN, where no GalT is present (normalized length > 0.8), galactose can no longer be attached and FA2G0 glycans are transported across the last part of the secretory pathway

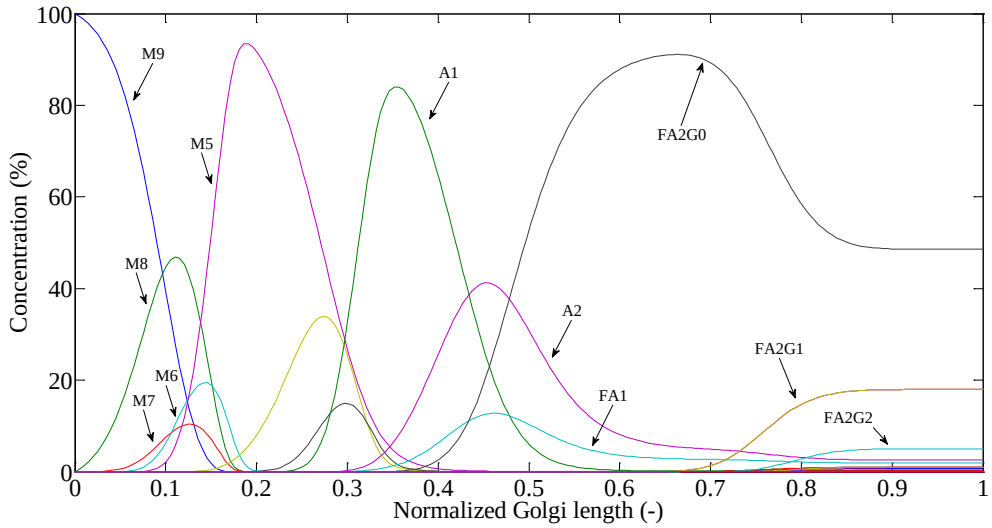

Figure 29 Intra-Golgi concentration profiles of the most important N-glycans.

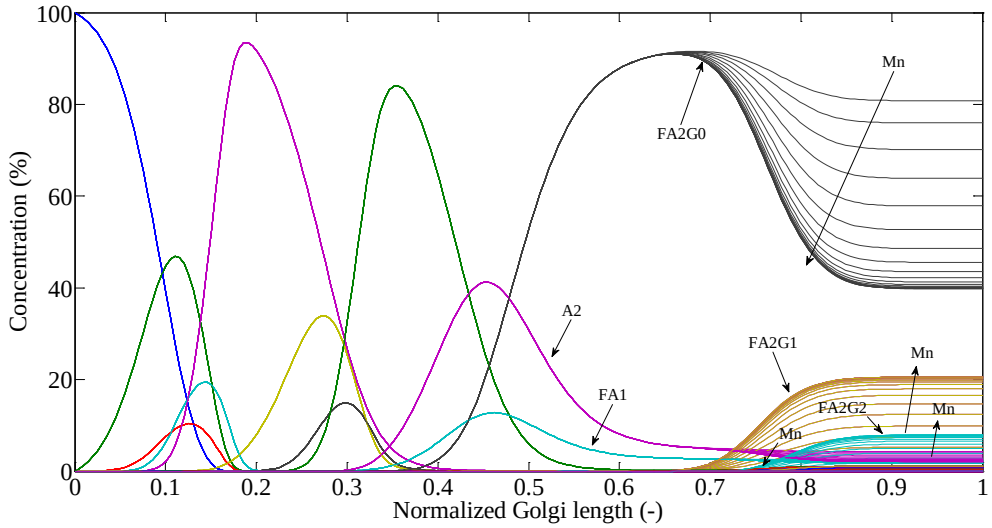

Figure 30 Change in the intra-Golgi concentration profiles of N-glycans in response to manganese supplementation

unmodified (flat line in the concentration profile).

Manganese and galactose were found to affect the Golgi profiles of oligosaccharides only after a certain position in the Golgi, mostly by decreasing the non-galactosylated form FA2G0 while increasing other oligosaccharides such as FA2G1, FA2G2 and sialylated glycans (Fig 30). This effect was registered by the model also for FA1 and A2, although only in minor quantity and only at the last stages of the trans-Golgi, where GalT is localized (normalized Golgi length between 0.7 and 0.8).In contrast, ammonia was found to influence the concentration profiles of every N-glycan because of the pH-dependency assumed for all the enzymes.

The final result was an increase in the fraction of low processed oligosaccharides like FA2G0 and a reduction of galactosylated and sialylated forms. Although ammonia had a profound effect on the final N-glycan distribution, it did not significantly change the intra-Golgi pattern of N-glycans (Fig. 31)

UDP-Galactose profile

The model can also be used to obtain information about non-measurable quantities, such as the fate of NSDs once imported inside the Golgi. Considering only UDP-Gal, it is possible

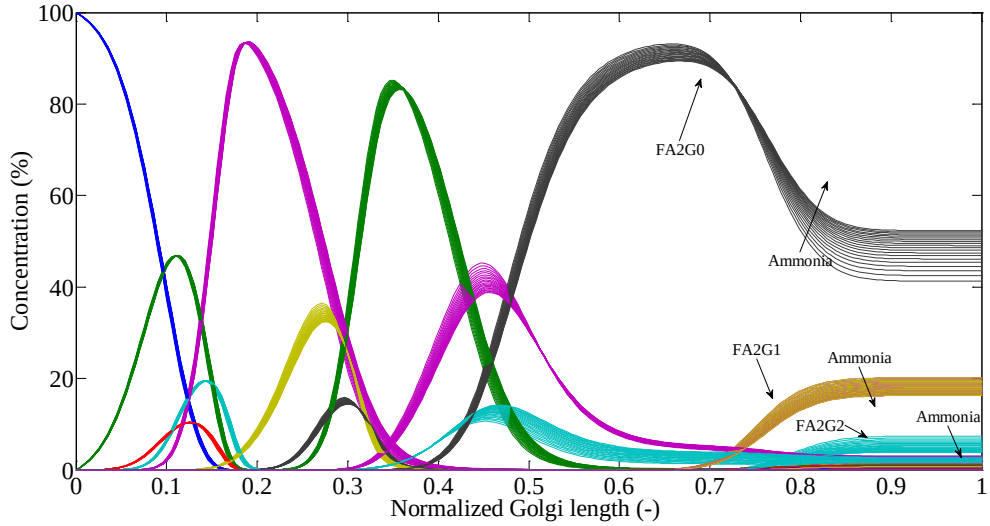

Figure 32 Change in the intra-Golgi concentration profiles of N-glycans in response to different ammonia levels.

to determine not only the Golgi compartment where it is transported, which is easily determinable by the transport protein concentration profile, but also where and how it is consumed. With the aid of computational tools, UDP-Gal concentration was found to rise together with the corresponding TP concentration (after 0.6 normalized Golgi length), and later dropping to lower values due to consumption by the GalT glycotransferase (Fig. 32). This behavior was predicted by the model for intracellular UDP-Gal concentrations

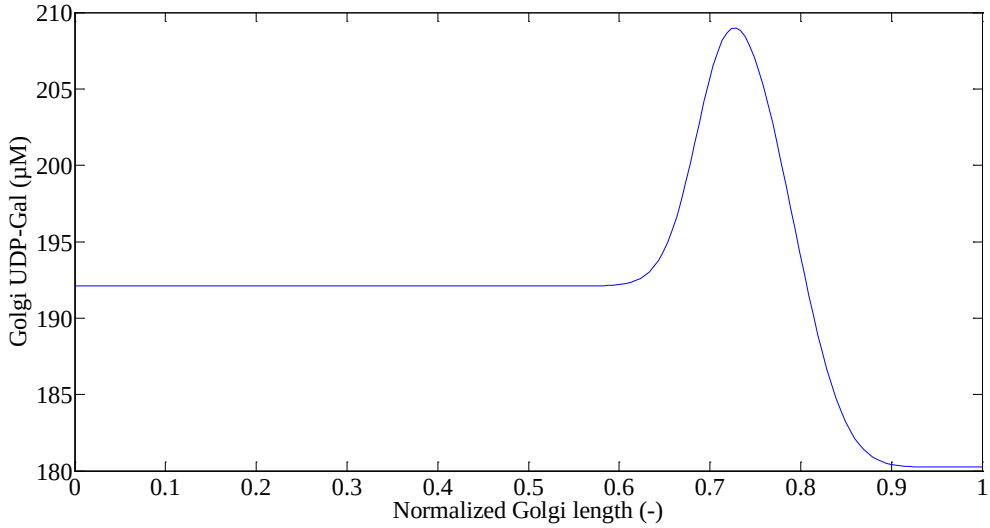

Figure 31 Illustrative UDP-Gal profile across the Golgi apparatus.

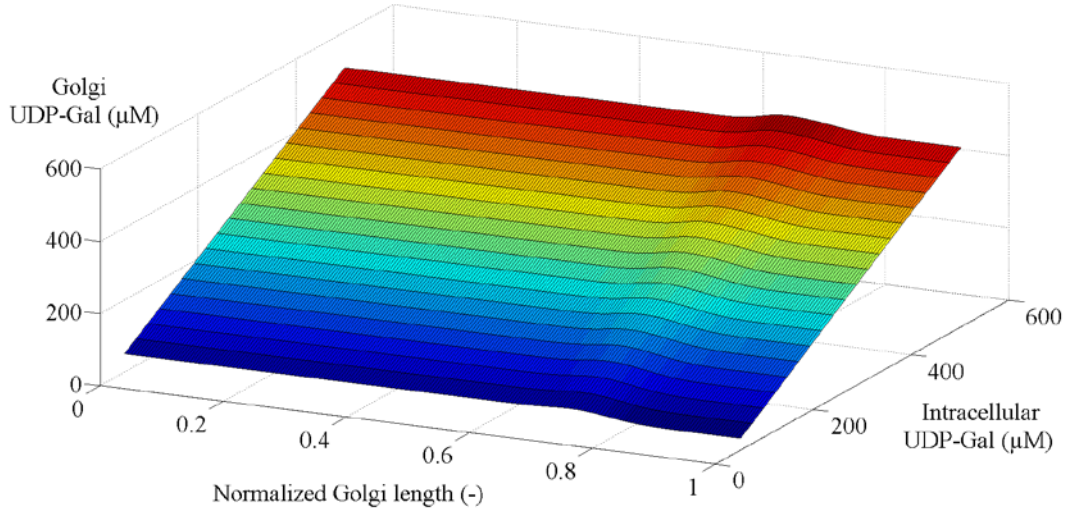

Figure 33 Golgi UDP-Gal concentration in response to galactose supplementation (intracellular UDP-Gal) along the Golgi.

ranging from 50 to 500 µM (Fig. 33). Although the nucleotide sugar concentration inside the Golgi increased in a quasi-linear manner, the drop caused by the consumption of the activated sugar did not change significantly, therefore galactosylation was not profoundly affected, as shown by the estimated FA2G1 concentration, which saturates at 300 µM intracellular UDP-Gal (Fig 34).

In turn, a major impact on the nucleotide sugar consumption was detected for different manganese and ammonia concentrations: increased manganese concentrations resulted in

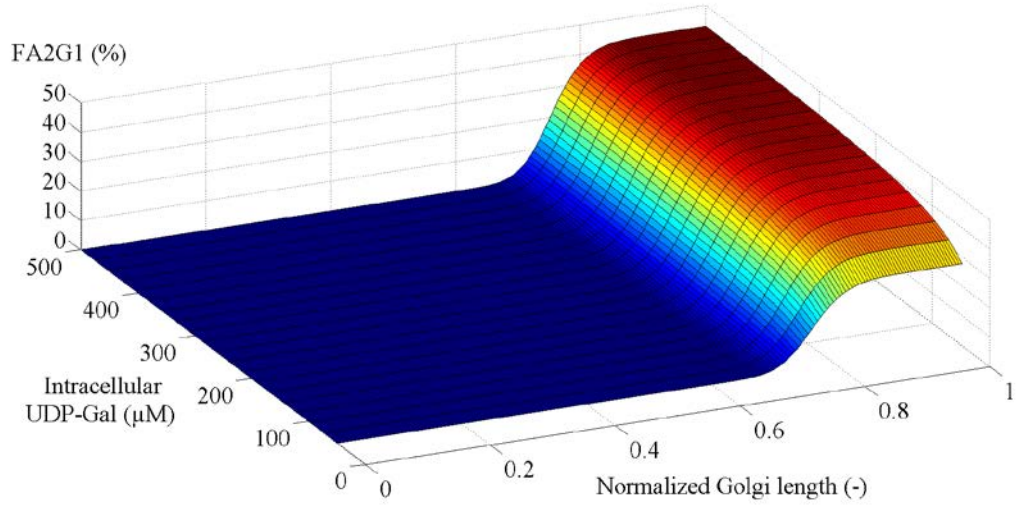

Figure 34 Non-linear variation of the FA2G1 concentration in response to galactose supplementation

higher UDP-Gal consumption due to the enhanced activity of GalT (Fig 35 A), while higher levels of ammonia resulted in lower nucleotide sugar utilization due to the corresponding Golgi pH shift and decreased activity of GalT (Fig 35 B).

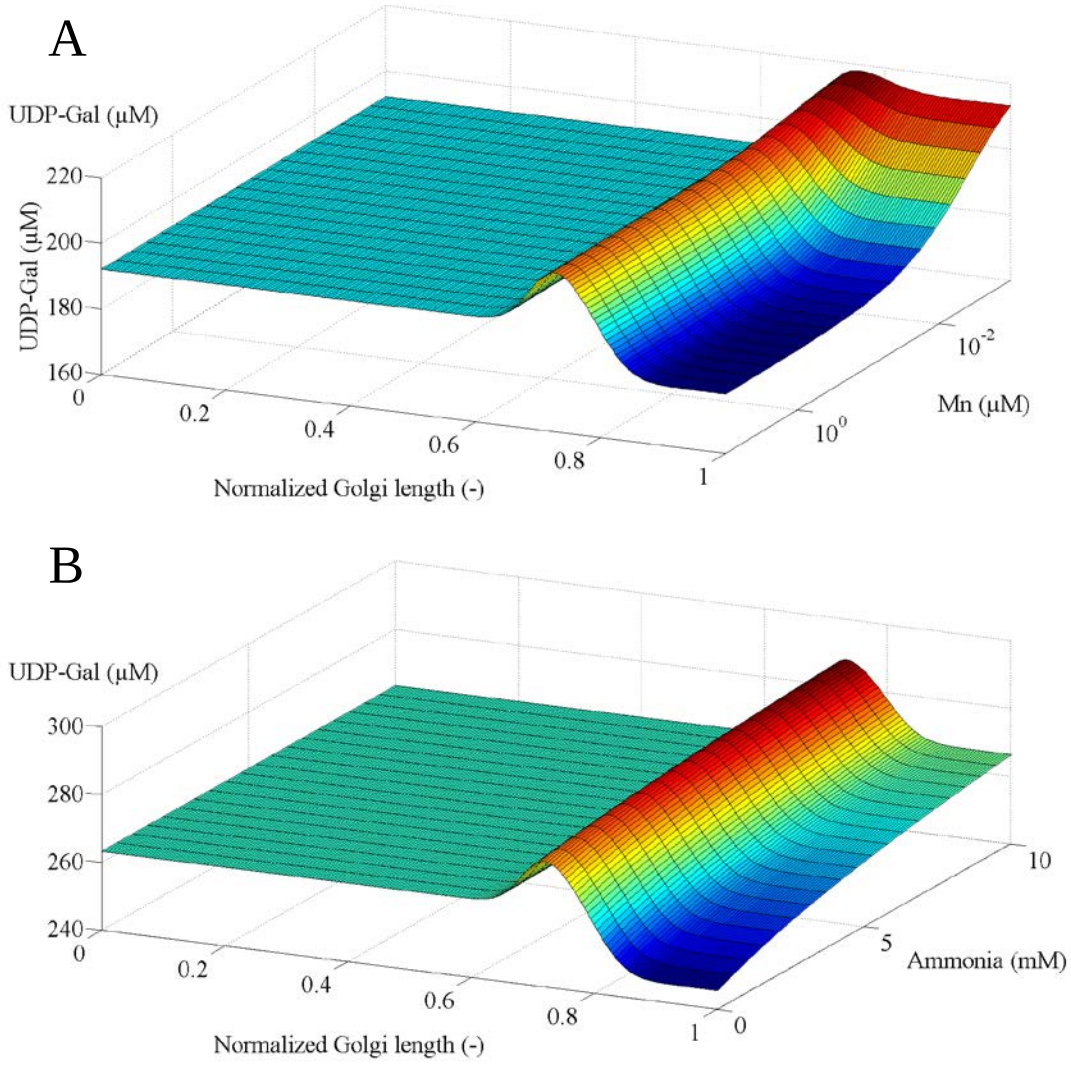

Figure 35 Different UDP-Gal consumptions inside the Golgi in response to different levels of ammonia (A) and manganese (B).

Chapter 5: Conclusions & Outlook

A series of continuous cell cultures using perfused bioreactors was successfully performed. It was shown that the N-glycosylation of mAbs in this type of system can be precisely controlled by medium compositions and average viable cell density.

Although powerful modulators of glycosylation, manganese and galactose were not show to significantly affect cell growth rate and antibody specific productivity. When one of these two components was added, an increase up to 1.5-fold in the amount of galactosylated Fc regions with a concomitant decrease terminal N-acetylglucosamine was detected. Moreover, manganese and galactose were found to have a synergic effect when supplemented at the same time. High ammonia levels inhibited both glycosylation and growth rate.

A mathematical model was developed to predict changes in N-glycosylation with respect to different process conditions by introducing new kinetic expressions. The model was able to reproduce the glycosylation pattern of the edge points of the DoE and successfully predicted the middle point. Moreover, the model was able to give insights about the concentration profiles across the Golgi of the species involved in this process.

The mechanistic model was compared to a statistical response surface methodology. It was found that the RSM, although capable of reproducing the glycosylation pattern of eight points of the DoE cube, was not able to correctly estimate the middle point and showed an inconsistent behavior outside the experimental space.

New experiments need to be carried out to demonstrate the N-glycosylation profile constancy in continuous bioreactors in a long term run. The assessment of the extrapolating capability of the mathematical model outside the experimental space and the robustness in terms of applicability to another mAb producing cell line will be the subject of future work.

Bibliography

[1] I. Jimenez del Val, J. M. Nagy, and C. Kontoravdi, “A dynamic mathematical model for monoclonal antibody N-linked glycosylation and nucleotide sugar donor transport within a maturing Golgi apparatus.,” *Biotechnol. Prog.*, vol. 27, no. 6, pp. 1730–43, 2011.

[2] H. Lis and N. Sharon, “Protein glycosylation. Structural and functional aspects.,” *Eur. J. Biochem.*, vol. 218, no. 1, pp. 1–27, Nov. 1993.

[3] R. G. Spiro, “Protein glycosylation: nature, distribution, enzymatic formation, and disease implications of glycopeptide bonds.,” *Glycobiology*, vol. 12, no. 4, p. 43R–56R, Apr. 2002.

[4] R. Apweiler, “On the frequency of protein glycosylation , as deduced from analysis of the SWISS-PROT database 1,” vol. 1473, pp. 4–8, 1999.

[5] A. Larkin and B. Imperiali, “The expanding horizons of asparagine-linked glycosylation.,” *Biochemistry*, vol. 50, no. 21, pp. 4411–26, May 2011.

[6] F. Schwarz and M. Aebi, “Mechanisms and principles of N-linked protein glycosylation,” *Current Opinion in Structural Biology*, vol. 21. pp. 576–582, 2011.

[7] G. Y. Wiederschain, “Essentials of glycobiology,” *Biochemistry (Moscow)*, vol. 74, no. 9. pp. 1056–1056, 2009.

[8] R. B. Parekh, R. A. Dwek, B. J. Sutton, D. L. Fernandes, A. Leung, D. Stanworth, T. W. Rademacher, T. Mizuochi, T. Taniguchi, K. Matsuta, F. Takeuchi, Y. Nagano, T. Miyamoto, and A. Kobata, “Association of rheumatoid arthritis and primary osteoarthritis with changes in the glycosylation pattern of total serum IgG,” *Nature*, vol. 316, no. 6027, pp. 452–457, Aug. 1985.

[9] J. N. Arnold, M. R. Wormald, R. B. Sim, P. M. Rudd, and R. a Dwek, “The impact of glycosylation on the biological function and structure of human immunoglobulins.,” *Annu. Rev. Immunol.*, vol. 25, pp. 21–50, Jan. 2007.

[10] J. Deisenhofer, “Crystallographic refinement and atomic models of a human Fc fragment and its complex with fragment B of protein A from Staphylococcus aureus at 2.9- and 2.8-A resolution.,” *Biochemistry*, vol. 20, no. 9, pp. 2361–70, Apr. 1981.

[11] R. Ghirlando, J. Lund, M. Goodall, and R. Jefferis, “Glycosylation of human IgG-Fc: influences on structure revealed by differential scanning micro-calorimetry.,” *Immunol. Lett.*, vol. 68, no. 1, pp. 47–52, May 1999.

[12] F. He, S. Hogan, R. F. Latypov, L. O. Narhi, and V. I. Razinkov, “High Throughput Thermostability Screening of Monoclonal Antibody Formulations,” vol. 99, no. 4, pp. 1707–1720, 2010.

[13] Y. Mimura, P. Sondermann, R. Ghirlando, J. Lund, S. P. Young, M. Goodall, and R. Jefferis, “Role of oligosaccharide residues of IgG1-Fc in Fc gamma RIIb binding.,” *J. Biol. Chem.*, vol. 276, no. 49, pp. 45539–47, Dec. 2001.

[14] T. Shinkawa, K. Nakamura, N. Yamane, E. Shoji-Hosaka, Y. Kanda, M. Sakurada, K. Uchida, H. Anazawa, M. Satoh, M. Yamasaki, N. Hanai, and K. Shitara, “The absence of fucose but not the presence of galactose or bisecting N-acetylglucosamine of human IgG1 complex-type oligosaccharides shows the critical role of enhancing antibody-dependent cellular cytotoxicity.,” *J. Biol. Chem.*, vol. 278, no. 5, pp. 3466–73, Jan. 2003.

[15] P. N. Boyd, A. C. Lines, and A. K. Patel, “The effect of the removal of sialic acid, galactose and total carbohydrate on the functional activity of Campath-1H,” *Mol. Immunol.*, vol. 32, no. 17–18, pp. 1311–1318, 1995.

[16] A. J. S. Jones, D. I. Papac, E. H. Chin, R. Keck, S. a Baughman, Y. S. Lin, J. Kneer, and J. E. Battersby, “Selective clearance of glycoforms of a complex glycoprotein pharmaceutical caused by terminal N-acetylglucosamine is similar in humans and cynomolgus monkeys.,” *Glycobiology*, vol. 17, no. 5, pp. 529–40, May 2007.

[17] V. Kayser, N. Chennamsetty, V. Voynov, K. Forrer, B. Helk, and B. L. Trout, “Glycosylation influences on the aggregation propensity of therapeutic monoclonal antibodies.,” *Biotechnol. J.*, vol. 6, no. 1, pp. 38–44, 2011.

[18] R. J. Solá and K. Griebenow, “Glycosylation of therapeutic proteins: an effective strategy to optimize efficacy.,” *BioDrugs*, vol. 24, no. 1, pp. 9–21, 2010.

[19] I. J. del Val, C. Kontoravdi, and J. M. Nagy, “Towards the implementation of quality by design to the production of therapeutic monoclonal antibodies with desired glycosylation patterns.,” *Biotechnol. Prog.*, vol. 26, no. 6, pp. 1505–1527, 2010.

[20] J. M. Reichert, “Marketed therapeutic antibodies compendium,” *mAbs*, vol. 4, no. 3. pp. 413–415, 2012.

[21] F. M. Wurm, “Production of recombinant protein therapeutics in cultivated mammalian cells.,” *Nat. Biotechnol.*, vol. 22, no. 11, pp. 1393–8, Nov. 2004.

[22] S. S. Ozturk and W. Hu, *Cell Culture Technology for Pharmaceutical and Cell-Based therapies*. CRC Press, 2005.

[23] A. Eon-Duval, H. Broly, and R. Gleixner, “Quality attributes of recombinant therapeutic proteins: an assessment of impact on safety and efficacy as part of a

quality by design development approach.," *Biotechnol. Prog.*, vol. 28, no. 3, pp. 608–622, 2012.

[24] L. Malphettes, Y. Freyvert, J. Chang, P.-Q. Liu, E. Chan, J. C. Miller, Z. Zhou, T. Nguyen, C. Tsai, A. W. Snowden, T. N. Collingwood, P. D. Gregory, and G. J. Cost, "Highly efficient deletion of FUT8 in CHO cell lines using zinc-finger nucleases yields cells that produce completely nonfucosylated antibodies.," *Biotechnol. Bioeng.*, vol. 106, no. 5, pp. 774–783, Aug. 2010.

[25] P. Umaña, J. Jean-Mairet, R. Moudry, H. Amstutz, and J. E. Bailey, "Engineered glycoforms of an antineuroblastoma IgG1 with optimized antibody-dependent cellular cytotoxic activity.," *Nat. Biotechnol.*, vol. 17, no. 2, pp. 176–80, Feb. 1999.

[26] W. S. Ahn, J.-J. Jeon, Y.-R. Jeong, S. J. Lee, and S. K. Yoon, "Effect of culture temperature on erythropoietin production and glycosylation in a perfusion culture of recombinant CHO cells.," *Biotechnol. Bioeng.*, vol. 101, no. 6, pp. 1234–44, Dec. 2008.

[27] M. Ivarsson, T. K. Villiger, M. Morbidelli, and M. Soos, "Evaluating the impact of cell culture process parameters on monoclonal antibody N-glycosylation.," *J. Biotechnol.*, vol. 188C, pp. 88–96, Aug. 2014.

[28] J. P. Kunkel, D. C. Jan, J. C. Jamieson, and M. Butler, "Dissolved oxygen concentration in serum-free continuous culture affects N-linked glycosylation of a monoclonal antibody.," *J. Biotechnol.*, vol. 62, no. 1, pp. 55–71, Jun. 1998.

[29] E. Pacis, M. Yu, J. Autsen, R. Bayer, and F. Li, "Effects of cell culture conditions on antibody N-linked glycosylation-what affects high mannose 5 glycoform.," *Biotechnol. Bioeng.*, vol. 108, no. 10, pp. 2348–2358, May 2011.

[30] J. I. Rearick, A. Chapman, and S. Kornfeld, "Glucose starvation alters lipid-linked oligosaccharide biosynthesis in Chinese hamster ovary cells," *J. Biol. Chem.*, vol. 256, no. 12, pp. 6255–6261, 1981.

[31] B. Liu, M. Spearman, J. Doering, E. Lattová, H. Perreault, and M. Butler, "The availability of glucose to CHO cells affects the intracellular lipid-linked oligosaccharide distribution, site occupancy and the N-glycosylation profile of a monoclonal antibody.," *J. Biotechnol.*, vol. 170, pp. 17–27, Jan. 2014.

[32] N. S. C. Wong, L. Wati, P. M. Nissom, H. T. Feng, M. M. Lee, and M. G. S. Yap, "An investigation of intracellular glycosylation activities in CHO cells: effects of nucleotide sugar precursor feeding.," *Biotechnol. Bioeng.*, vol. 107, no. 2, pp. 321–336, Oct. 2010.

[33] P. Hossler, S. McDermott, C. Racicot, C. Chumsae, H. Raharimampionona, Y. Zhou, D. Ouellette, J. Matuck, I. Correia, J. Fann, and J. Li, "Cell culture media supplementation of uncommonly used sugars sucrose and tagatose for the targeted

shifting of protein glycosylation profiles of recombinant protein therapeutics.," *Biotechnol. Prog.*, pp. 20–24, Aug. 2014.

[34] Y. Nishikawa, W. Pegg, H. Paulsen, and H. Schachter, "Control of glycoprotein synthesis. Purification and characterization of rabbit liver UDP-N-acetylglucosamine:alpha-3-D-mannoside beta-1,2-N-acetylglucosaminyltransferase I.," *J. Biol. Chem.*, vol. 263, no. 17, pp. 8270–81, Jun. 1988.

[35] B. Ramakrishnan, E. Boeggeman, V. Ramasamy, and P. K. Qasba, "Structure and catalytic cycle of beta-1,4-galactosyltransferase.," *Curr. Opin. Struct. Biol.*, vol. 14, no. 5, pp. 593–600, 2004.

[36] Q. Zhou, S. Shankara, A. Roy, H. Qiu, S. Estes, A. McVie-Wylie, K. Culm-Merdek, A. Park, C. Pan, and T. Edmunds, "Development of a simple and rapid method for producing non-fucosylated oligomannose containing antibodies with increased effector function," *Biotechnol. Bioeng.*, vol. 99, no. 3, pp. 652–665, 2008.

[37] Y. H. Sung, Y. J. Song, S. W. Lim, J. Y. Chung, and G. M. Lee, "Effect of sodium butyrate on the production, heterogeneity and biological activity of human thrombopoietin by recombinant Chinese hamster ovary cells.," *J. Biotechnol.*, vol. 112, no. 3, pp. 323–35, Sep. 2004.

[38] M. B. Garagba, S. Greco, P. George, I. Hugueny, and P. Louisot, "Polyamine Participation in the Maturation of Glycoprotein Fucosylation , but not Sialylation , in Rat Small Intestine," vol. 51, no. 5, pp. 625–634, 2002.

[39] N. Kochanowski, F. Blanchard, R. Cacan, F. Chirat, E. Guedon, A. Marc, and J.-L. Goergen, "Influence of intracellular nucleotide and nucleotide sugar contents on recombinant interferon-gamma glycosylation during batch and fed-batch cultures of CHO cells.," *Biotechnol. Bioeng.*, vol. 100, no. 4, pp. 721–33, Jul. 2008.

[40] D. C. F. Wong, N. S. C. Wong, J. S. Y. Goh, L. M. May, and M. G. S. Yap, "Profiling of N-glycosylation gene expression in CHO cell fed-batch cultures.," *Biotechnol. Bioeng.*, vol. 107, no. 3, pp. 516–528, 2010.

[41] P. Umaña and J. E. Bailey, "A mathematical model of N-linked glycoform biosynthesis.," *Biotechnol. Bioeng.*, vol. 55, no. 6, pp. 890–908, Sep. 1997.

[42] F. J. Krambeck and M. J. Betenbaugh, "A mathematical model of N-linked glycosylation.," *Biotechnol. Bioeng.*, vol. 92, no. 6, pp. 711–28, Dec. 2005.

[43] P. Hossler, B. C. Mulukutla, and W.-S. Hu, "Systems analysis of N-glycan processing in mammalian cells.," *PLoS One*, vol. 2, no. 8, p. e713, Jan. 2007.

[44] G. B. Nyberg, R. R. Balcarcel, B. D. Follstad, G. Stephanopoulos, and D. I. Wang, "Metabolic effects on recombinant interferon-gamma glycosylation in continuous culture of Chinese hamster ovary cells.," *Biotechnol. Bioeng.*, vol. 62, no. 3, pp. 336–47, Feb. 1999.

[45] E. Losev, C. A. Reinke, J. Jellen, D. E. Strongin, B. J. Bevis, and B. S. Glick, “Golgi maturation visualized in living yeast.,” *Nature*, vol. 441, no. 7096, pp. 1002–1006, 2006.

[46] B. S. Glick and A. Nakano, “Membrane traffic within the Golgi apparatus.,” *Annu. Rev. Cell Dev. Biol.*, vol. 25, pp. 113–32, Jan. 2009.

[47] W. C. Yang, J. Lu, C. Kwiatkowski, H. Yuan, R. Kshirsagar, T. Ryll, and Y.-M. Huang, “Perfusion seed cultures improve biopharmaceutical fed-batch production capacity and product quality.,” *Biotechnol. Prog.*, vol. 30, no. 3, pp. 616–25, 2014.

[48] M.-F. Clincke, C. Mölleryd, Y. Zhang, E. Lindskog, K. Walsh, and V. Chotteau, “Study of a recombinant CHO cell line producing a monoclonal antibody by ATF or TFF external filter perfusion in a WAVE Bioreactor™,” *BMC Proc.*, vol. 5, no. Suppl 8, p. P105, 2011.

[49] R. F. Steinhoff, M. Ivarsson, T. Habicher, T. K. Villiger, J. Boertz, J. Krismer, S. R. Fagerer, M. Soos, M. Morbidelli, M. Pabst, and R. Zenobi, “High-throughput nucleoside phosphate monitoring in mammalian cell fed-batch cultivation using quantitative matrix-assisted laser desorption/ionization time-of-flight mass spectrometry.,” *Biotechnol. J.*, p. n/a–n/a, Aug. 2014.

[50] N. Tomiya, E. Ailor, S. M. Lawrence, M. J. Betenbaugh, and Y. C. Lee, “Determination of nucleotides and sugar nucleotides involved in protein glycosylation by high-performance anion-exchange chromatography: sugar nucleotide contents in cultured insect cells and mammalian cells.,” *Anal. Biochem.*, vol. 293, no. 1, pp. 129–137, 2001.

[51] J. C. Bigge, T. P. Patel, J. A. Bruce, P. N. Goulding, S. M. Charles, and R. B. Parekh, “Nonselective and efficient fluorescent labeling of glycans using 2-amino benzamide and anthranilic acid.,” *Anal. Biochem.*, vol. 230, no. 2, pp. 229–38, Sep. 1995.

[52] A. H. Merry, D. C. a Neville, L. Royle, B. Matthews, D. J. Harvey, R. a Dwek, and P. M. Rudd, “Recovery of intact 2-aminobenzamide-labeled O-glycans released from glycoproteins by hydrazinolysis.,” *Anal. Biochem.*, vol. 304, no. 1, pp. 91–9, May 2002.

[53] A. Ceroni, K. Maass, H. Geyer, R. Geyer, A. Dell, and S. M. Haslam, “GlycoWorkbench: A tool for the computer-assisted annotation of mass spectra of glycans,” *J. Proteome Res.*, vol. 7, no. 4, pp. 1650–1659, 2008.

[54] W. G. Dunphy and J. E. Rothman, “Compartmentation of asparagine-linked oligosaccharide processing in the Golgi apparatus,” *J. Cell Biol.*, vol. 97, no. 1, pp. 270–275, 1983.

[55] T. Nilsson, C. E. Au, and J. J. M. Bergeron, “Sorting out glycosylation enzymes in the Golgi apparatus.,” *FEBS Lett.*, vol. 583, no. 23, pp. 3764–9, Dec. 2009.

[56] I. Tabas and S. Kornfeld, “Purification and characterization of a rat liver Golgi alpha-mannosidase capable of processing asparagine-linked oligosaccharides.,” *J. Biol. Chem.*, vol. 254, no. 22, pp. 11655–63, Nov. 1979.

[57] A. Velasco, L. Hendricks, K. W. Moremen, D. R. Tulsiani, O. Touster, and M. G. Farquhar, “Cell type-dependent variations in the subcellular distribution of alpha-mannosidase I and II.,” *J. Cell Biol.*, vol. 122, no. 1, pp. 39–51, 1993.

[58] U. M. Unligil, S. Zhou, S. Yuwaraj, M. Sarkar, H. Schachter, and J. M. Rini, “X-ray crystal structure of rabbit N-acetylglucosaminyltransferase I: catalytic mechanism and a new protein superfamily.,” *EMBO J.*, vol. 19, no. 20, pp. 5269–5280, 2000.

[59] B. Bendiak and H. Schachter, “Control of glycoprotein synthesis. Kinetic mechanism, substrate specificity, and inhibition characteristics of UDP-N-acetylglucosamine:alpha-D-mannoside beta 1-2 N-acetylglucosaminyltransferase II from rat liver.,” *J. Biol. Chem.*, vol. 262, no. 12, pp. 5784–90, Apr. 1987.

[60] H. Ihara, Y. Ikeda, S. Toma, X. Wang, T. Suzuki, J. Gu, E. Miyoshi, T. Tsukihara, K. Honke, A. Matsumoto, A. Nakagawa, and N. Taniguchi, “Crystal structure of mammalian alpha1,6-fucosyltransferase, FUT8.,” *Glycobiology*, vol. 17, no. 5, pp. 455–466, 2007.

[61] B. Bendiak and G. M. Cook, “Kinetic parameters of a beta-D-galactoside alpha 2 leads to 6 sialyltransferase from embryonic chicken liver.,” *Eur. J. Biochem.*, vol. 128, no. 2–3, pp. 355–362, 1982.

[62] K. Karaveg and K. W. Moremen, “Energetics of substrate binding and catalysis by class 1 (glycosylhydrolase family 47) alpha-mannosidases involved in N-glycan processing and endoplasmic reticulum quality control.,” *J. Biol. Chem.*, vol. 280, no. 33, pp. 29837–29848, 2005.

[63] K. W. Moremen, O. Touster, and P. W. Robbins, “Novel purification of the catalytic domain of Golgi alpha-mannosidase II. Characterization and comparison with the intact enzyme.,” *J. Biol. Chem.*, vol. 266, no. 25, pp. 16876–16885, 1991.

[64] N. Uozumi, S. Yanagidani, E. Miyoshi, Y. Ihara, T. Sakuma, C. X. Gao, T. Teshima, S. Fujii, T. Shiba, and N. Taniguchi, “Purification and cDNA cloning of porcine brain GDP-L-Fuc:N-acetyl-beta-D-glucosaminide alpha1--->6fucosyltransferase.,” *J. Biol. Chem.*, vol. 271, no. 44, pp. 27810–27817, 1996.

[65] B. Bendiak, L. D. Ward, and R. J. Simpson, “Proteins of the Golgi apparatus. Purification to homogeneity, N-terminal sequence, and unusually large Stokes radius of the membrane-bound form of UDP-galactose:N-acetylglucosamine beta 1-4galactosyltransferase from rat liver.,” *Eur. J. Biochem.*, vol. 216, no. 2, pp. 405–417, 1993.

[66] J. Weinstein, U. de Souza-e-Silva, and J. C. Paulson, “Purification of a Gal beta 1 to 4GlcNAc alpha 2 to 6 sialyltransferase and a Gal beta 1 to 3(4)GlcNAc alpha 2 to 3

sialyltransferase to homogeneity from rat liver.," *J. Biol. Chem.*, vol. 257, no. 22, pp. 13835–44, Nov. 1982.

[67] E. V Chandrasekaran, M. Davila, D. Nixon, and J. Mendicino, "Purification and properties of alpha-D-mannose:beta-1,2-N-acetylglucosaminyl-transferases and alpha-D-mannosidases from human adenocarcinoma.," *Cancer Res.*, vol. 44, no. 9, pp. 4059–68, Sep. 1984.

[68] F. J. Krambeck, S. V Bennun, S. Narang, S. Choi, K. J. Yarema, and M. J. Betenbaugh, "A mathematical model to derive N-glycan structures and cellular enzyme activities from mass spectrometric data.," *Glycobiology*, vol. 19, no. 11, pp. 1163–1175, 2009.

[69] W. Chen, U. M. Unligil, J. M. Rini, and P. Stanley, "Independent Lec1A CHO glycosylation mutants arise from point mutations in N-acetylglucosaminyltransferase I that reduce affinity for both substrates. Molecular consequences based on the crystal structure of GlcNAc-TI.," *Biochemistry*, vol. 40, no. 30, pp. 8765–8772, 2001.

[70] M. R. Pâquet, S. Narasimhan, H. Schachter, and M. A. Moscarello, "Branch specificity of purified rat liver Golgi UDP-galactose: N-acetylglucosamine beta-1,4-galactosyltransferase. Preferential transfer of of galactose on the GlcNAc beta 1,2-Man alpha 1,3-branch of a complex biantennary Asn-linked oligosaccharide.," *J. Biol. Chem.*, vol. 259, no. 8, pp. 4716–4721, 1984.

[71] A. K. Datta and J. C. Paulson, "The sialyltransferase 'sialylmotif' participates in binding the donor substrate CMP-NeuAc.," *J. Biol. Chem.*, vol. 270, no. 4, pp. 1497–1500, 1995.

[72] A. Mcqueen and J. E. Bailey, "Bioprocess Engineering Growth inhibition of hybridoma cells by ammonium ion : correlation with effects on intracellular pH," vol. 6, pp. 49–61, 1991.

[73] "http://plotdigitizer.sourceforge.net/."

[74] J. Llopis, J. M. McCaffery, A. Miyawaki, M. G. Farquhar, and R. Y. Tsien, "Measurement of cytosolic, mitochondrial, and Golgi pH in single living cells with green fluorescent proteins.," *Proc. Natl. Acad. Sci. U. S. A.*, vol. 95, no. 12Llopis, J., McCaffery, J. M., Miyawaki, A., Farquhar, M. G., & Tsien, R. Y. (1998). Measurement of cytosolic, mitochondrial, and Golgi pH in single living cells with green fluorescent proteins. Proceedings of the National Academy of Sciences of the Unit, pp. 6803–8, Jun. 1998.

[75] P. Paroutis, N. Touret, and S. Grinstein, "The pH of the secretory pathway: measurement, determinants, and regulation.," *Physiology (Bethesda).*, vol. 19, pp. 207–15, Aug. 2004.

[76] E. Monis, P. Bonay, and R. C. Hughes, “Characterization of a mannosidase acting on alpha 1----3- and alpha 1----6-linked mannose residues of oligomannosidic intermediates of glycoprotein processing.,” *Eur. J. Biochem.*, vol. 168, no. 2, pp. 287–94, Oct. 1987.

[77] W. Zhang, D. Betel, and H. Schachter, “Cloning and expression of a novel UDP-GlcNAc:alpha-D-mannoside beta1,2-N-acetylglucosaminyltransferase homologous to UDP-GlcNAc:alpha-3-D-mannoside beta1,2-N-acetylglucosaminyltransferase I.,” *Biochem. J.*, vol. 361, no. Pt 1, pp. 153–62, Jan. 2002.

[78] M. G. Shoreibah, O. Hindsgaul, and M. Pierce, “Purification and characterization of rat kidney UDP-N-acetylglucosamine: alpha-6-D-mannoside beta-1,6-N-acetylglucosaminyltransferase.,” *J. Biol. Chem.*, vol. 267, no. 5, pp. 2920–7, Feb. 1992.

[79] N. Uozumi, S. Yanagidani, E. Miyoshi, Y. Ihara, T. Sakuma, C. X. Gao, T. Teshima, S. Fujii, T. Shiba, and N. Taniguchi, “Purification and cDNA cloning of porcine brain GDP-L-Fuc:N-acetyl-beta-D-glucosaminide alpha1-->6fucosyltransferase.,” *J. Biol. Chem.*, vol. 271, no. 44, pp. 27810–7, Nov. 1996.

[80] M. Gawlitzek, T. Ryll, J. Lofgren, and M. B. Sliwkowski, “Ammonium alters N-glycan structures of recombinant TNFR-IgG: degradative versus biosynthetic mechanisms.,” *Biotechnol. Bioeng.*, vol. 68, no. 6, pp. 637–646, 2000.

[81] C. K. Crowell, G. E. Grampp, G. N. Rogers, J. Miller, and R. I. Scheinman, “Amino Acid and Manganese Supplementation Modulates the Glycosylation State of Erythropoietin in a CHO Culture System,” vol. 96, no. 3, pp. 538–549, 2007.

[82] L. W. Sommers and C. B. Hirschberg, “liver Golgi . A new Golgi marker activity . Transport of Sugar Nucleotides into Rat Liver Golgi,” pp. 10811–10817, 1982.

[83] B. C. Waldman and G. Rudnick, “UDP-GlcNAc transport across the Golgi membrane: electroneutral exchange for dianionic UMP.,” *Biochemistry*, vol. 29, no. 1, pp. 44–52, 1990.

[84] L. W. Sommers and C. B. Hirschberg, “Transport of sugar nucleotides into rat liver Golgi. A new Golgi marker activity.,” *J. Biol. Chem.*, vol. 257, no. 18, pp. 10811–10817, 1982.

[85] M. E. Milla, C. A. Clairmont, and C. B. Hirschberg, “Reconstitution into proteoliposomes and partial purification of the Golgi apparatus membrane UDP-galactose, UDP-xylose, and UDP-glucuronic acid transport activities,” *J. Biol. Chem.*, vol. 267, no. 1, pp. 103–107, 1992.

[86] A. Lepers, L. Shaw, R. Cacan, R. Schauer, J. Montreuil, and A. Verbert, “Transport of CMP-N-glycoloylneuraminic acid into mouse liver Golgi vesicles.,” *FEBS Lett.*, vol. 250, no. 2, pp. 245–250, 1989.

[87] J. A. Egea, D. Henriques, T. Cokelaer, A. F. Villaverde, A. Macnamara, D. Danciu, J. R. Banga, and J. Saez-rodriguez, "Open Access MEIGO : an open-source software suite based on metaheuristics for global optimization in systems biology and bioinformatics," pp. 1–9, 2014.

[88] A. Khetan, Y. Huang, J. Dolnikova, N. E. Pederson, D. Wen, H. Yusuf-Makagiansar, P. Chen, and T. Ryll, "Control of misincorporation of serine for asparagine during antibody production using CHO cells.," *Biotechnol. Bioeng.*, vol. 107, no. 1, pp. 116–23, Sep. 2010.

[89] L. L. Lairson, B. Henrissat, G. J. Davies, and S. G. Withers, "Glycosyltransferases: structures, functions, and mechanisms.," *Annu. Rev. Biochem.*, vol. 77, pp. 521–55, Jan. 2008.

Supplementary material

S1 Mn-dependent rate expression derivation

The rate expression derived hereby applies only for GalT. This enzyme was found to follow sequential order Bi-Bi kinetics, meaning that the substrates bind the enzyme in a specific order, with the presence of the Mn being necessary for UDP-Gal to occur. Once the enzyme binds the activated sugar, it undergoes a conformational change that allows the successive binding of the N-glycan [35]. Because of this, release of the reaction products occurs in the reverse order with the sugar released first. Mn is assumed to be released together with the phosphate group during the catalytic act [89]. Other assumptions, taken from [1] are listed below:

- Equilibrium is reached rapidly for each reaction.
- Competitive and product inhibition are assumed.
- The rate limiting step is the transfer of the sugar to the growing oligosaccharide and is assumed to be irreversible.

According to these considerations, the reaction mechanisms can be schematized as follows:

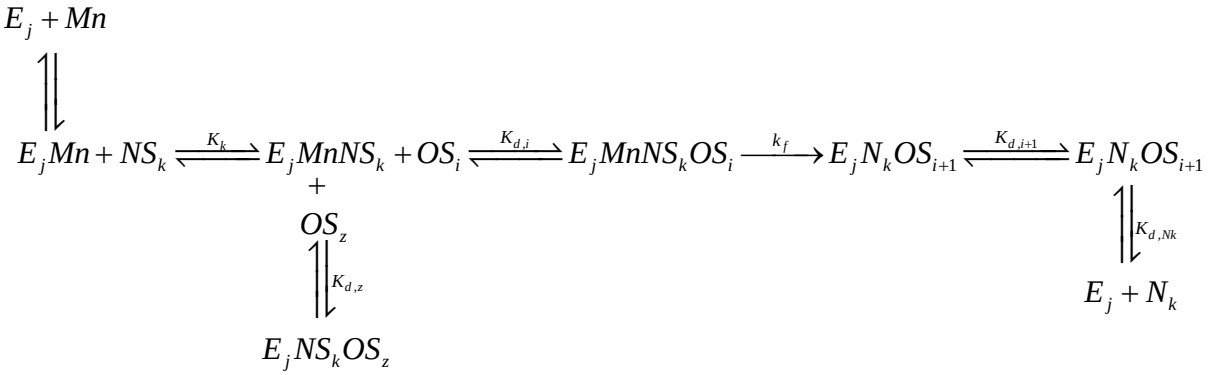

From the reaction scheme, the dissociation constants and different expressions for the enzyme concentrations can be derived:

$$K_{d,Mn} = \frac{[Mn][E_j]}{[E_jMn]} \longrightarrow [E_jMn] = [E_j]\frac{[Mn]}{K_{d,Mn}} \tag{23}$$

$$K_k = \frac{[NS_k][E_jMn]}{[E_jMnNS_k]} \longrightarrow [E_jMnNS_k] = [E_jMn]\frac{[NS_k]}{K_k} \tag{24}$$

$$K_{d,i} = \frac{[OS_i][E_jMnNS_k]}{[E_jMnNS_kOS_i]} \longrightarrow [E_jMnNS_kOS_i] = [E_jMnNS_k]\frac{[OS_i]}{K_{d,i}} \tag{25}$$

$$K_{d,z} = \frac{[OS_z][E_jMnNS_k]}{[E_jMnNS_kOS_z]} \longrightarrow [E_jMnNS_kOS_z] = [E_jMnNS_k]\frac{[OS_z]}{K_{d,z}} \tag{26}$$

$$K_{d,i+1} = \frac{[OS_{i+1}][E_jN_k]}{[E_jN_kOS_{i+1}]} \longrightarrow [E_jN_kOS_{i+1}] = [E_jN_k]\frac{[OS_{i+1}]}{K_{d,i+1}} \tag{27}$$

$$K_{d,N_k} = \frac{[E_j][N_k]}{[E_jN_k]} \longrightarrow [E_jN_k] = [E_j]\frac{[N_k]}{K_{d,Nk}} \tag{28}$$

The total enzyme balance can be computed:

$$E_j^{tot} = E_j + E_jMn + E_jMnNS_k + E_jN_k \tag{29}$$

Combining the dissociation constant with the enzyme balance:

$$E_j^{tot} = E_j + E_j\frac{[Mn]}{K_{d,Mn}} + E_j\frac{[Mn]}{K_{d,Mn}}\frac{[NS_k]}{K_k} + E_j\frac{[Mn]}{K_{d,Mn}}\frac{[NS_k]}{K_k}\frac{[OS_i]}{K_{d,i}} + \ldots \tag{30}$$

$$+\ldots E_j\frac{[Mn]}{K_{d,Mn}}\frac{[NS_k]}{K_k}\sum_z^{NC}\frac{[OS_z]}{K_{d,z}} + E_j\frac{[OS_{i+1}]}{K_{d,i+1}}\frac{[N_k]}{K_{d,Nk}} + E_j\frac{[N_k]}{K_{d,Nk}}$$

$$E_j^{\text{tot}} = E_j + E_j \frac{[Mn]}{K_{d,Mn}} + E_j \frac{[Mn]}{K_{d,Mn}} \frac{[NS_k]}{K_k} + E_j \frac{[Mn]}{K_{d,Mn}} \frac{[NS_k]}{K_k} \frac{[OS_i]}{K_{d,i}} + \ldots$$
$$+ \ldots E_j \frac{[Mn]}{K_{d,Mn}} \frac{[NS_k]}{K_k} \sum_z^{NC} \frac{[OS_z]}{K_{d,z}} + E_j \frac{[OS_{i+1}]}{K_{d,i+1}} \frac{[N_k]}{K_{d,Nk}} + E_j \frac{[N_k]}{K_{d,Nk}} \quad (31)$$

Solving for *Ej*:

$$E_j = \frac{E_j^{\text{tot}}}{1 + \frac{[Mn]}{K_{d,Mn}} + \frac{[Mn]}{K_{d,Mn}} \frac{[NS_k]}{K_k} + \frac{[Mn]}{K_{d,Mn}} \frac{[NS_k]}{K_k} \frac{[OS_i]}{K_{d,i}} + \frac{[Mn]}{K_{d,Mn}} \frac{[NS_k]}{K_k} \sum_z^{NC} \frac{[OS_z]}{K_{d,z}} + \frac{[OS_{i+1}]}{K_{d,i+1}} \frac{[N_k]}{K_{d,Nk}} + \frac{[N_k]}{K_{d,Nk}}} \quad (32)$$

Combining Eq.23-25:

$$\left[E_j MnNS_k OS_i\right] = \left[E_j MnNS_k OS_i\right] \frac{K_{d,Mn} K_k K_{d,i}}{[Mn][NS_k][OS_i]} \quad (33)$$

Inserting the expression found for *Ej* in Eq. 33:

$$\left[E_j MnNS_k OS_i\right] \frac{K_{d,Mn} K_k K_{d,i}}{[Mn][NS_k][OS_i]} = \frac{E_j^{\text{tot}}}{1 + \frac{[Mn]}{K_{d,Mn}} + \frac{[Mn]}{K_{d,Mn}} \frac{[NS_k]}{K_k} + \frac{[Mn]}{K_{d,Mn}} \frac{[NS_k]}{K_k} \frac{[OS_i]}{K_{d,i}} + \frac{[Mn]}{K_{d,Mn}} \frac{[NS_k]}{K_k} \sum_z^{NC} \frac{[OS_z]}{K_{d,z}} + \frac{[OS_{i+1}]}{K_{d,i+1}} \frac{[N_k]}{K_{d,Nk}} + \frac{[N_k]}{K_{d,Nk}}} \quad (34)$$

Rearranging:

$$\left[E_j MnNS_k OS_i\right] = \frac{E_j^{\text{tot}} \frac{[Mn][NS_k][OS_i]}{K_{d,Mn} K_k K_{d,i}}}{1 + \frac{[Mn]}{K_{d,Mn}} + \frac{[Mn]}{K_{d,Mn}} \frac{[NS_k]}{K_k} + \frac{[Mn]}{K_{d,Mn}} \frac{[NS_k]}{K_k} \frac{[OS_i]}{K_{d,i}} + \frac{[Mn]}{K_{d,Mn}} \frac{[NS_k]}{K_k} \sum_z^{NC} \frac{[OS_z]}{K_{d,z}} + \frac{[OS_{i+1}]}{K_{d,i+1}} \frac{[N_k]}{K_{d,Nk}} + \frac{[N_k]}{K_{d,Nk}}} \quad (35)$$

The reaction rate for the limiting step is defined as:

$$r_j = k_{f,j} \cdot \left[EMnNS_k OS_i \right] \tag{36}$$

Inserting Eq. 36 in Eq. 35 and rearranging:

$$r_j = \frac{k_{f,j} E_j^{\text{tot}} [Mn][NS_k][OS_i]}{K_{d,Mn} K_k K_{d,i} \left(1 + \frac{[Mn]}{K_{d,Mn}} + \frac{[Mn]}{K_{d,Mn}} \frac{[NS_k]}{K_k} + \frac{[Mn]}{K_{d,Mn}} \frac{[NS_k]}{K_k} \frac{[OS_i]}{K_{d,i}} + \frac{[Mn]}{K_{d,Mn}} \frac{[NS_k]}{K_k} \sum_z^{NC} \frac{[OS_z]}{K_{d,z}} + \frac{[OS_{i+1}]}{K_{d,i+1}} \frac{[N_k]}{K_{d,Nk}} + \frac{[N_k]}{K_{d,Nk}} \right)} \tag{37}$$

$$r_j = \frac{k_{f,j} E_j^{\text{tot}} [NS_k][OS_i]}{K_k K_{d,i} \left(1 + \frac{K_{d,Mn}}{Mn} + \frac{[NS_k]}{K_k} + \frac{[NS_k]}{K_k} \frac{[OS_i]}{K_{d,i}} + \frac{[NS_k]}{K_k} \sum_z^{NC} \frac{[OS_z]}{K_{d,z}} + \frac{K_{d,Mn}}{Mn} \frac{[OS_{i+1}]}{K_{d,i+1}} \frac{[N_k]}{K_{d,Nk}} + \frac{K_{d,Mn}}{Mn} \frac{[N_k]}{K_{d,Nk}} \right)} \tag{38}$$